TAMPEREEN TEKNILLINEN YLIOPISTO
TAMPERE UNIVERSITY OF TECHNOLOGY

Jie Zhang

Advanced Signal Processing in Multi-mode Multi-frequency Receivers for Positioning Applications

Julkaisu 1176 • Publication 1176

Tampere 2013

Tampereen teknillinen yliopisto. Julkaisu 1176
Tampere University of Technology. Publication 1176

Jie Zhang

Advanced Signal Processing in Multi-mode Multi-frequency Receivers for Positioning Applications

Thesis for the degree of Doctor of Science in Technology to be presented with due permission for public examination and criticism in Sähkötalo Building, Auditorium SJ204, at Tampere University of Technology, on the 3rd of December 2013, at 12 noon.

Tampereen teknillinen yliopisto - Tampere University of Technology
Tampere 2013

ISBN 978-952-15-3187-3 (printed)
ISBN 978-952-15-3503-1 (PDF)
ISSN 1459-2045

Abstract

The demands for positioning services are increasing steadily since the first Global Navigation Satellite Systems (GNSS), NAVSTAR Global Positioning System, also known as GPS was introduced in the early 80s. The increasing demands for positioning services have accelerated the advent of other satellite-based systems, such as the Russian GLONASS, the European Galileo and the Chinese Compass/Beidou-2 system. However, the GNSS fail to provide accurate positioning solution indoors, which is one of the demanding environments. Therefore developing indoor positioning techniques has become a very important topic, mainly in terms of continuity of services and seamless localization. This has led to many theoretical and experimental studies in this field using a wide range of techniques, from purely GNSS approach to methods employing networks of physical sensors or Wireless Local Area Networks (WLAN). These systems, together with satellite-based ones, all have their advantages, but they also face different challenges. Most of these are related to the physical channel containing various error sources that affect the quality of the received signal and degrade the receiver's positioning performance.

The users will benefit from having multiple systems with more satellites and different positioning methods available. In this way, the positioning performance against the errors and challenges will be superior to having only a single system. This can be realized by the multi-mode multi-frequency receiver, which is able to process jointly the new signals, modulations and frequencies introduced in modern positioning systems.

The work presented in this thesis focuses on the signal processing part for research and development of such a receiver and outlines the potential capability of the future receivers for positioning applications. More specifically, this thesis studies the narrowband interference effects on the future GNSS signals in both single-frequency and multi-frequency receivers, makes a performance analysis of dual-frequency ionosphere delay estimation methods under strong multipath errors and presents an optimized multi-correlator based multipath mitigation technique for future GNSS signals. In addition, the performance of four multipath mitigation techniques under time-varying, measurement-based channel models is compared. Finally, a new Non-Line-of-Sight identification based on non-GNSS signal is proposed for improving the path-loss modeling based indoor positioning in multi-mode multi-frequency receivers.

This thesis consists of an introductory part with five chapters and a compendium of six original publications ([I] − [VI]), attached as appendices.

Acknowledgements

This research work has been conducted in the period 2010-2013 in the Department of Communications Engineering and Department of Electronics and Communications Engineering (during the year 2013) at Tampere University of Technology, Tampere, Finland. The research was funded by the EU FP7 under project “Galileo Ready Advanced Mass Market Receiver (GRAMMAR)”, the Academy of Finland under the research project “Digital Signal Processing Algorithms for Indoor Positioning Systems (ACAPO)”, the Graduate School in Electronics, Telecommunications and Automation (GETA; 2012-2013), the Tampere Doctoral Program in Information Science and Engineering (TISE; 2012-2013), Nokia Foundation (2010) and Tekniikka Edistämissäätiö (TES; 2011). The financial support is gratefully acknowledged.

The work presented in this thesis would not have this form without the support of many people. I would like to take this opportunity and thank all those who contributed to the successful completion of this thesis. First of all, I would like to express my deepest gratitude to my supervisor, Adjunct Professor, Dr. Elena Simona Lohan for providing me the opportunity to enter the wireless positioning field and for her dedication, continuous guidance and encouragement throughout my research years. I express my appreciation to all my present and former colleagues at the department for their support and contributions on the published research work that form the basis of this thesis. Special thanks are reserved to Dr. Mohammad Zahidul Hasan Bhuiyan and Dr. Danai Skournetou for fruitful discussions and great collaborations in the research, Elina Laitinen for sharing your ideas and helping with the language revision of the manuscript. I would like to thank Dr. Jussi Salmi from Aalto University, Dr. Stephan Sand and Wei Wang from German Aerospace Center (DLR) for the great joint-research. Finally, I would like to extend my gratitude to the other former and present members Bashir Siddiqui, Shweta Shresha, Parinaz Kaseb Zadeh in wireless positioning group for the enthusiastic and pleasant work atmosphere.

I also would like to acknowledge the pre-examiners, Professor Pratap Misra from Tufts University and Dr. Heidi Kuusniemi from Finnish Geodetic Institute for reviewing my thesis and for their valuable comments to improve this thesis. I am also very grateful to Professor Kai Borre from Aalborg University for agreeing to act as opponent in the public defense of my dissertation.

I wish to extend my thanks to all my friends in Finland for the enjoyable moments we spend together in numerous gathering and parties. It has been a real pleasure to stay in

Finland for seven years which could not be possible without you. I am also very thankful to my friends in China who didn't let the distance separate us.

Finally, I express my gratitude to my parents for their endless love and inspiration. Last but not least, I would like to thank my love, Toni Björninen, for truly supporting me, helping me, believing in me and loving me.

Tampere, November 2013

Jie Zhang

List of publications

This thesis consists of six publications, which are referred as [I] – [VI] in the text. None of these publications have been used or planned to be used as a part of any other thesis and all co-authors have given permission to use the joint articles.

I. J. Zhang, E. S. Lohan, "Effect of narrowband interference on Galileo E1 signal receiver performance," *International Journal of Navigation and Observation*, vol. 2011, Article ID 959871, 10 pages, 2011. DOI:10.1155/2011/959871.

II. J. Zhang, E. S. Lohan, "Galileo E1 and E5a link-level performance for dual frequency overlay structure," *ICST Transactions on Ubiquitous Environments*, 2012. DOI: 10.4108/trans.ubienv.2012.e3.

III. M. Z. H. Bhuiyan, J. Zhang, E. S. Lohan, W. Wang, S. Sand, "Analysis of multipath mitigation techniques with land mobile satellite channel model," *Radioengineering*, vol. 21, no. 4, December 2012.

IV. J. Zhang, E. S. Lohan, "Multi-correlator structures for tracking Galileo signals with CBOC and SinBOC(1,1) reference receivers and limited front-end bandwidths," *Proc. of The 7th IEEE Workshop on Positioning, Navigation and Communication 2010 (WPNC)*, pp. 179-186, March 2010, Dresden, Germany.

V. J. Zhang, D. Skournetou, W. Wang, S. Sand, E. S. Lohan, "Performance analysis of dual-frequency range estimation methods in the presence of ionospheric and multipath propagation effects," *Proc. of the International Conference on Localization and GNSS (ICL-GNSS)*, June 2012, Starnberg, Germany.

VI. J. Zhang, J. Salmi, E. S. Lohan, "Analysis of kurtosis-based LOS/NLOS identification using indoor MIMO channel measurements," *IEEE Transactions on Vehicular Technology*, vol. 62, issue 6, pp. 2871-2874, July 2013.

Author's contribution

The publications [I] − [V] focus on the satellite-based positioning. Specifically, the first two publications [I] − [II] are related to the research on interference effects in both single and multi-frequency Galileo receivers. The publications [III] − [IV] deal with multipath mitigation algorithms for the new GNSS signals. The publication [V] is related to the research on dual-frequency ionosphere estimation methods. The last publication [VI] focuses on the Non-Line-of-Sight identification for indoor positioning operations in future multi-mode receivers. The publications can be seen as building blocks towards multi-mode multi-frequency receivers, having dealt with multiple Galileo frequencies and with supplementing GNSS via non-GNSS approaches (such as MIMO WLAN) in indoor cases.

I. The author analyzed the robustness of Galileo CBOC-modulated signal against the narrowband interference, taking into account the impact of different modulation types in the receiver, namely CBOC and SinBOC(1,1). The author had a major contribution to the analytical derivation and performed all the simulations. The author is the main writer of the publication text.

II. The author analyzed the performance of a dual frequency receiver with overlay structure in the presence of narrowband interference. The idea of the publication was proposed by the author. The author implemented a dual-frequency receiver simulator with overlay structure and performed all the simulations. The author is the main writer of the publication text.

III. This publication has compared different multipath mitigation algorithms in realistic measurement-based channel models in co-operation with Dr. Mohammad Zahidul H. Bhuiyan from Finnish Geodetic Institute, the thesis supervisor and two researchers from DLR, Germany, with whom the author collaborated in GRAMMAR EU FP7 project. The author has contributed in the implementation of channel model and multipath mitigation algorithms in the simulators. The publication text was prepared together with the co-authors.

IV. The author optimized a multipath mitigation method based on a multi-correlator structure for tracking Galileo CBOC-modulated signal with limited front-end bandwidth. The idea was originally from the discussion with the thesis supervisor of

the author. The author has performed the optimization. Both implementations of the optimized algorithm in the simulator and simulations were conducted by the author. The author is the main writer of the publication text.

V. The author has analyzed three dual-frequency ranging estimation methods in the presence of multipath and ionosphere effects. The ionosphere correction methods were initially devised based on an idea by Dr. Danai Skournetou. The author implemented these estimation methods and performed all the simulations. The author is the main writer of the publication text.

VI. The author has proposed a new form for kurtosis-based NLOS identification and analyzed the kurtosis-based NLOS identification with two different system parameters in terms of both simulations and MIMO channel measurements. The measurement data was provided by Dr. Jussi Salmi from Aalto University, Helsinki, Finland. The model implementation and the simulations were conducted by the author, with feedback from co-authors. The author was the main writer of the manuscript.

Continuation of some of the work presented here and complementary research results have been presented by the author in publications [128] [131] [146].

List of abbreviations

ADC	Analog-to-Digital Conversion
AGNSS	Assisted Global Navigation Satellite Systems
AltBOC	Alternative Binary Offset Carrier
AM	Amplitude Modulation
AOA	Angle of Arrival
ARNS	Aeronautical Radio Navigation Services
AWGN	Additive White Gaussian Noise
BFC	Brute Force Constraint
BOC	Binary Offset Carrier
BPSK	Binary Phase Shift Keying
BPF	Band-pass filter
BS	Base Station
C/A	Coarse/Acquisition
CBOC	Composite Binary Offset Carrier
CosBOC	Cosine Binary Offset Carrier
CDMA	Code Division Multiple Access
CIR	Channel Impulse Response
CLS	Constrained Least Square
CNSS	Compass Navigation Satellite System
COO	Cell of Origin
CS	Commercial Service in Galileo
CS	Control Segment in GPS
CWI	Continuous Wave Interference
DBOC	Double Binary Offset Carrier
DLL	Delay Lock Loop
DoD	Department of Defense

DS-CDMA	Direct-Sequence Code Division Multiple Access
DSSS	Direct Sequence Spread Spectrum
E	Early correlator
EC	European Commission
EML	Early-minus-Late
ESA	European Space Agency
EU	European Union
FDMA	Frequency Division Multiple Access
FFT	Fast Fourier Transform
FLL	Frequency Lock Loop
FM	Frequency Modulation
FPP	First Path Power
GCC	Galileo Control Center
GEO	Geostationary Orbit
GLONASS	GLObalnaya NAvigatsionnaya Sputnikovaya Sistema
GNSS	Global Navigation Satellite Systems
GPS	Global Positioning System
GSS	Galileo Sensor Stations
HRC	High Resolution Correlator
IF	Intermediate Frequency
IGSO	Inclined Geosynchronous Satellite Orbit
IOV	In-orbit Validation
L	Late correlator
LBS	Location-based Service
LOS	Line-of-Sight
LS	Least Square
MBOC	Multiplexed Binary Offset Carrier
MCS	Master Control Station
MEE	Multipath Error Envelope
MEO	Medium Earth Orbit
MGD	Multiple Gate Delay
NCO	Numerically Controlled Oscillator

NLOS	Non-Line-of-Sight
OS	Open Service
P	Prompt correlator
PLL	Phase Lock Loop
POA	Phase of Arrival
PPS	Precise Positioning Service
PRN	Pseudo-Random Noise
PRS	Public Regulated Service
PSD	Power Spectral Density
PVT	Position, Velocity, Time
RAIM	Receiver Autonomous Integrity Monitoring
RF	Radio Frequency
RFI	Radio Frequency Interference
RHCP	Right-Hand Circularly Polarization
RMS	Root Mean Square
RMSE	Root Mean Square Error
RNSS	Radio Navigation Satellite Services
RSS	Received Signal Strength
RSSI	Received Signal Strength Indicator
SinBOC	Sine Binary Offset Carrier
SoL	Safety of Life service
SNIR	Signal to Noise and Interference Ratio
SNR	Signal to Noise Ratio
SOP	Signals of Opportunity
SPS	Standard Positioning Service
SV	Space Vehicle
TDOA	Time Difference of Arrival
TEC	Total Electron Content
TECU	Total Electron Content Unit
TMBOC	Time-Multiplexed Binary Offset Carrier
TOA	Time of Arrival
TT&C	Telemetry, Tracking and Control

TUT	Tampere University of Technology
UHF	Ultra High Frequency
ULS	Uplink Stations
UMTS	Universal Mobile Telecommunications System
UTC	Coordinated Universal Time
UWB	Ultra-Wideband
VHF	Very High Frequency
WLAN	Wireless Local Area Networks

List of symbols

$\otimes$	Convolution operator
b_n	n^{th} complex data symbol
$c_{k,n}$	k^{th} chip corresponding to the n^{th} symbol
c	Speed of light
C/N_0	Carrier-to-Noise density Ratio
d	Length of the path
d_0	Reference distance
$d(t)$	Data sequence after spreading
$\delta(t)$	Discrete Dirac pulse
δ_t	Clock bias
Δf	Frequency search resolution
σ_X	Standard deviation of random variable X
ε_i	Measurement error
$\mathcal{E}_{all\_k}$	The errors that contaminate the received signal k
$E(\cdot)$	Expectation
f_c	Carrier frequency
f_i	Carrier frequency i
f_{sc}	Sub-carrier frequency
ϕ_0	Phase at t=0
$h(t)$	Channel impulse response
$G_{BPSK}(f)$	Normalized PSD of BPSK modulation
$G_{MBOC}(f)$	PSD of MBOC modulation
$G_{SinBOC}(f)$	Unit-power PSD of SinBOC modulation
I_i	First-order of ionosphere delay at carrier frequency f_i
κ	Kurtosis
μ_X	Mean of random variable X
n	Number of half period of the sub-carrier during one code chip

N_{BOC}	BOC modulation order
N_{BOC_1}	BOC modulation order of the first stage
N_{BOC_2}	BOC modulation order of the second stage
$P_{DBOC}(f)$	Power spectral density of DBOC modulation
PL	Total path loss in dB
PL_0	Path loss in dB at the reference distance d_0
$\mathcal{R}$	Real function
S_F	Spreading factor
$S_{E5}(t)$	Baseband E5 signal
$Sign(\cdot)$	Signum operator
$S_{SinBOC}(t)$	SinBOC signal waveform
T_{B_1}	Sub-chip interval after the first modulation stage
T_B	Sub-chip interval after the second modulation stage
T_c	Chip period
T_{coh}	Coherent integration time in second
T_{sym}	Symbol period
ρ	True satellite-receiver range
ρ_i	Measured pseudorange corresponding to the signal transmitted at carrier frequency f_i
ω_{E5}	Angular E5 carrier frequency
X_g	Gaussian random variable with zero mean
w	Amplitude weighting factor
$x(t)$	Modulated signal
x_j	j^{th} satellite latitude
x_u	User's latitude
X	Random variable under evaluation
y_j	j^{th} satellite longitude
y_u	User's longitude
z_j	j^{th} satellite altitude
z_u	User's altitude

Contents

1 Introduction

For the readers' convenience, the road map to the contents of this work is provided in Figure 1.1. The introduction part of the thesis consists of five sections discussing the essential background knowledge regarding the research results. The main research results are given in publications [I]−[VI].

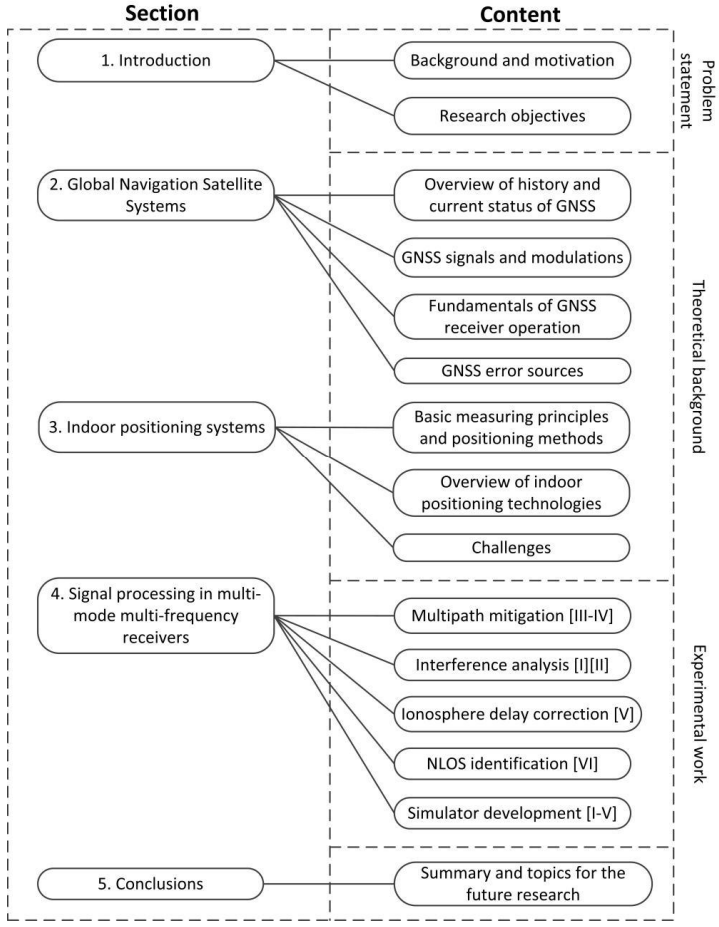

Figure 1.1: Structure and contents of the thesis

1.1 Background and motivation

Positioning is a function that has been playing a significant role in people's life, whether to explore new lands or plan routes. In the past decades, thanks to the advent of electronics and wireless communication technologies, positioning methods have undergone a qualitative leap. They can be accessible to individuals with sufficiently low cost and low power devices. A leap in these technologies occurred with the introduction of the NAVSTAR Global Positioning System (GPS) in the 1980s. It is the first of global navigation satellite systems to become operational and serve to the civilian users. Its great availability, accuracy and reliable performance outdoors have resulted in a rapid and revolutionary adoption of the system worldwide. The increasing demands for positioning services have accelerated the advent of new satellite navigation systems. Russia runs its own system, called GLObalnaya NAvigatsionnaya Sputnikovaya Sistema (GLONASS), which achieved global coverage and full operation capability at the end of 2011. The European Union has devoted a lot of efforts on building an own satellite positioning system, known as Galileo, that should become fully operational in the next 5-10 years. China is also developing a global system known as Compass, which is the second generation of their regional navigation system BeiDou. The advent of all these satellite-based systems has resulted in the use of more generic term, namely Global Navigation Satellite Systems (GNSS) for a technology that is increasingly considered as a public utility. In the coming decade, there will be the next generations of GNSS that are currently being developed. Major activities include modernization of the US GPS and the Russian GLONASS. We will also see the completion of two new GNSS, the Galileo system and the Chinese Compass, which already covers the Asia Pacific region and will grow to achieve global coverage around 2020. New systems and the modernization programs will introduce new frequencies and modulations, which could potentially improve the service capability of the systems. GNSS have a special place among various positioning technologies. This is mainly due to the fact that they have brought such simplicity of use and low cost that many applications and domains have taken advantage of positioning.

GNSS systems are global by nature, but they cannot provide reliable positioning anytime, anywhere due to several, yet unsolved challenges. A number of well-known environments exist, such as indoors, urban canyons and underground, where GNSS signals lose significant power. Consequently, GNSS operations become difficult or impossible. In addition, according to the Environment Protection Agency, people spend about 89-90 percent of their time indoors [1][2]. Moreover, people are willing to have a smart guide to direct them to the destination without any detours, especially in large and unfamiliar spaces, such as airports, office buildings and shopping malls. All the demands and challenges have motivated the innovative thinking worldwide focused on developing technologies for positioning in challenging environments. This has led to many theoretical

and experimental works in the field using a wide range of techniques. One leading technology is the inertial navigation system. It is based on a package of gyroscopes and accelerometers to continuously calculate the position, orientation and velocity via dead reckoning [3][4]. Ranging-based positioning technologies based on radio frequency signals are also used widely. Moreover, positioning with signals of opportunity becomes a popular concept. It exploits the existing wireless transmissions, such as TV, radio and area network signals to calculate the user's location [5][6]. It can be seen that, there is no overall solution based on a single technology, such as that provided outdoors by GNSS. However, the diversity of indoor positioning technology shows how profoundly interdisciplinary the field is and reflects that almost any signal/sensor technique can be exploited for this purpose.

These systems, together with the satellite-based ones, all have their advantages, but they also face different challenges. Most of these challenges are related to the physical signal channel which introduces various error sources that affect the quality of the received signal, and degrade the receiver's positioning performance. These errors include the ionosphere induced propagation delay errors, un-/intentional interferences and multipath/Non-Line-of-Sight (NLOS) propagation.

The users will benefit from having multiple systems with more satellites and different positioning methods available [7][8]. This can be realized by the multi-mode multi-frequency receiver, which is able to process jointly the new signals, modulations and frequencies introduced in the modern positioning systems. One of the main benefits of using multiple frequencies is to provide ionosphere estimation capabilities – removing one of the most significant errors in the current standalone GNSS. In addition, tracking different frequencies in the receiver potentially increases the robustness against jamming attempts. Moreover, a better performance in multipath mitigation could be achieved through tracking the signal, which has higher chip rate and wider bandwidth. The extra positioning methods in the receiver could enable high accuracy positioning in urban canyon and indoors.

To summarize, the multi-mode multi-frequency receiver, which is able to fully utilize the diversity of future GNSS and indoor positioning technologies could provide superior positioning performance compared with the situation with a single-mode receiver. On the other hand, the advantage of multi-mode multi-frequency receivers mentioned above is usually based on certain assumptions. The potential capabilities of such a receiver overcome various challenges, such as multipath/ NLOS propagation, ionosphere delay under strong multipath error, and interferences still need to be investigated. These challenges are what have motivated the author. The work presented in this thesis is dedicated to offer solutions to such challenges.

1.2 Scope and objectives of the thesis

The work presented in this thesis focuses on the signal processing part for research and development of multi-mode multi-frequency receivers, and outlines the potential capability of the future receiver for positioning applications. The main objective of this thesis is to evaluate and improve the performance of multi-mode multi-frequency receivers under various challenges through advanced signal processing. The particular sub-objectives of the thesis can be listed as follows.

- ❖ Work dedicated to improve multipath mitigation performance in GNSS receiver:
  - Optimization of a multiple correlator structure multipath mitigation technique for CBOC-modulated signal with limited bandwidth.
  - Exploring multipath mitigation performance of the new wideband signals.
  - Performance evaluation of multipath mitigation algorithms for CBOC-modulated signal in realistic measurement-based channel models.

- ❖ Analysis of interference effects on the future GNSS signals in both single-frequency and multi-frequency GNSS receivers:
  - Analytical model derivation and performance evaluations of Galileo E1 under narrowband interference.
  - Evaluations of narrowband interference effect on a dual-frequency receiver.

- ❖ Studies on ionosphere delay estimation methods in multi-frequency receivers:
  - Evaluations of dual-frequency ionosphere delay correction methods under strong multipath errors.

- ❖ Improving the indoor positioning accuracy, as a building block of future multi-mode receivers:
  - Development of new NLOS identification methods based on non-GNSS signals.

- ❖ Development of multi-frequency GNSS receivers as research tools:
  - Development of open-source Simulink-based GNSS signal simulators for Galileo E1 and E5 bands.

The research in this thesis has been conducted at the Department of Communications Engineering and the Department of Electronics and Communications Engineering (during the year 2013) at Tampere University of Technology, Tampere, Finland. The research has

been carried out during several projects: “Galileo Ready Advanced Mass MArket Receiver (GRAMMAR)” project funded by EU FP7, “Digital Signal Processing Algorithms for Indoor Positioning Systems (ACAPO)” project and CALM-rest project funded by the Academy of Finland. Additional funding supports are provided by Graduate School in Electronics, Telecommunications and Automation (GETA), Tampere Doctoral Programme in Information Science and Engineering (TISE), Nokia Foundation and Tekniikka Edistämissäätiö (TES). All the work presented in this thesis has been supervised by Adj. Prof. Dr. Elena Simona Lohan.

1.3 Parallel work

As the multi-mode multi-frequency receiver is an awareness raising concept after the introduction of the new signals for positioning applications, it is natural that parallel work has been independently done in other research groups as well. For example, in [9] and [10], the interference studies developed in [I, II] have been extended. The effect of GNSS jammer on the satellite navigation receivers has been studied in [11]. A multipath mitigation study based on S-curve shaping for the new BOC family signals have been performed in [12]. In [12], a one-correlator based S-curve shaping is developed and our study in [IV] has been cited. Parallel studies regarding NLOS identification with multi-antenna configurations for mobile positioning application have been recently reported in [13][14], but the algorithms described there are different from that presented in the publication [VI]. In [15], graphical interfaces and simulators for GNSS signals are discussed and our Simulink model is cited.

1.4 Structure of the thesis

This compendium-type thesis is composed of an introductory part with five chapters and a collection of six original publications. The introductory part provides readers with essential background knowledge on the principle of positioning in terms of both GNSS and indoor positioning systems. The error sources and challenges that degrade receiver’s positioning performance and an overview on the methods developed for mitigating and overcome the various errors and challenges are also discussed. The publication part includes the detailed description of the proposed algorithms, comparison with the state-of-the-art methods and performance analysis. These include four articles published in international journals and two articles published in peer-reviewed international conferences. They are briefly referred in the text as [I], [II], …, [VI]. It is remarked that the novel parts of this thesis stay in the publications. The remaining of this thesis is organized as follows.

Chapter 2 provides the essential background of satellite-based positioning systems. It starts with an overview of the history and current status of GNSS. The modulations used in the future GNSS signals, are then discussed. After that, the main functionalities of a GNSS receiver are described, with particular attention to the baseband signal processing, and finally, various error sources in satellite-based positioning are briefly described.

Chapter 3 gives an overview of indoor positioning systems. The basic measuring principles and positioning methods are described first. A brief introduction of different indoor positioning technologies is presented next. In the end, the challenges in indoor positioning are discussed.

Chapter 4 discusses the various state-of-the-art methods for mitigating the errors. The algorithms proposed in this thesis are presented with respect to the state-of-the-art methods. The development of Simulink-based GNSS signal receiver simulators as a research tool and the basic functionalities of the simulators are presented.

Chapter 5 concludes the thesis with a summary and some prospects for future research.

Finally, the original results of the thesis, which are summarized in the introductory part, are reported in the publications, attached as appendices to the thesis.

2 Global navigation satellite systems

This chapter presents an overview of current and future GNSS. A global navigation system is a system that offers global navigation at any point of the Earth within the system limitation (such as reduced indoor coverage). First we present a brief history and current status of the satellite navigation systems. Next, the discussions focus on the satellite signal characteristics. The typical receiver structure and the functionality of each component in the receiver are then presented. In the end, various error sources and their effects on GNSS performance are discussed.

2.1 Brief history of satellite navigation systems

Satellite-based navigation started in the early 1960s. The first satellite navigation system was the U.S. Navy Navigation Satellite System (as referred to “TRANSIT”). Its operation was based on the Doppler Effect. The receiver’s location was determined by monitoring the frequency shift between the broadcast frequency and received frequency [16]. The success of TRANSIT brought the follow-on programs for space-based navigation systems. The U.S Department of Defense (DoD) developed Navstar GPS. Nowadays, GPS is not the only system of its kind. Russian military space operates the GLONASS in order to provide global coverage. GPS and GLONASS became fully operational in 1995 and 1996, respectively. Since then, GLONASS was not operational for a long period, due to the collapse of the Russian economy and until the end of 2011, after which the system was again updated and modernized. In 1998, the European Union (EU) decided to develop a satellite navigation system, which is independent of GPS and designed specifically for civilian use worldwide. Meanwhile, China is developing its own satellite navigation system. By the end of 2020, there will be at least four independent global navigation systems, the U.S. GPS, the Russian GLONASS, the European Galileo and the Chinese Compass/Beidou-2 with virtually around 120 navigation satellites in the sky. Next section provides further details about these four systems.

2.2 Current and future GNSS

2.2.1 GPS

In the early 1960s, several U.S. government organizations, including DoD were interested in developing satellite systems for three-dimensional positioning, meaning latitude, longitude and altitude. Their targets were to achieve a system with the following attributes: global coverage, operation in all weather, serving high-dynamic platform ability and high accuracy. Presently, GPS is the first and the one of the two fully operational satellite navigation systems. It meets the criteria established in the 1960s for an optimum positioning system. Although GPS was primarily developed for military purpose, it has been widely used in civilian applications as well during the past few decades. The system is offering two types of service: a Standard Positioning Service (SPS) for public use and an encoded Precise Positioning Service (PPS), dedicated to military and selected government agency users. The SPS is free of direct charge to all the users worldwide.

GPS is comprised of three segments: satellite constellation, ground control/monitoring network, and user equipment. The satellite constellation contains the satellites in orbit that provide the ranging signals and data messages to the user equipment. The Air Force manages the constellation to ensure the availability of at least 24 GPS satellites during 95% of the time. For the past several years, the Air Force has been flying 31 operational GPS satellites plus 3−4 decommissioned satellites that can be reactivated if needed [17]. The most recent GPS satellite launch was scheduled on May 15th 2013 [18]. GPS satellites fly in Medium Earth Orbit (MEO) at an altitude of approximately 20,200 km. The satellites in the GPS constellation are placed in six Earth-centered orbital planes with a minimum of four satellites in each plane. The Control Segment (CS) tracks/maintains the satellites in their positions and monitors the health and status of satellite subsystem. Furthermore, the CS collects pseudorange and carrier phase measurement at the remote monitor stations to determine satellite clock corrections, almanac and ephemeris [19]. In order to accomplish these functions, the CS consists of three different components: the Master control station (MCS) located at Schriever Air Force Base near Colorado Springs in US [16], several monitor stations and the ground antennas. The user equipment performs the navigation, timing and other related functions.

GPS signals use a Direct Sequence Spread Spectrum (DSSS) technique [20] and are based on Code Division Multiple Access (CDMA) principle to distinguish signals coming from different satellites. The legacy GPS satellites broadcast ranging code and navigation data on two frequencies. These two radio frequencies are referred to L1 centered at 1575.42 Megahertz (MHz) and L2 centered at 1227.60 MHz. Each GPS satellite transmits two different signals: Coarse/Acquisition or C/A code at L1, and Precision signal or P(Y) at

both L1 and L2. The L1 and L2 carrier signals are currently modulated by the pseudorandom noise (PRN) sequences using Binary Phase Shift Keying (BPSK) modulation. Since each satellite uses the same carrier frequencies, the signals are separated with a unique PRN sequence associated with each satellite.

In order to improve the performance of GPS receivers and to remain competitive with international satellite navigation systems, the growing demand on the existing system has led to the effort to modernize the GPS system. In the late 1990s, the US government started a GPS modernization program, which involves upgrading the GPS space and control segments with new features to upgrade GPS performance for both military and civilian applications. A major focus in this program is adding new navigation signals to the satellite constellation. These new signals are designed for civilian use: L2C, L5 and L1C [21]. The current C/A signal will continue to be transmitted in the future. Therefore, there will be a total of four civil GPS signals. Among these new signals, L2C is designed specifically to meet commercial needs. Combined with the current L1 signal in a dual frequency receiver, L2C enables ionosphere error correction, whereby the user of a dual-frequency GPS receiver could enjoy the same accuracy as the military applications. The L5 is the third civilian GPS signal, centered at 1176.45 MHz. It features higher power, wider bandwidth and more advanced signal structure and is designed for meeting demanding requirements for safety-of-life transportation and other high-performance applications. L1C is the fourth civilian GPS signal, designed to enable the interoperability between GPS and other international satellite navigation systems, such as the European Galileo system. It features a Multiplexed Binary Offset Carrier (MBOC) modulation scheme that enables international cooperation in particular with Galileo system, which will improve mobile GPS reception in cities and other challenging environments.

2.2.2 GLONASS

When GPS was under development in the 1970s, the former Union of Soviet Socialist Republics (USSR) developed a similar system called GLONASS. Similar to GPS, GLONASS was designed primarily for the military applications. The first GLONASS satellite was launched in 1982 and the system was declared fully operational in 1996. After the completion, the system fell into decay rapidly with the collapse of the Russian economy. The old satellites were taken out of service after their design life time had been exceeded. To change this situation, Vladimir Putin made the decision on restoration of the system as a top government priority and funding was substantially increased [22]. By 2010, GLONASS reached full coverage in Russian territory and since December 2011, it has been fully operational, providing worldwide coverage and acceptable accuracy for most users.

Functionally, GLONASS consists of a 21 satellite constellation plus 3 active spares. The 24 satellites operate at an altitude of 19,100 km and are uniformly located in three

orbital planes 120° apart in right ascension. Traditionally, each GLONASS satellite transmits navigation signals in two frequency bands, L1 (1598.0625 − 1609.3125 MHz) and L2 (1242.9375 – 1251.6875 MHz). Unlike all other GNSS systems, GLONASS employs frequency division multiple access (FDMA) technique in order to make the separation between satellites. Aiming to provide better accuracy, multipath resistance and especially greater interoperability with GPS and future Galileo, new GLONASS−K satellites will transmit CDMA signals in addition to the FDMA signals.

A number of ground support segments are scattered throughout Russia that control, track and upload ephemeris, timing information and other information to the satellites. In the system modernization, the ground segment will produce an extension monitoring-station network providing more frequent updates to make the system time scale for stable and better synchronized with Coordinated Universal Time (UTC). Although GLONASS is fully operational, its commercialization, especially the development of the user device, has been lacking compared with the GPS. In order to improve the situation, the Russian government has been actively promoting GLONASS for civilian use. Several private manufacturers – Javad Navigation Systems, Leica, NovAtel and Trimble – currently offer combined GPS/GLONASS receivers, used for the survey market.

2.2.3 Galileo

A new promising GNSS under development is the European navigation system, Galileo. Galileo will provide a highly accurate, guaranteed global positioning service under civilian control. It will interoperate with GPS and GLONASS, the two other GNSS currently operational. The development and In-Orbit Validation (IOV) of the Galileo programme is carried out by the European Space Agency (ESA) and the European Commission (EC). The system is expected to be fully operational by 2020.

The full deployed Galileo system will consist of 30 satellites (27 operational + 3 active spares), equally distributed in three orbital planes. Each plane is at 23,222 km altitude above the Earth, and at an inclination of the orbital planes of 56 degrees to the equator [23]. The first two experimental navigation satellites, Galileo In-Orbit Validation Element GIOVE−A and GIOVE−B were launched in 2005 and 2008, respectively, for testing the key Galileo technologies. The first two Galileo IOV satellites were carried into orbit from European Spaceport on 21st October 2011 and second pair was launched on 12nd October 2012 [24]. The Galileo IOV phase will validate the system design using these four satellites – the minimum required to provide exact positioning and timing at the test locations [25].

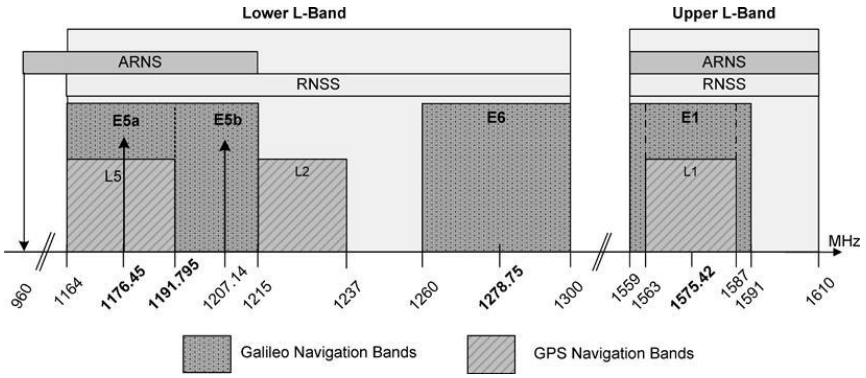

Figure 2.1: Galileo and GPS Frequency plan [30][31]

The Galileo satellites will transmit navigation signals at four different frequency bands, namely E5a, E5b, E6 and E1 as shown in Figure 2.1. They have been selected in the allocated spectrum for Radio Navigation Satellite Services (RNSS). In addition to that, E5a, E5b and E1 bands are included in the allocated spectrum for Aeronautical Radio Navigation Services (ARNS), employed by Civil-Aviation users. It can be seen that, in the lower L-Band, E5a (overlapping with the future GPS L5) and E5b with 24 MHz each, E6 with 40 MHz are planned. In the upper band, E1 with 32 MHz are planned. The frequency band overlapping enables the inter-operational capability between Galileo and GPS. The interference between the signals in the same band will be kept as small as possible by implementing new modulations [26].

The Galileo ground segment is responsible for maintaining proper operations of the system. The basic functions include: 1) control/maintenance of the status and configuration of the satellite constellation; 2) prediction of ephemeris and satellite clock evolution; 3) keeping the corresponding GNSS time scale and 4) updating the navigation messages for all the satellites. The ground segment consists of two Galileo Control Centers (GCCs) in Europe, five Telemetry, Tracking and Control (TT&C) stations, new Mission Uplink Stations (ULS), and a global network of Galileo Sensor Stations (GSS) [27].

The Galileo user segment is composed by Galileo receivers. The receiver development activities have been initiated within the Galileo programme, addressing different needs of the system development process and covering the range of signals and services that will be offered [23].

The current plans in Galileo are to provide four levels of services worldwide [28][29]:

- ***Open Service*** **(OS)** gives basic level services, dedicated to consumer applications. The service provides positioning, velocity, and timing information that can be accessed free of charge by mass-market receivers. The OS performance is expected to be competitive with the existing GNSS in terms of both accuracy and availability; moreover, the service will also be interoperable with those systems, e.g., the receiver may use both Galileo and GPS signals in order to provide seamless services performance in urban canyons.
- ***Safety of Life Service*** **(SoL)** is designed for use in most transportation applications where the degraded navigation information will endanger lives. SoL will provide to its users not only a global positioning service as OS, but it will also have the provision of integrity information at the global level.
- ***Commercial Service*** **(CS)** is a restricted-access service level for commercial and professional applications where higher accuracy is required. The CS is based on adding to the OS signals two additional signals, which are protected through commercial encryption. Within CS, the users will be offered high data rate throughput, high accurate positioning and several value-added applications, such as service guarantees, provision of ionosphere delay models.
- ***Public Regulated Service*** **(PRS)** is intended for groups such as police and customs. It is encrypted and operational at all time and circumstances. A major advantage of PRS is that it is designed to be robust against jamming and spoofing.

2.2.4 Compass/Beidou-2

Compass Navigation Satellite System (CNSS), also named BeiDou-2, is China's second generation satellite navigation system. In December 2011, the Compass/Beidou-2 system was officially announced to provide initial navigation and timing services for the whole Asia-Pacific region with a constellation of ten satellites (five geostationary orbit (GEO) satellites and five Inclined Geosynchronous Satellite Orbit (IGSO) satellites) [31][33]. During 2012, five more satellites (one GEO satellite and four MEO satellites) were launched. By the end of 2012, there are five GEO, four MEO and five IGSO BeiDou navigation satellites in orbit [34].

Similar to other GNSS, Compass/Beidou-2 is composed of three main parts: space section, ground section and user section. The space section of Compass will consist of 5 GEO satellites, 27 MEO satellites and 3 IGSO satellites. The GEO satellites are operating in orbit at an altitude of 35,786 kilometers and MEO satellite are operating in orbit at an altitude of 21,528 kilometers and an inclination of 55° to the equatorial plane [34]. The IGSO satellites are operating in orbit at an altitude of 35,786 kilometers and an inclination

of 55° to the equatorial plane. Frequencies for Compass are allocated in four bands: B1 and B1−2 centered at 1561.0 MHz and 1589.7 MHz, respectively, with 4 MHz bandwidth each, B2 and B3 centered at 1207.14 MHz and 1268.51 MHz, respectively, with 24 MHz bandwidth each. The ground section includes a main control station, upload stations and monitor stations. The ground section is responsible for controlling the satellite constellation and uploading the orbital correction and navigation message to Compass satellites. The user section consists of Compass user terminals, which should be compatible with other navigation satellite systems.

The Compass system will provide global coverage with positioning and timing services, including two kinds of services: 1) an open service that will be free of change; 2) an authorized service that will provide more secure communication services as well as a higher level of integrity. The Compass system will also provide two regional services, which are the wide area differential service with one meter positioning accuracy and a short message communication service that can be exchanged between stations and users [33].

2.3 GNSS signals and modulations

In order to design signal processing algorithms for the GNSS receivers, it is necessary to know the characteristics of the signals. In this section, different signal modulations that will be used in modernized GPS and Galileo systems are explained. The work carried out in this thesis mainly focuses on three different signal modulations, namely Multiplexed Binary Offset Carrier (MBOC) modulation used in Galileo E1 signal and modernized GPS L1C signal, Alternate Binary Offset Carrier (AltBOC) modulation used in Galileo E5 signal and Sine BOC (SinBOC) modulation that can be used as an alternative to demodulate MBOC signal at the receiver side.

2.3.1 BPSK

A very important and useful signal in satellite navigation is the BPSK modulation, which was in fact the first one to be used for satellite navigation. In spite of its simplicity, it is still used nowadays and in the future navigation systems. A BPSK-modulated signal can be seen as the convolution between a code part $d(t)$ (including navigation data) and a modulation pulse as follows:

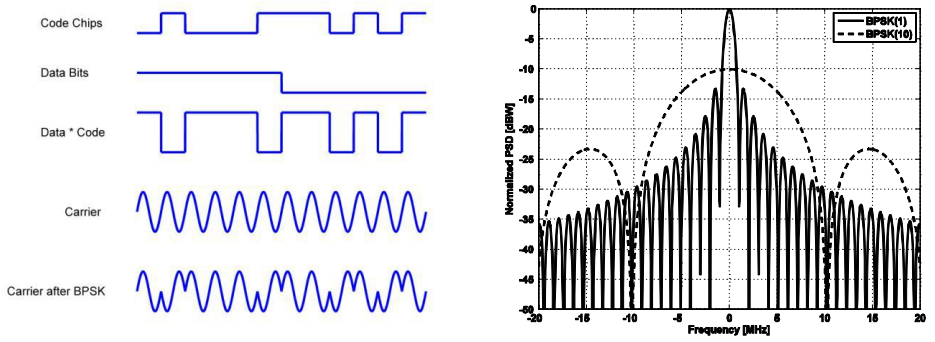

(a) (b)

Figure 2.2: (a) Example of BPSK modulation of the carrier wave with code chips and navigation data; (b) Normalized PSD of BPSK(1) and BPSK(10) modulation.

$$s(t) = p_{T_C}(t) \otimes \sum_{n=-\infty}^{+\infty} b_n \sum_{k=1}^{S_F} c_{k,n}\delta(t - nT_{sym} - kT_C), \quad b_n = \begin{cases} +1 & \text{for binary symbol "1"} \\ -1 & \text{for binary symbol "0"} \end{cases} \qquad (1)$$
$$= s_{BPSK} \otimes d(t)$$

where $\otimes$ is the convolution operator, T_C is the chip period, b_n is the n^{th} complex data symbol, $d(t)$ is the data sequence after spreading, $\delta(t)$ is the Dirac Pulse function, T_{sym} is the code symbol period, $c_{k,n}$ is kth chip corresponding to the nth symbol, S_F is the spreading factor ($S_F = T_{sym} / T_C$), $p_{T_C}(t)$ is a rectangular pulse of unit amplitude and width T_C defined as

$$p_{T_C}(t) \triangleq \begin{cases} 1 & \text{if } 0 \le t < T_C \\ 0 & \text{otherwise} \end{cases} \qquad (2)$$

Then the analog passband signal at carrier frequency f_C becomes

$$m(t) = A_C s(t) \cos(2\pi f_C t) \qquad (3)$$

Above, A_C is the amplitude of the carrier frequency.

Figure 2.2 (a) shows the generation of a BPSK modulated signal at carrier frequency. The code chips are combined with the navigation data bits through modulo-2 adders (* in the figure). The final signal is created by BPSK where the carrier phase is instantaneously shifted by 180°, depending on the data-modulated code chips. When a navigation data bit transition occurs, the phase of the resulting signal is also phase-shifted 180° [35] . In the literature, BPSK(n) form is commonly used, which describes a signal with BPSK modulation and the spreading code rate n×1.023 MHz. For example, the future Galileo will use BPSK(10) for E5a and E5b signals, which means the PRN code chip rate is 10.23 MHz. The normalized power spectral density (PSD) of a BPSK signal under ideal codes assumption can be defined as in Eq. (4) [36]. Figure 2.2 (b) presents the normalized PSD of BPSK(1) and BPSK(10) modulation.

$$G_{BPSK}(f) = f_C \left(\frac{\sin(\pi f / f_C)}{\pi f} \right)^2 \tag{4}$$

2.3.2 BOC

The concept of Binary Offset Carrier (BOC) modulation was allegedly first introduced by Betz [37] as an effort for GPS modernization. It provides a simple and efficient way of offering a low spectral interference with the existing GPS signal and potentially better time-resolution capabilities compared with the traditional BPSK modulation [38][39].

BOC modulation is a square sub-carrier modulation, where a signal is multiplied by a rectangular sub-carrier frequency f_{SC} . This sub-carrier frequency splits the spectrum of the signal into two parts. A BOC modulation is defined via two parameters BOC(*m,n*), related to reference frequency 1.023 MHz, $m = f_{SC} / 1.023 \text{ MHz}$ and $n = f_C / 1.023 \text{ MHz}$, where f_C is chip rate. From the equivalent baseband signal point of view, the BOC modulation can be defined via a single parameter, denoted as the BOC modulation order [40]:

$$N_{BOC} \triangleq 2\frac{m}{n} = 2\frac{f_{SC}}{f_C} \tag{5}$$

where *m* and *n* are two positive indices (not necessarily integers but they should be chosen in such a way that N_{BOC} remains an integer).

BOC modulation has two main variants: sine-BOC (SinBOC) and cosine-BOC (CosBOC). Any SinBOC or CosBOC-modulated signal *x(t)* can be seen as the convolution between Sin/CosBOC waveform and a modulating waveform *d(t)*, as follows [41]:

$$\begin{aligned} x(t) &= \sum_{n=-\infty}^{\infty} b_n \sum_{k=1}^{S_F} c_{k,n} s_{Sin/CosBOC}(t - nT_{sym} - kT_C) \\ &= s_{Sin/CosBOC}(t) \otimes \sum_{n=-\infty}^{\infty} \sum_{k=1}^{S_F} b_n c_{k,n} \delta(t - nT_{sym} - kT_C) \\ &\triangleq s_{Sin/CosBOC}(t) \otimes d(t) \end{aligned} \tag{6}$$

According to its original definition in [42], s_{SinBOC}, s_{CosBOC} and their equivalences are shown in Eq. (7) and Eq. (8) [41]. Figure 2.4 gives an example of time domain waveform for SinBOC(1,1) modulated chip sequences.

$$\begin{cases} s_{SinBOC}(t) = sign\left(\sin\left(\dfrac{N_{BOC}\pi t}{T_C}\right)\right), 0 \le t \le T_C \\ s_{CosBOC}(t) = sign\left(\cos\left(\dfrac{N_{BOC}\pi t}{T_C}\right)\right), 0 \le t \le T_C \end{cases} \tag{7}$$

$$\begin{cases} s_{SinBOC(m,n)}(t) = p_{T_{B_1}}(t) \otimes \sum_{i=0}^{N_{BOC}-1} (-1)^i \delta(t - iT_{B_1}), 0 \le t < T_C \\ s_{CosBOC(m,n)}(t) = p_{T_{B_1}}(t) \otimes \sum_{i=0}^{N_{BOC}-1} \sum_{k=0}^{1} (-1)^{i+k} \delta(t - iT_{B_1} - \dfrac{kT_{B_1}}{2}), 0 \le t \le T_C \end{cases} \tag{8}$$

where $sign(\bullet)$ is the signum operator, N_{BOC} is the BOC modulation order defined in Eq. (5); $p_{T_{B_1}}(\bullet)$ is the rectangular pulses of amplitude 1 and support $T_{B_1} = T_C / N_{BOC}$.

For even and odd N_{BOC}, the normalized Power Spectral Density (PSD) of SinBOC- and CosBOC-modulated signal is defined in Eq. (9) and Eq. (10), respectively [43]. The expression for even and odd N_{BOC} in both sine and cosine phase modulations are very similar. The only difference is whether a sine or cosine appears in the numerator. Figure 2.3 shows the normalized PSD of SinBOC(1,1) and BPSK modulations.

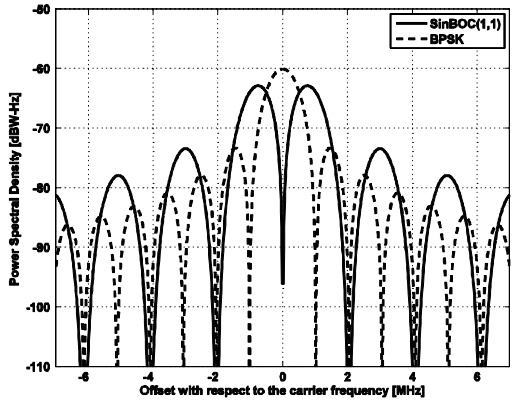

Figure 2.3: Normalized PSD of SinBOC(1,1)- and BPSK-modulated signal

$$G_{SinBOC(m,n)}(f) = \frac{1}{T_C}\left(\frac{\sin\left(\pi f \frac{T_C}{N_{BOC}}\right) \text{sin/ cos}(\pi f T_C)}{\pi f \cos\left(\pi f \frac{T_C}{N_{BOC}}\right)} \right)^2, \begin{cases} \text{"sin" if } N_{BOC} \text{ is even} \\ \text{"cos" if } N_{BOC} \text{ is odd} \end{cases} \tag{9}$$

$$G_{CosBOC(m,n)}(f) = \frac{1}{T_C}\left(\frac{\text{sin/ cos}(\pi f T_C)\left(\cos\left(\pi f \frac{T_C}{N_{BOC}}\right)-1\right)}{\pi f \cos\left(\pi f \frac{T_C}{N_{BOC}}\right)} \right)^2, \begin{cases} \text{"sin" if } N_{BOC} \text{ is even} \\ \text{"cos" if } N_{BOC} \text{ is odd} \end{cases} \tag{10}$$

2.3.3 MBOC

In 2007, the United States and the European Union announced an agreement for a common GPS-Galileo signal modulation, Multiplexed BOC (MBOC), for civilian use. MBOC introduces small amount of power on higher frequencies in order to improve the performance in tracking [44][45][46]. According to Galileo Joint Undertaking (GJU) recommendation [46], the PSD of the entire MBOC signal, denoted MBOC(6,1,1/11) is defined as:

$$G_{MBOC(6,1,1/11)}(f) = \frac{10}{11} G_{SinBOC(1,1)}(f) + \frac{1}{11} G_{SinBOC(6,1)}(f) \tag{11}$$

where $G_{SinBOC(m,n)}$ is the unit-power PSD of a sine-phased BOC modulation and 1/11 denotes the percentage of power of SinBOC(6,1) with respect to the total MBOC signal power. The MBOC PSD in Eq. (11) is the total PSD of pilot and data signals together, thus there are many possible practical ways to implement it. There are two main implementations to achieve MBOC PSD: Composite BOC (CBOC) and Time-Multiplexed (TMBOC), which are currently selected for Galileo E1 and modernized GPS L1 signals, respectively.

Composite BOC (CBOC): A possible CBOC implementation is based on the four level spreading symbols formed by sum of weighted SinBOC(1,1) and SinBOC(6,1) symbols as shown in Eq. (12) (where SinBOC(1,1) part is passed through a hold block in order to match the rate of SinBOC(6,1) part) .

$$s_{CBOC}(t) = w_1 s_{SinBOC(1,1),held}(t) \pm w_2 s_{SinBOC(6,1)}(t) \tag{12}$$

In above, when the two right-band terms are added, CBOC('+') is formed, and when the two terms are subtracted, we have the CBOC('−') implementation. CBOC('+/−') can also be used, where odd chips are CBOC('+') modulated and even chips are CBOC('−')-modulated [45]. Currently, CBOC('+') and CBOC('−') have been used for E1B data channel and E1C pilot channel in Galileo E1 signal [30]. In Eq. (12), w_1 and w_2 are amplitude weighting factors which need to be chosen in such a way that PSD is as in Eq. (11) and $w_1^2+w_2^2=1$. One possible choice is to select $w_1 = \sqrt{10/11}$ and $w_2 = \sqrt{1/11}$ if 50% of the total power is placed on the pilot channel. The example of CBOC modulated time domain waveform is presented in Figure 2.4.

Time-Multiplexed BOC (TMBOC): In TMBOC modulation, the whole signal is divided into blocks of N code chips and M of N code chips ($M<N$) are SinBOC(1,1) modulated, while $N - M$ code chips are SinBOC(6,1) modulated. The choice of N and M parameters depends on the power percentage of pilot channels with respect to the data channel [44]. An example of TMBOC modulated time domain waveform is shown in Figure 2.4 with N=5 and M=4.

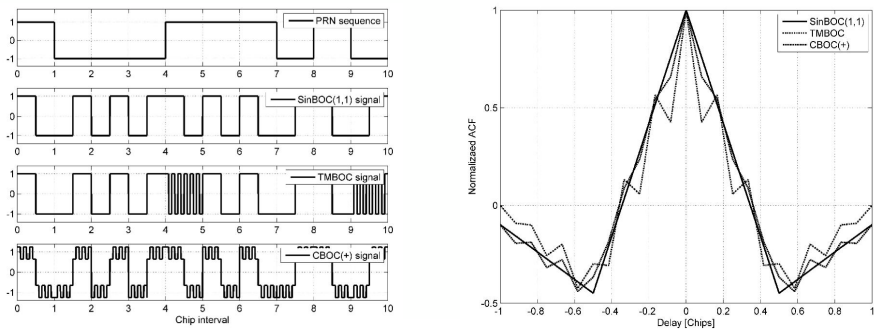

Figure 2.4: Waveforms for SinBOC, TMBOC and CBOC modulated signals (left) and their normalized ACFs for single path channel, no noise, infinite bandwidth (right).

Figure 2.4 also presents the normalized Autocorrelation Function (ACF) of SinBOC, CBOC and TMBOC with infinite receiver bandwidth. It can be observed that the main peak of TMBOC is narrower than other BOC modulations. The shape of the ACF will affect the tracking performance [47].

2.3.4 AltBOC

The Galileo E5 signal employs a special modulation known as constant envelope Alternative BOC (AltBOC) modulation. The sub-carrier waveforms are chosen so as to obtain a constant envelop at the transmitter. The result of this AltBOC modulation is a split spectrum around the center frequency as shown in Figure 2.5. Each sideband comprises two PRN codes modulated onto the orthogonal components. The in-phase components E5aI and E5bI carry the navigation messages. The quadrature components E5aQ and E5bQ are data-free pilot signals. The Galileo E5 transmitted signal can be represented as [48]:

$$S_{E5}(t) = \mathcal{R}\left[s_{E5}(t) e^{j(\omega_{E5} t + \phi_0)} \right] \tag{13}$$

where $s_{E5}(t)$ is the baseband signal, ω_{E5} is the angular E5 carrier frequency, ϕ_0 is the phase at $t = 0$ and $\mathcal{R}$ denotes the real functions.

As shown in [49], the expression of the constant envelope AltBOC modulation PSD can be presented as:

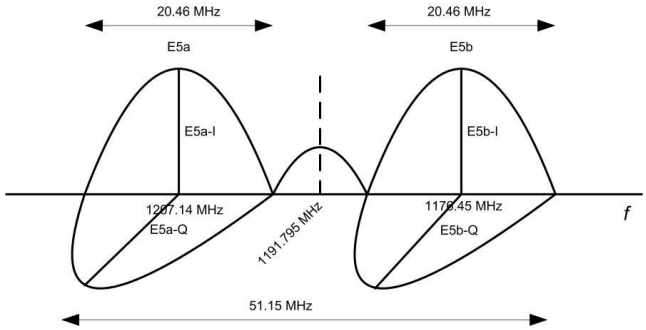

Figure 2.5: Galileo E5 signal spectrum [48]

$$G_{AltBOC(m,n)}(f) = \frac{4}{\pi^2 f^2 T_C} \frac{\cos^2(\pi f T_C)}{\cos^2\left(\pi f \frac{T_C}{N}\right)} \left[\begin{array}{l} \cos^2\left(\pi f \frac{T_S}{2}\right) - \cos\left(\pi f \frac{T_S}{2}\right) \\ -2\cos\left(\pi f \frac{T_S}{2}\right)\cos\left(\pi f \frac{T_S}{4}\right) + 2 \end{array} \right] \tag{14}$$

where m defines the sub-carrier rate and n defines the spreading code rate; The ratio $N = 2f_S / f_C = 2m/n$ is the number of half period of the sub-carrier during on code chip. $T_S = 1/f_S$, where $f_S = m \cdot 1.023$ MHz and $f_C = n \cdot 1.023$ MHz. This ratio can be odd or even [49][50].

The constant envelope AltBOC modulation has many advantages to the users and gives flexibility to receiver manufactures to choose between different receiver designs [50] and the performance of these different configurations can be found in [51][52][53].

- Tracking only E5a or E5b for a simple receiver.
- Tracking both E5a and E5b independently. This also provides dual frequency measurements, spectral isolation and frequency diversity against interference.
- Tracking the main lobe with BOC(15,10), which allows a high precision tracking while limiting the susceptibility to interference.
- Using BOC(15,10) in an extra wide bandwidth for very high accuracy receivers.

2.3.5 CDBOC

A new class of BOC modulation, namely the Complex Double-BOC (CDBOC) modulation has been introduced in [54]. This modulation generalizes the main modulation types used in GPS and Galileo under a single, unified formula, and allows extra-flexibility in design of the suitable spectral shaping for future GNSS signals. A CDBOC waveform can be defined as:

$$s_{CDBOC(N_1,N_2,N_3,N_4,f_C)}(t) = x_1(t) \otimes p_{T_{B_{12}}}(t) \otimes \sum_{i=0}^{N_1-1}\sum_{k=0}^{N_2-1}(-1)^{i+k}\,\delta\left(t - iT_{B_1} - kT_{B_{12}}\right) + jx_2(t) \otimes p_{T_{B_{12}}}(t) \otimes \sum_{l=0}^{N_3-1}\sum_{m=0}^{N_4-1}\sum_{p=0}^{P_{res}-1}(-1)^{l+m}\,\delta\left(t - lT_{B_3} - mT_{B_{34}} - pT_{B_{12}}\right) \quad (15)$$

Above, N_1, N_2, N_3 and N_4 are four positive integer numbers, satisfying the condition that N_3N_4 is a divisor of N_1N_2 (i.e., $N_1N_2/(N_3N_4) \triangleq P_{res} \in \mathbb{N}$); $T_{B_i} = T_C/N_i$ and $T_{B_{ij}} = T_C/(N_iN_j)$; $x_1(t)$ and $x_2(t)$ are the modulating signals. As summarized in [54], most of the modulations proposed so far for GPS and Galileo signals, namely BPSK, SinBOC, CosBOC, QPSK and AltBOC are only particular cases of the CDBOC modulation as shown Table 2.1 [54].

Table 2.1: Relationship of CDBOC-modulation family with GPS/Galileo modulation types

N_1	N_2	N_3	N_4	$x_i(t)$, i = 1, 2	Modulation type
1	1	–	–	$x_1(t)$ = binary complex signal $x_2(t)$ = 0	BPSK
>1	1	–	–	$x_1(t)$ = binary complex signal $x_2(t)$ = 0	SinBOC((aN_1/2), a), a>0 [e.g. a=1, N_1=2 → SinBOC(1, 1)]
>1	2	–	–	$x_1(t)$ = binary complex signal $x_2(t)$ = 0	CosBOC((aN_1/2), a), a>0 [e.g. a=2.5, N_1=12 →CosBOC(15, 2.5)]
>1	2	N_3= N_1	1	$x_1(t)$, $x_2(t)$ distinct signals	Non-constant envelope AltBOC((aN_1/2), a), a>0 [e.g. a=10, N_1=3 → AltBOC(15, 10)]

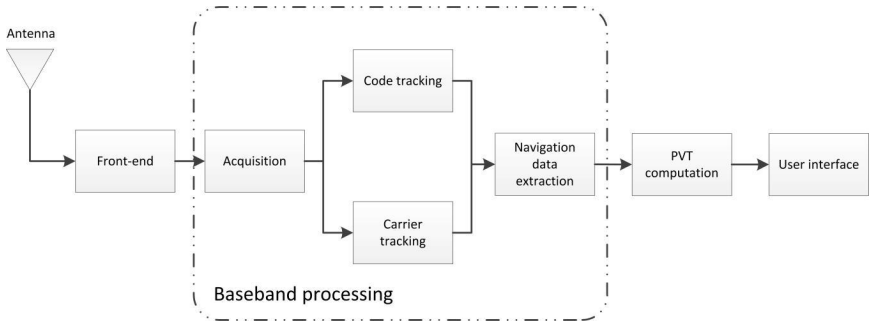

Figure 2.6: Diagram of a typical GNSS receiver

2.4 Fundamentals of GNSS receiver operation

GNSS receiver is a radio navigation device that aims at tracking the GNSS signals, in order to correctly extract navigation message information and calculate the user's position. In order to hold a deeper understanding on how the user's position is computed, the fundamental operations of a GNSS receiver need to be described.

Figure 2.6 shows the diagram of a typical GNSS receiver structure. The signals transmitted from the satellites are first received by the receiver's antenna. Through the front-end, the input signal is amplified and down-converted to a desired frequency. The signal will be further digitized for baseband processing. In the baseband processing, which is the main focus of this thesis, the presence of the signal is detected by an acquisition method. Once the signal is detected, the necessary parameters must be obtained and passed to the tracking process. The tracking task is to follow continuously the code and carrier parameters of the incoming signal in order to accurately extract the navigation data. Afterwards, the navigation unit provides the complete navigation solution, which is composed of position, velocity, and time (PVT solution). The final data are passed to the interface for application specific purpose [55].

2.4.1 Receiver front-end

A GNSS signal is captured through the receiver's antenna and is fed to the front-end section. The front-end is responsible for constructing the received signals for signal processing. Figure 2.7 illustrates a typical front-end structure in GNSS receivers. The GNSS antennas employ Right-Hand Circularly Polarization (RHCP). The main motivation for choosing RHCP is that GNSS antenna could provide a significant level of suppression

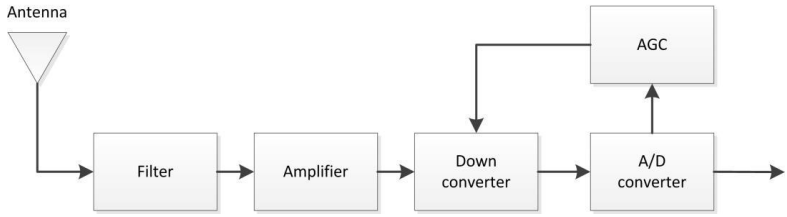

Figure 2.7: Typical GNSS receiver front-end structure

from erroneous multipath reflection [35]. The preferred antenna pattern is hemispherical since the satellites are over head for most applications. The RF chain in the front-end includes several signal processing operations, such as amplification, filtering, down-conversion, Automatic Gain Control and Analog-to-Digital conversion (ADC). The functionality of each component is well-documented in literature, for example, in [16][19][35][55].

In general, the receiver designs aim to minimize the cost and the complexity of the front-end section. It is expected to convert the signal to digital form as soon as possible, because the digital components are not influenced by temperature or humidity and the digital components can be reprogrammable if the design is changed. In contrast, the analog components change character with the environment and may require individual tuning, which can significantly increase the cost. Moreover, it has to be replaced if the design change is desired. [16]

2.4.2 Signal acquisition

After the incoming signal has been digitalized, a series of baseband signal processing will be conducted, among which signal acquisition is the first one. The purpose of acquisition is to determine all the satellites visible to user and to estimate the coarse values of carrier frequency and code phase of the satellite signal. In other words, acquisition is a three-dimensional search process, where the satellite code number, code delay and frequency need to be estimated.

It is known that in CDMA-based GNSS, each satellite transmits a unique PRN code. The presence of satellite signals is found through correlation between the incoming signal and each satellite PRN code. A high enough correlation peak with a certain PRN will indicate the visibility of the corresponding satellite. The coarse frequency and code delay then can be estimated. In order to determine the code delay and frequency, a search space needs to be defined. The search space must cover the full range of uncertain code delay and

frequency. The code search space is usually equal to the length of spreading code, for example, 1023 chips for GPS C/A signal and 4092 chips for Galileo E1 signal. The resolution of the code delay search (code bin) can be a fraction of one chip or a number of samples specified by the sampling frequency in the receiver. The frequency of the received signal from a specific satellite can differ from its nominal value. The relative motion of the satellite and receiver causes a Doppler effect. The frequency search range must take the Doppler shift into account. In the case of the receiver moving toward the satellite at a high speed, the Doppler frequency shift is around ±5 kHz. Therefore, in a GNSS receiver design, the search frequency range can be assumed as the nominal frequency plus a maximum Doppler shift ±5 kHz [55]. The frequency resolution (frequency bin) is determined by the coherent integration time defined in the receiver. According to [19], the rule of thumb is: $\Delta f = 2/(3T_{coh})$, where Δf is frequency search resolution in Hertz and T_{coh} is the coherent integration time in second.

A single code bin and a frequency bin compose a search bin. The whole code delay and frequency search space consists of thousands of search bins and can be divided into several search windows depending on the search techniques. Several search techniques have been proposed in literature in order to obtain a faster and a more efficient signal acquisition, for example in [40] [56]. These search techniques can be classified in three major categories as serial search, parallel search and combined serial/parallel search.

The ***serial search*** is based on the multiplication between incoming signal and each search bin. The search window consists of only one search bin. Hence, all the search bins are examined one by one in a serial manner. The serial search technique has quite straightforward implementation. However, due to its searching manner, the acquisition time is too long to meet today's user requirements.

The ***parallel search*** parallelizes the search for one parameter. Typically, Fourier transform is utilized to perform a transformation from time into frequency domain, which allows to parallelize the search in the frequency space [35][57]. Such design significantly reduces the acquisition time, nonetheless, at the expense of higher power consumption [58]. Towards the end of 1990's, consumer receivers employing parallel correlator banks became available and nowadays, it is a commonly used approach.

The ***hybrid search*** is the combination of serial search and parallel search in order to achieve a better trade-off in the acquisition time and complexity.

After the search stage is finished, a grid of correlation values at different code delay and frequency combinations is built. If the correlation value at certain search bin exceeds a predefined threshold, the satellite signal is present and the frequency and code delay associated with this search bin are found, and they can be passed to the tracking stage.

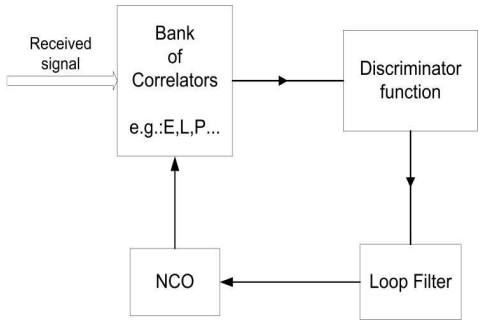

Figure 2.8: Generic block diagram of a code tracking loop

2.4.3 Signal tracking

In order to obtain the navigation messages, the receiver needs to perfectly align the replica with the incoming signal. The main purpose of tracking is to refine the coarse values of code phase and frequency phase estimations and to keep track of these as the signal properties change over time. The tracking is conducted with code tracking, carrier frequency and carrier frequency phase tracking. These three tracking functions work together in an interactive process, aiding each other. The accuracy of the final value at tracking stage output is connected with the accuracy of unknown distance between the satellite and a receiver (also known as pseudorange) computed later on.

Code tracking

The general idea of code tracking is to estimate the delay of the received signal as accurately as possible. This is done by generating a replica of the PRN code that transmitted by the satellite being acquired by the receiver. Then the receiver must shift the phase of the replica codes until it reaches the maximum correlation with the incoming signal. After the alignment is accomplished, the PRN code is removed from the signal, leaving the carrier modulated by the navigation message [16]. One common structure used in GNSS receiver for code tracking is based on a feedback loop, namely delay lock loop (DLL) as shown in Figure 2.8. Among the DLL varieties that exist in the literature, the Early-minus-Late (EML) structure is the most popular one. In this structure, we have three correlators: one Early (E), one Prompt (P) and one Late (L) correlator. The E and L correlators are nominally generated with a spacing of ±0.5 chip with respect to the P correlator. The incoming signal is correlated with each of these correlators. The correlation

outputs are then used in the discriminator function in order to detect the code phase difference between the incoming signal and replica code. The output of the discriminator function is fed into the Numerically Controlled Oscillator (NCO) in order to generate a precise replica code. Before feeding the output of a discriminator into the NCO, it passes through a loop filter, which is used to reduce the noise in order to produce an accurate estimate for an original signal at its output.

Carrier tracking

Another important processing in the signal tracking is to refine the estimation of Doppler frequency and carrier phase. Like the DLL, the carrier tracking can be implemented by a feedback loop, which is characterized by pre-detection integrators, the carrier loop discriminators and carrier loop filters. The carrier loop discriminator defines the type of the tracking loop as a phase lock loop (PLL) or a frequency lock loop (FLL). The PLL discriminator produces phase error estimation at its output. A commonly used PLL is known as Costas loop [59], which is insensitive to the phase transitions due to navigation bits. The FLL discriminator produces a frequency error estimate by replicating the approximate frequency [19]. The objective of the loop filter is to filter the discriminator output in order to reduce noise. The FLL and PLL can be used together as a FLL-assisted PLL loop to achieve better carrier tracking.

2.4.4 Navigation data extraction

The last task performed in the baseband processing is to extract the navigation data bits, from which the beginning of the subframe must be found in order to find the time when the data was transmitted from the satellites. Since the bit rate of navigation data is different than the sample rate at the output from the tracking loop, the bit transition time must be found before decoding the navigation data bits. When the bit transition times are located, the data bit sequence can be extracted. This procedure is called bit synchronization. When the GNSS navigation bits have been obtained from the bit synchronization, the ephemeris data for the satellite must be decoded. This is used later on to compute the position of the satellite at the time of transmission [35].

2.4.5 User location computation

Before making position computation, the pseudoranges, i.e., the true satellite-receiver ranges are first estimated as the multiplication of transmission time from the satellites to the receiver by the speed of the signal (e.g., the speed of light). The user's position is computed from pseudoranges and the satellite positions obtained from ephemeris data. In many

position applications, it is often desired to know the position of user U in terms of latitude (x_u), longitude (y_u) and altitude (z_u). With the computed pseudorange and satellite position, we can build the following system of non-linear equations:

$$\begin{cases} \rho_1 = \sqrt{(x_1 - x_u)^2 + (y_1 - y_u)^2 + (z_1 - z_u)^2} + c\delta_t + \mathcal{E}_{all\_1} \\ \rho_2 = \sqrt{(x_2 - x_u)^2 + (y_2 - y_u)^2 + (z_2 - z_u)^2} + c\delta_t + \mathcal{E}_{all\_2} \\ \rho_3 = \sqrt{(x_3 - x_u)^2 + (y_3 - y_u)^2 + (z_3 - z_u)^2} + c\delta_t + \mathcal{E}_{all\_3} \\ \rho_4 = \sqrt{(x_4 - x_u)^2 + (y_4 - y_u)^2 + (z_4 - z_u)^2} + c\delta_t + \mathcal{E}_{all\_4} \end{cases} \quad (16)$$

where ρ_j is the measured pseudorange between receiver and j^{th} satellite, whose position in three dimension is x_j, y_j and z_j; x_u, y_u and z_u are the unknown user location, c is the speed of light, δ_t refer to the clock bias between the satellite and receiver and $\mathcal{E}_{all\_k}$ refers to the errors that contaminate the received signal k. Assuming that the satellite and receiver clocks are synchronized and that there are no other errors, it is possible to solve above equations with the help of linear algebra [19].

2.5 Error sources in GNSS

In ideal conditions, a GNSS receiver can accurately estimate the user's position. However, in reality, there are various error sources that affect the positioning accuracy and receiver's performance. These errors in the satellite navigation system can be split into three categories, depending on where they take place: space segment related errors, propagation channel errors and receiver-related errors.

2.5.1 Space segment related errors

The satellites contain atomic clocks that control all onboard timing operations, including broadcast signal generation. Although these clocks are highly stable, the time deviation can be up to 1 millisecond (ms) from GPS system time. An offset of 1 ms translates to an 300 km pseudorange error. It is expected that the clock error will decrease when the newer satellites with better performing clocks are launched [60].

Another space segment-related error is ephemeris error. The ephemeris error is usually decomposed into components along three orthogonal directions defined relative to the satellite orbit: radial, along-track and cross track [16]. Among these components in the ephemeris error, the radial component tends to be the smallest one. The error in a

pseudorange measurement is the projection of the satellite position error vector on the satellite-receiver line-of-sight, which depends mostly on the radial component of the ephemeris error. The other two components along the line-of-sight are small [16].

2.5.2 Propagation channel errors

The GNSS signals are affected by the medium through which they travel from the satellites to a receiver. There is a variety of error sources associated with the propagation environment. More precisely, the main error sources are: 1) ionosphere, 2) troposphere, 3) multipath and 4) interference.

Ionosphere

The ionosphere is a dispersive medium located in the region of the atmosphere between about 70 km and 1000 km above the Earth's surface. Within this region, ultra rays from the sun ionize a portion of gas molecules and release free electrons. The corresponding amount of free electrons depends on the latitude of the observation points and on the activity of the Sun. Furthermore, the time of the year, seasons, and time of the day also have high impact on the density of these ionized particles. These free electrons have direct influence on electromagnetic wave propagation delay, including the GNSS satellite signals broadcasts.

The first-order ionosphere delay accounts for about 99% of ionosphere delay and is proportional to the amount of the free electrons and inversely proportional to the square of frequency. More precisely, it is defined as [61]

$$I_i = \frac{40.3}{f_i^2} TEC \tag{17}$$

where TEC is the total electron content measured in the TEC Unites (TECUs) with 1 TECU=10^{16} electrons/m^2 and f_i is the i-th frequency. Eq. (17) is effective for only narrowband signals, such as E1 or L1 signal. As the frequency range gets wider, the ionosphere variation within the band is larger. For example, the ionosphere effect on Galileo E5 signal is much bigger than that on Galileo E1 signal since Galileo E5 signal has lower carrier frequency and much wider bandwidth [62].

As it was mentioned earlier, typical TEC value varies according to the time and the location. A typical TEC range at GNSS frequency (1100 MHz − 1600 MHz) at mid-latitude daytime is 1−100 TECU. During the night time, typical TEC values are between 0 and 30. In low latitudes and during a solar max, TEC can be up to 200 TECU [V] [63]. As shown in [57], the ionosphere delay induced into the Galileo E1 signal at night time can be low as

few centimeters, but in the day time the ionosphere delay would be in the range of 10 – 40 meters depending on the latitude and the solar activity.

Troposphere

The troposphere is the lower part of the atmosphere that is non-dispersive for frequencies up to 15 GHz [64]. Therefore, the troposphere is frequency independent for GNSS signals. The effect of the troposphere on the GNSS signals appears as an extra delay in the time measurement of the signal traveling from the satellites to a receiver. This delay depends on the local temperature, pressure and relative humidity. Due to the non-dispersive property, the carrier phase and code measurement are affected by the same delay.

The troposphere consists of a hydrostatic part (i.e., dry gases, mainly N_2 and O_2) and a wet part (i.e., wet vapor), causing the GNSS signals to be refracted [16]. The delay caused by the hydrostatic part varies with local temperature and atmosphere pressure and is about 90% of the magnitude of the troposphere delay. It can be easily estimated based on the user latitude, altitude and season. On the other hand, the wet component, which consists of water vapor and condensed water in form of clouds, is very difficult to model since it varies with local weather and can change rapidly.

Multipath

Multipath is considered as one of the dominant sources of ranging errors in GNSS. It is caused by, i.e., reflection, scattering, refraction, shadowing, diffraction off the surrounding objects, such as buildings and walls (see the left plot in Figure 2.9). Since the path travelled by reflection is always longer than the direct path, multipath signal arrives later with respect to the direct path. Then the receivers receive multiple copies of the desired signal. When the multipath delay is large, the receiver can readily resolve the multipath as long as the receiver tracks the direct path [19]. However, in the urban area, the multipath reflection from nearby objects can arrive at short delays after the arrival of the direct path. Such multipath distorts the correlation function between the received composite signal and local replica as shown in the right plot in Figure 2.9 where a direct line-of-sight (LOS) signal is added constructively with an in-phase delayed and an attenuated version of it to form a compound signal. The distorted correlation introduces error in pseudorange and carrier phase measurement. The shadowing attenuates the direct path signal, introduced typically when the direct path propagates through foliage or a structure, as shown in the left plot in Figure 2.9. In some cases, the multipath which does not suffer from the same attenuation may be even stronger than the direct path. The shadowing of the direct path may be so severe that the receiver can only track the multipath signals. The characteristics of multipath signals, besides their delays, also depend on power and phase relative to the direct path. Multipath with much lower power level than that with the direct path has little distortion on the direct path and consequently produces little error. The phase of multipath

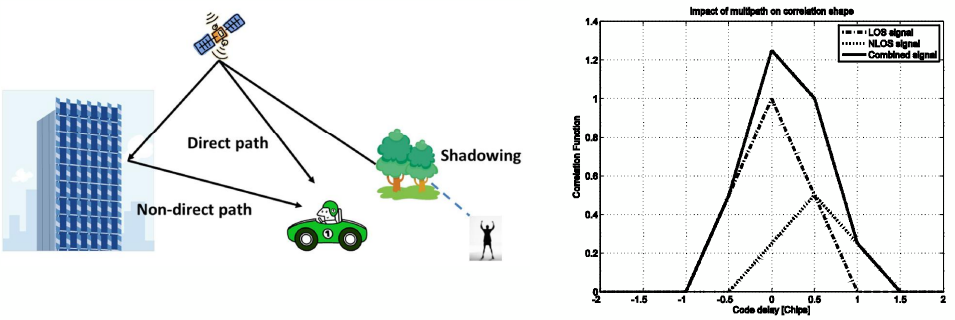

Figure 2.9: Left: Multipath propagation example; Right: Received correlation function in two-path static channel model; path delay [0 0.5] chips, path amplitude: [0 -3] dB, in phase combination.

also has direct influence on the degree and character of the correlation function distortion [19].

Interference

Besides the multipath, an important error that degrades the GNSS signal is interference. Interference can be defined as "disturbances that affect an electrical circuit due to either electromagnetic conduction or electromagnetic radiation emitted from an external source" [65]. In GNSS, the most common source of interference is radio-frequency interference (RFI), which is presented as extra electromagnetic signals in the radio link frequencies or in the adjacent spectrum. The GNSS deployed Direct-Sequence CDMA (DS-CDMA) technique has high processing gain, which offers protection against low power RFI. The moderate and high power interference, which makes the Signal-to-Noise-and-interference-Ratio (SNIR) in the receiver is very low, can easily degrade the receiver's performance or even completely block the GNSS service [66]. Furthermore, the planned deployment of a 4G network from LightSquared, now brought to an end, could have created a new interference situation especially when using 1552.7 MHz band [67].

Considering the spectral characteristics, the interferences can be classified in:

- Narrowband interference, which has a limited fraction of the bandwidth. The potential narrowband interferences are the spurious emissions and out-of-band emission of many broadcast and communication services, such as mobile stations, broadcast television and fixed Very High Frequency (VHF) and Ultra High Frequency (UHF) transmitters [19]. The effect of partial-band and narrowband interference on GPS are reported in [68][69] and in [I] for Galileo E1 signal.

- Wideband interference, which contains energy on the whole radio link bandwidth. Potential sources include Ultra-wide Band (UWB) transmission, see e.g., [70][71][72], inter-system interferences between GNSS systems and intra-system interference between signals of in the same system sharing the same bands, see e.g. [73][74].

If the interference signal is designed to degrade the performance of GNSS receiver, it is called intentional interference. According to the American Volpe National Transportation System Center, the intentional interference can be classified as follows [75]:

- Jamming, where a high-power interference signal is transmitted, causing the receiver not to be able to detect the navigation signal.
- Spoofing, is intended to produce a false position within the receiver through the broadcast of false GNSS signals.
- Meaconing, which is the interception and rebroadcasting of navigation signals in order to confuse navigation and timing.

2.5.3 Receiver-related errors

The accuracy and stability of the receiver clock is not as good as the atomic clocks on the satellites, due to the size and price. The time difference between the receiver and satellite can cause very large errors in the pseudorange computation. As shown in Eq. (16), if the clock in the receiver and satellites are well synchronized, the user position can be calculated by solving three non-linear equations. However, in the reality, the time difference introduces another temporal parameter that needs to be taken into account in the measured pseudorange. In other words, in order to estimate the receiver's position in three dimensions, we actually need four satellites as shown in Eq. (16).

Measurement errors are also induced by the receiver tracking loops. In a typical modern receiver, receiver noise and resolution error made by the DLL are relatively small and negligible in comparison with the errors induced by multipath. PLL also introduces errors, which affect carrier phase measurement. The PLL measurement errors are on the order of millimeters in nominal conditions. User equipment bias errors are introduced by the receiver hardware, such as delay induced by hardware, hardware-induced multipath [76]. These errors can be removed or reduced by calibration or careful design of the receiver front-end.

3 Indoor positioning systems

In the outdoor environment where multipath is low and sufficient number of satellites is available, the satellite-based positioning systems are able to provide autonomous geo-spatial positions with worldwide coverage. However, in urban and indoor environments, various obstacles, such as for example, walls, human beings and various other obstacles lead to multipath effects and the satellite signals lose significant power. As a consequence, the satellite signals become nearly undetectable in such environments. Due to the greater mobility, a significant need for localization has emerged and technical solutions for indoor positioning are needed, not only for automotive applications, but also for personal purpose. In general, there are two directions that can be taken. The first direction relies on increasing the sensitivity of the GNSS receiver without adding any extra electronics to achieve the indoor positioning function. The second one is to implement a different technique or a hybridization of different techniques indoors. Then the final system will consist of the integration of GNSS for outdoors and this newly developed one for indoors, which is also the core concept of multi-mode multi-frequency receivers [77].

These two trends have been utilized in various wireless indoor positioning systems and have become very popular in the last decade. These wireless indoor positioning systems can be used in many applications, such as medical care, social networking, firefighting and intelligent transportation. At the highest level, all technologies for indoor positioning can be divided into three main groups employing different physical principles: electromagnetic waves (i.e., microwave, radio wave); mechanical waves (i.e., ultra sound) and inertial navigation (accelerometers and gyroscopes) [78]. In this chapter, we describe the basic measuring principles and positioning methods used in the indoor positioning technologies. Various indoor positioning technologies are reviewed. In the end, the challenges in indoor positioning are discussed.

3.1 Basic measuring principles

The following basic measuring principles are common techniques for distance and angular observations.

TOA/TDOA

The principle of Time of Arrival (TOA) is based on measuring the absolute travel time of a signal between the transmitter and the receiver. The distance between a transmitter and a receiver can be derived by the multiplication of the signal travel time by the wave speed (i.e., the speed of light). This is also the principle used in GNSS. TOA relies on precise time synchronization of two devices [79]. For example, one nanosecond (10^{-9} s) time error in synchronization translates into a distance error of 30 cm if radio frequency is used (10^{-9} s $\times$*speed of light* = 30 cm). Moreover, severe and complex indoor multipath leads to inaccurate estimates of the TOA [80].

Time Difference of Arrival (TDOA) measures the time difference of signal arrival at the same receiver from two transmitters. TDOA has the advantage that a possible receiver clock bias can be ignored. Any constant clock bias in a receiver is eliminated by subtraction. With two transmitters at known locations, the position of a receiver can be located onto a hyperboloid. With three or more transmitters, the position of a receiver can be determined by the intersection of two or more hyperboloids.

AOA

Angle of Arrival (AOA) measures the angles of arriving signals with the receiver antenna. One common approach to obtain AOA measurement is to use an antenna array or antenna beamforming. It has the advantage that only few measurements are needed and high precision can be achieved. This method requires high antenna complexity, leading to quite expensive solutions. The AOA measurement is also sensitive to multipath and shadowing since it depends on the antenna radiation patterns [81].

POA

Phase of Arrival (POA) uses the received carrier phase to determine the distance between transmitters and a receiver, which is the same as the carrier phase synchronization used in GNSS. It requires that the transmitters are placed at particular locations and they emit pure sinusoidal signals [82]. In order to mitigate phase wrapping, the received signal phase is evaluated on multiple frequencies. The distance is then determined by the rate of phase changes. The disadvantage of POA measurement is that a Line-of Sight signal path is necessary to limit localization errors [79].

RSSI

Received Signal Strength Indicator (RSSI) shows the Received Signal Strength (RSS) averaged over a certain sampling period [83]. This received power can be used to estimate the distance of a mobile unit with the help of propagation modeling, because the RSS is a function of the propagation distance. For example, the free space propagation model is based on a RSS signal variation inversely proportional to the square of travelling distance.

Theoretically, the estimated distances to multiple beacons can be used to determine the receiver position by multilateration.

3.2 General positioning methods

Cell of Origin

The Cell of Origin (COO) is used to determine the position of a mobile device by its presence in a particular area or based on a physical phenomenon with limited range [78]. This method is used mainly for positioning in cellular networks. It uses the cell area in which the mobile device is registered to identify the corresponding Base Station (BS) in GSM cellular network or Node B in Universal Mobile Telecommunications System (UMTS) network. This method is also known as Cell ID based method. The location of the mobile device can be calculated by known properties, such as signal strength. COO is a very simple positioning technology and its accuracy is dependent on the cell size.

Trilateration/multilateration

Similar to the trilateration method used in GNSS, trilateration/multilateration can be used to determine the position from distance measurements no matter what distance estimation method has been used (for example distance estimation based on TOA, TDOA, AOA or RSS). With the measured distances, circles are drawn around each transmitter with the radius equal to the measured distance. The device is at the position where the circles from each transmitter coincide. With three transmitters, the technique is called trilateration. With more than three transmitters, it is called multilateration. With perfect distance measurements, this method will give an exact, unique answer, i.e., a single point at the intersection of the circles as shown in Figure 3.1(a). With imperfect distance measurements, the circles will not intersect at a single point, even the circles may not intersect at all. In this situation, an estimated position is found by looking for the point that simultaneously minimizes the distance to all circles (see Figure 3.1(b)). It needs to be mentioned that this circle concept is only valid for two-dimensional positioning. If three-dimensional positioning is required, four spheres are needed to intersect at a unique valid point as in the satellite-based positioning.

Fingerprinting

In this technique, no distance measurements between a receiver and transmitters are needed. Generally, fingerprinting can be divided into two phases. First phase is the offline phase, where the data from different reference points in the coverage area is collected. The standard data for fingerprinting is RSS, but the data can also be audio or images [78]. The collected data are then stored in a database. The second phase is the positioning phase. The

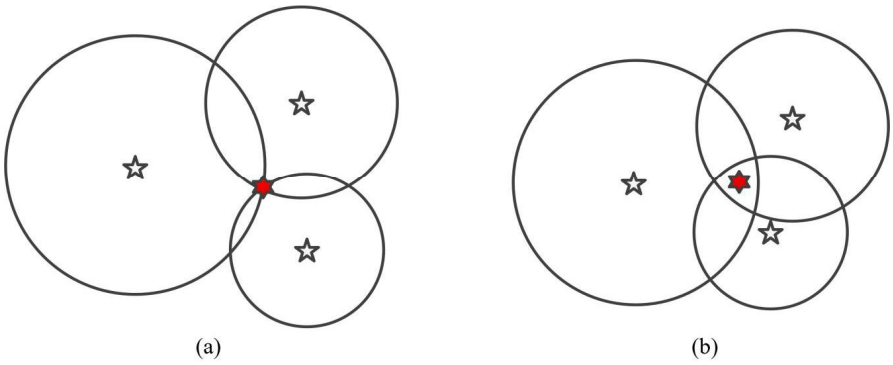

Figure 3.1: Positioning method by trilateration (a) perfect information (b) imperfect information

current RSS at the mobile device is compared with the database and the closest match is found in the database through various matching approaches, such as a nearest neighbor approach or an average over a number of nearest neighbors. The location of the mobile device can be determined as the location of the reference point with the best match. The fingerprinting position method has been widely studied in the literature, for example, in [84][85] and it is typically used in WLAN-based indoor positioning.

Path-loss probabilistic modeling

Another possible positioning method is the propagation modeling or path-loss modeling, based on RSS. Similar to fingerprint methods, this method also consists of two phases. The first phase is a data collection phase similar to the fingerprinting method. However, we do not store all the original fingerprints. Instead, a path-loss model is built based on the collected data, which connects the distance values to the RSS values. We only store a few parameters for each transmitter. Different propagation models have been introduced to model the path-loss depending on the environment and applications, for example, free space path-loss model, log-distance path-loss model, Okumura-Hata model. In this phase, the parameters in the path-loss model need to be estimated. Since the locations of transmitters are usually unknown in many environments, the location estimation of transmitters is also required. Once the path-loss model and transmitter location are estimated, the location of the mobile device can be determined using different algorithms, such as Bayesian [86] or even by recreating an own RSS database of the area based on the estimated parameters [87]. In reality, due to the interference, multipath and presence of obstacles, the RSSI values lead to a complex spatial distribution, which is unfavorable for the estimation of distance from RSSI [78]. Therefore, fingerprinting has become more popular than propagation modeling.

3.3 Overview of indoor positioning technologies

Developing indoor positioning techniques has become a very important topic. This has led to many theoretical and experimental works in this field using a large range of techniques, from purely GNSS approaches to networks of physical sensors or Wireless Local Area Networks (WLAN). In this section, several technologies, including GNSS-related or non-GNSS technologies are briefly introduced.

3.3.1 High sensitivity receiver & AGNSS

Satellite signal attenuation from walls causes a standard GNSS receiver to perform poorly in indoor environments. The weak satellite signals become nearly undetectable for the receivers. The attenuation on GNSS signal can be up to 20 – 30 dB depending on the electrical properties of building materials [88]. The propagation of GNSS signal also suffers from severe multipath and NLOS conditions [89]. To overcome these limitations, a number of advanced signal processing techniques used in GNSS receiver have been proposed in the past few years. The high signal attenuation can be overcome by the joint use of coherent correlation and non-coherent integration. This technique has given rise to the so-called high sensitivity GNSS receivers. This type of receiver processes a long period of signals. For example, the traditional GPS receiver has 1 ms coherent integration time, corresponding to one GPS C/A-code length. High sensitivity receivers usually extend this up to 20 ms, corresponding to the length of one GPS navigation data bit. By using long non-coherent integration, they can achieve high sensitivity and avoid the effect of bit transitions and clock drift [90]. The high sensitivity receivers usually make use of Assisted-GNSS (A-GNSS) for position determination in order to overcome some problems, such as impossibility to demodulate the navigation data in high attenuation conditions [89]. The wireless network provides the information, such as ephemeris, almanac, differential correction and other relevant information that are normally obtained from the GNSS satellites directly [88]. Assistance data can also be used to reduce the frequency and code-delay search space [91]. However, the performance of A-GNSS enabled high sensitivity receivers, as shown in [78], is severely degraded indoors or in poor signal conditions compared with the achievable performance level typically outdoors. Therefore, high sensitivity GNSS is not ready to be used for pedestrian navigation in most public buildings. Indeed, the location-based service (LBS) with high sensitivity GNSS alone is not ready to be utilized, but it can be combined with multi-sensor systems to provide occasional position

updates. Various high sensitivity GNSS solutions and experimental studies can be found in [92]–[94].

3.3.2 WLAN/Wi-Fi

WLAN or Wi-Fi (a trademark term meaning IEEE 802.11x standard) can be used to estimate the location of a mobile device within its network. WLAN positioning systems have become the most widespread approach for indoor positioning. The use of WLAN signals has the advantage that the WLAN access points are readily available in many indoor environments and it is possible to use standard mobile devices. Different distance measurement methods can be used in WLAN-based positioning. The most popular WLAN distance measurement is to make use of RSSI, which is easy to extract in its network. TOA and TDOA or AOA are less common in WLAN due to the complexity of time delay and angular measurement. With the new standard in WLAN, which supports multiple antenna configurations, known as Multiple-Input and Multiple-Output (MIMO), AOA can be used for distance measurement to improve the positioning accuracy [95]. Either fingerprinting or path-loss modeling can be used as positioning methods. The main challenges for WLAN RSSI-based positioning methods are high time-variability of signal strength and the complexity of modeling the signal propagation according to attenuation patterns in indoor environment. The Channel Impulse Response (CIR) obtained in WLAN system can be used for distinguishing the LOS and NLOS scenarios in order to improve the signal propagation modeling [VI]. Localization approaches using WLAN and reported performance can be found in [96]-[98].

3.3.3 Ultra-Wideband

Ultra-Wideband (UWB) is a short-range, high bandwidth radio communication system. It has the properties of strong multipath resistance and to some extent penetrability for building material, which can be favorable for indoor positioning [78]. UWB usually occupies a large frequency band (>500 MHz) or a large relative bandwidth (larger than 20% of the carrier frequency) [99]. A large bandwidth allows for high resolution in time so that a large number of multipath delay components appear in the signal and become resolvable. The ranging techniques in UWB can be either TOA or TDOA. Since achievable accuracy of TOA measurement is directly correlated to the signal bandwidth, UWB is well suited for precise ranging. One commonly used positioning method in UWB is fingerprinting. In UWB, a CIR contains large amount of information from multiple multipath components. Therefore, the CIR can be used as a unique fingerprint assigned to each location and stored in the database. In the second phase, the current CIR is compared

with the database. The location of the fingerprint with optimum correlation is returned as the current position. Therefore, UWB fingerprinting has potentially better performance than WLAN fingerprinting. The RSSI can also be used as fingerprints, but the high resolution benefit of UWB will be lost. The reason why UWB has not entered the mass market is the requirement for a dedicated transmitter-receiver infrastructure. Localization systems using UWB and their performance parameters can be found in different reports, for example, in [100]−[102].

3.3.4 Other signals of opportunity

By signals of opportunity (SOP), we mean those signals that are not originally intended for positioning but they are freely available all the time within certain range and they can be used also for navigation through proper exploitation. The signals can be transmitted from land-based or space-based transmitters, for example, Amplitude Modulation/Frequency Modulation (AM/FM) radio broadcast stations, analog/digital television broadcasting and satellite communication transmitters from the space. In urban area, SOP can provide many measurements which may potentially be used to overcome blocked signals and identify multipath signals through a Receiver Autonomous Integrity Monitoring (RAIM) technique [103] [104]. SOP usually has a much higher received signal power, possibly allowing the signals to be received and exploited indoors [105]. The exploitation of the signals is challenging. First of all, the signal transmitters are usually not synchronized, the transmit time is unknown, and the signal is not maintained by the navigational users. Secondly, due to the limited terrestrial transmitter height, the solution is more likely two-dimensional than three-dimensional. Compensation for slant ranges is required if the height difference is significant [106]. The SOP concept has become very popular in recent year and the studies on positioning with signals of opportunity have been conducted intensively in both academic and industrial fields. The exploitation and the analysis of positioning performance with different signals of opportunity can be found in literature, for example, in [107]−[111].

3.4 Open challenges

Judging from the diversity of present indoor positioning technologies, there is no overall winning solution to positioning yet and the future is likely to stay in hybrid multi-mode multi-signal solutions. Each of them faces different challenges. In the following, the various challenges of indoor positioning are discussed.

- **Accuracy:** accuracy is the most important parameter in any positioning system. Among various indoor positioning systems, most systems suffer from unstable

signal propagation due to the complex indoor environment, affecting the accuracy, for example, the severe multipath from signal reflection, high attenuation and signal scattering due to greater density of obstacles. The performance of some positioning methods, such as trilateration, is affected significantly by the NLOS propagation. Therefore, distinguishing between LOS and NLOS scenarios is very important. Moreover, it is clear that the higher the accuracy, the better the system; however, there is often a tradeoff between the accuracy and other characteristics. Some compromises between satisfactory accuracy and other characteristics are needed.

- **Complexity:** complexity of a positioning system can be attributed to hardware, software, and operation factors [88]. In order to achieve high indoor positioning accuracy, different positioning techniques could be combined into one single mobile device, which requires sophisticated implementations. Consequently, the cost of the mobile device will be increased. Therefore, developing low-cost architectures in multi-mode receivers for combining GNSS and non-GNSS techniques is necessary. Moreover, the processing power is limited in the user devices; sophisticated algorithms in the user device will cause long processing time and short battery life.
- **Scalability:** the scalability character of a system ensures the normal positioning system function when the positioning scope gets large [78]. Usually the positioning performance degrades when the distance between the transmitter and receiver increases. When a larger area is covered, wireless signal channels may become congested, more calculation may be needed to perform positioning, or more communication infrastructure may be required.
- **Other challenges:** in many indoor positioning applications, a map of the building floor plan is required. However, gathering indoor maps presents a unique challenge because it requires building maps from building owners or accurate automatic ways to build the maps based on measurements, such as simultaneous Localization and Mapping (SLAM) [112]. Many businesses would not like to provide their maps because of the privacy concern and little consumer demand. From the design and layout of building aspect, multiple floors, inconsistent Wi-Fi coverage, poor calibrated sensors, all these limit the indoor positioning performance.

4 Advanced signal processing in multi-mode multi-frequency receivers

In Chapter 2 and Chapter 3, it was shown that there are various propagation channel-related errors in both outdoor and indoor environments, such as multipath/NLOS propagation, ionosphere and interferences. These errors affect the quality of the received signal and degrade the receiver's positioning performance. In this chapter, we outline various state-of-the-art signal processing methods, which can be used in multi-mode multi-frequency receivers for mitigating these errors. In addition, we position our analysis and proposed methods in this thesis with respect to the state-of-the-art.

4.1 Multipath mitigation

Multipath propagation remains as one of the dominant error sources in GNSS. Several approaches have been implemented in the last few decades to reduce the multipath effect on a GNSS receiver. One important group of multipath mitigation techniques is based on baseband receiver processing. Some baseband processing techniques, such as [113][114], rely on prior knowledge of the correlation function of the signal. They employ advanced receiver processing methods that attempt to match the ideal correlation function to the observed correlation function in multipath. The most commonly used techniques are based on the variation of early-late processing. These variations of early-late processing are enhanced classical correlation-based code delay estimator Early-Minus-Late (EML). In the classical EML, the early-late correlators spaced at one chip and fails to cope with the multipath propagation [115][116]. A first approach to reduce the influence of multipath effects is based on the idea of narrowing the spacing between early and late correlators, i.e., nEML or Narrow Correlator [117][118][119]. The choice of the correlator spacing depends on the receiver's available front-end bandwidth along with the associated sampling frequency [120]. Correlator spacing in the range of 0.05 to 0.2 chips are commercially available for Narrow Correlator based GPS receivers [121]. Narrow Correlator has also been used as a benchmark algorithm for our studied algorithms in publications [I] − [V].

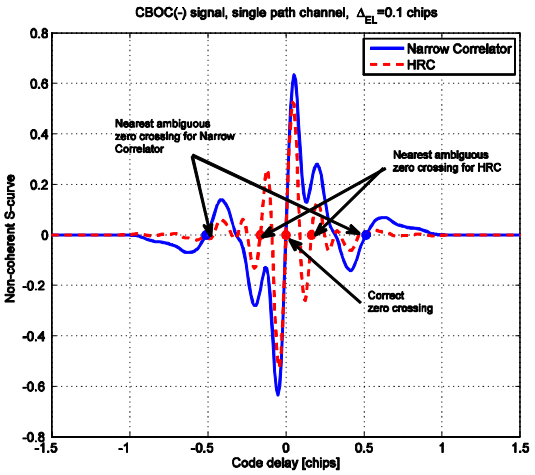

Figure 4.1: A non-coherent S-curve for CBOC('−') modulated signal in single path channel

Another early-late correlator processing based multipath mitigation approach uses five correlators in the tracking loop, i.e., Double Delta (ΔΔ) technique [122]. ΔΔ technique offers better multipath mitigation in medium-to-long delay multipath in good Carrier-to-Noise-density-Ratio (C/N_0) compared with Narrow Correlator [122]. Several well-known particular cases of ΔΔ technique are Strobe Correlator [123] and High Resolution Correlator (HRC) [124]. An example of non-coherent S-curve is shown in Figure 4.1 for a CBOC('−') modulated signal in a single-path channel. The nearest ambiguous zero crossing for HRC (around ±0.16 chips) is much closer as compared with that of Narrow Correlator (around ±0.51 chips) in this particular case. This indicates that the probability of locking to any of the side peaks is much higher for HRC than that of Narrow Correlator.

Another similar tracking structure is the Multiple Gate Delay (MGD) correlator, where the number of early and late correlators and their weighting factors can be optimized according to the signal and multipath profile as illustrated in [IV][125]. The results in [126] and [127] showed that the optimized MGD for the SinBOC(1,1) modulated signal with infinite front-end bandwidth has promising tracking performance in short delay multipath scenarios. In order to evaluate the performance of MGD for the CBOC modulated signal, which will be used in Galileo E1 signal, the author optimized the correlator spacing and weighting factor for CBOC modulated signals, taking into account the limited front-end bandwidth aspect, as described in [IV]. Meanwhile, two receiver types have also been taken into account: one using CBOC reference waveform, another one using SinBOC(1,1) reference waveform. The MGD performance was compared with Narrow Correlator and HRC method in terms of both Multipath Error Envelope (MEE) and Root Mean Square

Error (RMSE). The results reported in [IV], show that the optimized MGD gives significantly better multipath mitigation than the Narrow Correlator and HRC in short delay scenarios with wide front-end bandwidth at middle to high C/N_0. The Narrow Correlator performed the best at very low C/N_0. Based on this discovery, a C/N_0-based two-stage delay tracker has been proposed in [128], where the MGD and Narrow Correlator were used jointly according to the estimated C/N_0. In addition, most multipath mitigation algorithms in the literature are often based on optimistic channel assumptions. Therefore, this thesis includes a performance comparison of four multipath mitigation techniques, namely Narrow Correlator, HRC, Two-stage MGD and Reduced Search Space Maximum Likelihood (RSSML) for CBOC modulated signals in realistic measurement-based channel models [III].

Besides the advanced processing techniques discussed above, the multipath mitigation can also be improved with the deployment of new GNSS systems and the accompanying of available new signals. The CBOC signal structure allows the receivers to obtain high performance in terms of multipath rejection and tracking [44]. This is mainly due to a higher transition rate brought by the BOC(6,1) on top of the BOC(1,1) [129]. In addition, European Galileo system provides a unique broadband E5 signal with 51.15 MHz authorized bandwidth [30]. Processing AltBOC modulated E5 signal leads to a better tracking performance in terms of noise and multipath mitigation at the expense of a large front-end bandwidth. As the results shown in [130][131], assuming a GNSS receiver with built-in Narrow Correlator for multipath mitigation, the level of code noise of Galileo E5 is much lower than that for Galileo E1. The multipath errors for Galileo E5 are reduced by a factor of three to five. However, processing the whole E5 signal requires a large front-end

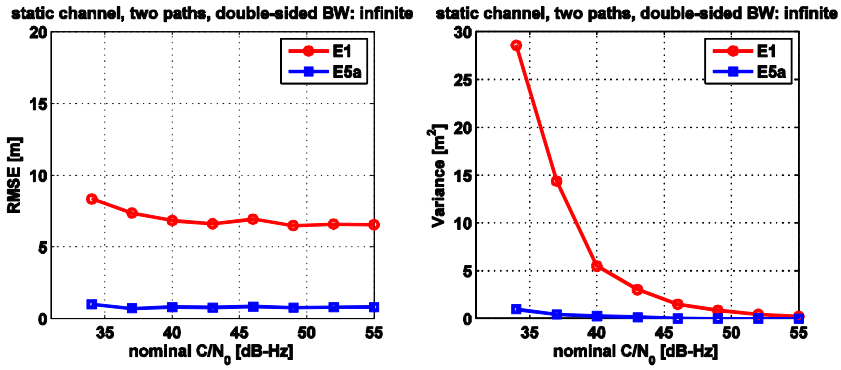

Figure 4.2: Example of code tracking RMSE and variance of E1 and E5a signal in a two-path channel profile with infinite bandwidth

filter bandwidth. Consequently, a high sampling frequency is a prerequisite, which will lead to higher power consumption. On the other hand, the E5 signal has the advantage that the E5a and E5b can be processed independently as traditional BPSK(10) signal. High chip rate in E5a and E5b signal can also improve the multipath mitigation performance in the receiver compared with processing GPS C/A or Galileo E1 signals as the results shown in [130]. As the example shown in Figure 4.2, in the same multipath channel condition, tracking E5a signal have much lower code tracking RMSE and code tracking variance compared with that of E1 signal. Furthermore, the required correlator spacing should be smaller than half of the one-side width of the autocorrelation main peak. BPSK(10) modulation provides a wider choice for correlator spacing compared with AltBOC(15,10) modulation, which could give the receiver designers more freedom on selecting the parameters for their designs [132].

4.2 NLOS identification for indoor positioning

The indoor positioning function, as an important part in the multi-mode multi-frequency receiver has also suffered from the NLOS propagation. The NLOS propagation introduces positive biases in the distance estimation, seriously affecting the positioning performance for those algorithms based on distance measures, such as trilateration and probabilistic models [133]. Therefore, it is critical to identify the NLOS conditions in positioning system and to develop techniques that mitigate their effects.

One approach to identify NLOS is to use measurement metrics, such as RSS or TOA estimations [134][135]. This type of technique is simple and offers low-complexity solution. The accuracy might be low, but it can be robust in isolating the really bad channel conditions. Technically, the identification can be achieved by comparing the variance of RSS or TOA against a threshold resulting in a simple hypothesis test [136]. It is also possible to combine the information from RSS and TOA estimation to improve NLOS identification as introduced in [137]. An alternative NLOS identification based on evaluating the envelope of the received signal has been proposed in [138]. The basic idea behind this technique is to distinguish the envelope of the received signal in LOS and NLOS environments, as if there is a LOS path, the power envelope will have a Ricean distribution and otherwise it will have Rayleigh distribution.

Another category of NLOS identification techniques is based on the channel statistics, because the statistics of the received multipath components such as amplitude, mean, excess and root mean square (RMS) delay can be easily exploited. The typical metrics can be used are: the ratio of the First Path Power (FPP) to the total power, the RMSE delay spread or kurtosis. The channel condition can be indicated by the ratio of the FPP to the total power technique. The results shown in [139] highlight the capability of this method on

distinguishing the LOS and NLOS conditions. This technique is simple but requires estimating the power of the first arriving path, which requires channel estimation. A better technique is based on the Root Mean Square (RMS) delay spread as proposed in [140]. Similar to the techniques based on RSS/TOA, the identification in this method is based on comparing the RMS delay spread with a suitable threshold that provides a desired probability of correct detection. The different channel conditions can also be characterized by the kurtosis metric. The results presented in [140] showed that the kurtosis outperformed the mean excess delay and RMS delay spread. The kurtosis characterizes the peakedness of the data samples. For example, the data samples with high kurtosis tend to have a distinct peak near the mean, while data sets with low kurtosis tend to have a flat top near the mean rather than a sharp peak. Kurtosis can be defined as the ratio of the fourth order moment of the data to the square of the second-order moment as shown in Eq. (18).

$$\kappa = \frac{E\left[\left(X-\mu_X\right)^4\right]}{E\left[\left(X-\mu_X\right)^2\right]^2} = \frac{E\left[\left(X-\mu_X\right)^4\right]}{\sigma_X^4} \tag{18}$$

where X is the random variable under evaluation, μ_X and σ_X are the mean and the standard deviation of X, respectively. Figure 4.3 shows an example of CIR in LOS and NLOS conditions. As we can see, the CIR in NLOS condition has longer delay and more multipath components compared with that in LOS condition. Thus, the kurtosis metric can be used to

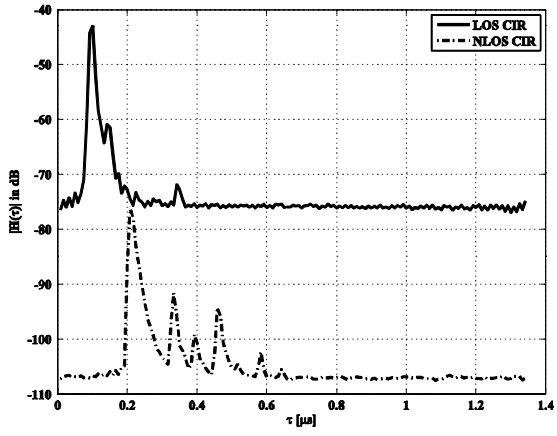

Figure 4.3: Example of channel impulse response in LOS and NLOS conditions

identify LOS channel since the CIR are peakier with respect to a flat NLOS CIR. The advantage of kurtosis is that it is calculated directly on the received signal, no estimation algorithm is needed. This keeps the identification process easy and quick and it implies that no estimation errors of the estimation algorithm are introduced [141].

In [140] and [142], the CIR amplitude has been taken as the data samples for kurtosis calculation in UWB system. However, the kurtosis shows high sensitivity to the system parameters, such as bandwidth as reported in [VI] and the performance of kurtosis-based NLOS identification in other systems is still unknown. Motivated by this, the author has proposed to use a different form of CIR for kurtosis calculation in [VI]. By using the logarithm of CIR amplitude, which is supported by the often assumed lognormal of CIR amplitude fading, the kurtosis value is less sensitive to the system parameters and shows more consistent and clearer separation for LOS and NLOS conditions. In [VI], the author also compared the proposed kurtosis-based identification in both Single Input Single Output (SISO) channels and MIMO channels in WLAN system. The results show that if multi-antennas are available, the average kurtosis, which is averaged over all the kurtosis values of all the antenna pairs gives even better indication of LOS/NLOS condition than that in SISO channel.

4.3 Interference analysis

Among all the different error sources that can potentially corrupt satellite navigation waveforms, the interference is particularly harmful since, in some cases, it cannot be mitigated by a simple correlation process. In the recent years, many efforts have been made on developing interference mitigation techniques for positioning systems. One of the most powerful technologies against radio interference is the multi-element antenna arrays with adaptive beam-forming and null-steering capabilities. A number of antenna array techniques for radio interference mitigation in GNSS receivers has been intensively studied in the last two decades, showing that space-time adaptive processing allows for significant improvement [143][144][145]. This kind of spatial processing technique can suppress multiple wideband and narrowband interference at the same time. However, it has the disadvantages of complex hardware, large scale and high cost.

Frequency excision technique is another approach to mitigate interference, especially narrowband interference. In this technique, the data samples are converted to the frequency domain. By comparing the magnitude of each frequency component with a pre-defined threshold, the interferences are detected and then suppressed down to the thermal noise level, but this also suppresses the energy of the useful signal in those frequency regions. The signal energy loss will have a small effect on the receiver tracking performance if only a small percentage of the signal spectrum is suppressed as shown in [146]. Figure 4.4

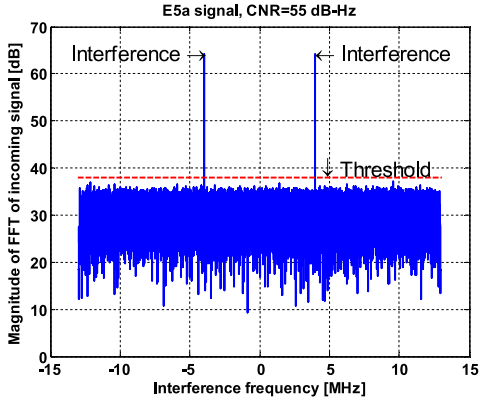

Figure 4.4: An example of continuous wave interference in frequency domain

shows an example of the signal frequency domain spectral in the presence of continuous wave interference (CWI). The strong CWI appears clearly above the noise floor in the frequency domain. Figure 4.5 shows that the code tracking error and estimated C/N_0 before and after frequency excision interference mitigation at several scenarios, which include different interference frequencies and power at different C/N_0 as listed in [146], in where only a single continuous wave interference is present as in Figure 4.4. As we can see that, after the mitigation, the code tracking error is slightly higher and the estimated C/N_0 is slightly lower than that without any interference. It is because the small part of signal energy is lost after the FFT excision.

Besides the techniques discussed above, the modernized navigation signals could also enhance the interference tolerance. The new modulations show high robustness against the narrowband interference. In [I], the author has presented an interference effect assessment on the new CBOC-modulated signal, taking into account the receiver modulation type. As reported in [I], CBOC signal is more robust than the GPS C/A BPSK-modulated signal against the narrowband interference and different modulation types in the receiver have impact on the code tracking performance in the presence of narrowband interference. The use of new wideband signals can also help to increase the anti-jam performance by increasing the processing gain with higher chip rate [147]. Such method is effective on both intentional and unintentional interference. As the results shown in [II], the wideband E5a signal is more robust against the interference than E1 signal. Moreover, in the modernized GNSS signal, the pilot signals are introduced, which are modulated by long-period PRN code without the navigation message. Receivers can extend the coherent integration time as long as possible to improve Signal-to-Noise-Ratio (SNR). Consequently, the sensitivity of a

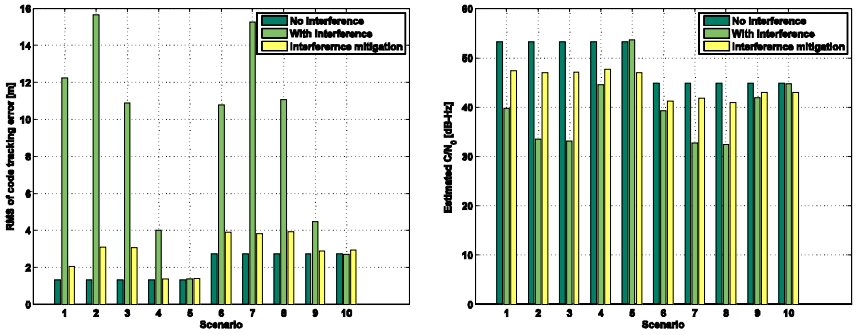

(a) (b)

Figure 4.5: Comparison between no interference, with interference and with frequency excision interference mitigation technique in a) code tracking error and b) estimated C/N_0

receiver can be significantly improved; the robustness of the receiver is thus enhanced to the interference condition. The new message error correction coding scheme can also improve the continuity of navigation in various kinds of interference [147].

The frequency diversity provides higher robustness against jamming since one signal band may still be usable while the other is jammed. This is equivalent to increased tolerance. The disadvantage of multi-band is a noticeable increase in receiver complexity, size and power consumption, especially for the RF front-end. The complexity of multi-frequency front-end can be considerably reduced by sharing front-end components or stages using intentional signal overlay [148]. With this structure, multiple signals are combined before the baseband processing, in which way the signals could interfere with each other, especially when external interference exists in one of the signal bands. The author has analyzed the impacts of interference due to the signal superposition in an E1-E5a dual-frequency receiver with overlay structure in [II]. The reason of choosing E1-E5a combination is that it yields the best performance in range estimation [149] and other criteria, such as acquisition time, power containment and compatibility with GPS [150]. The results in [II] show that the signal superposition in the baseband significantly increases the noise level on code tracking. The external narrowband interference introduced by E5a signal affects the code tracking performance of E1 signal; even it is not located in the E1 signal band after the superposition.

4.4 Ionosphere delay mitigation

Among the various error sources, ionosphere accounts for the biggest part of signal's total delay and therefore, it is essential to mitigate its effects. The employed methods of removing the ionosphere error from the pseudoranges can be grouped into two main categories, depending on the receiver type: single frequency and multi-frequency. In the conventional receivers, which receive signals from only one frequency, the unknown TEC can be obtained from TEC monitoring map or model computations, such as Klobuchar [151][152] and NeQuick, which has been proposed for the Galileo-enabled receivers [153][154].

Unlike in single-frequency receivers, no ionosphere modeling is needed when more than one carrier frequency are available. For example, a dual-frequency receiver measures the pseudoranges of two received signals at different frequencies. If both of the pseudoranges are contaminated by the same ionosphere effect, proper combination of the available measurements allows the receiver to completely remove the first order ionosphere. This is one of the main advantages of dual-frequency receiver over single-frequency ones. More precisely, in a dual-frequency receiver, we can model the available pseudoranges as:

$$\begin{cases} \rho_1 = \rho + \dfrac{40.3}{f_1^2} TEC + \varepsilon_1 + \mathcal{E}_{all\_1} \\ \rho_2 = \rho + \dfrac{40.3}{f_2^2} TEC + \varepsilon_2 + \mathcal{E}_{all\_2} \end{cases} \tag{19}$$

where ρ is the true satellite-receiver range, ρ_i are the measured pseudorange corresponding to the signal transmitted in f_i carrier frequency, ε_i is the measurement error (e.g., due to the multipath propagation effects), $\mathcal{E}_{all\_k}$ encompasses all the error sources on all the received signals (e.g., clock bias, tropospheric delay). In this model, the error sources $\mathcal{E}_{all\_k}$ can be ignored if all the signals are from a particular satellite since their effects contaminate both frequencies in the same way and do not affect the validity of the results [155]. If there are no measurement error (ε_i=0 for i=1, 2), we can estimate TEC accurately and consequently the satellite-receiver range by solving the linear system of two equations and two unknowns. In the presence of errors (i.e., due to multipath delay tracking errors), the linear Least Square (LS) can be used. With the help of vector notations, we can write the system given in Eq.(19) in a compact form as

$$\begin{bmatrix} \rho_1 \\ \rho_2 \end{bmatrix} = \begin{bmatrix} 1 & \frac{40.3}{f_1^2} \\ 1 & \frac{40.3}{f_2^2} \end{bmatrix} \begin{bmatrix} \rho \\ TEC \end{bmatrix} + \begin{bmatrix} \varepsilon_1 \\ \varepsilon_2 \end{bmatrix} \tag{20}$$

$$\mathbf{r} = \mathbf{A}\mathbf{x} + \mathbf{e}$$

where **r** is the observation vector that contains the pseudorange measurements. **A** is a 2×2 matrix, **x** is the unknown parameter vector to be estimated and **e** is the measurement error vector. The unknown TEC and true range parameters can be estimated by LS as

$$\hat{\mathbf{x}}_{LS} = (\mathbf{A}^T\mathbf{A})^{-1}\mathbf{A}^T\mathbf{r} \tag{21}$$

where *T* denotes the operation of transposition.

One limitation of LS method is that it does not account for physically invalid solutions. One way to avoid the aforementioned problem is to impose certain constrains in the solution for the ordinary LS, leading to what is commonly known as Constrained Least Square (CLS). The idea is to minimize the squared difference between the observed data and **Ax**, subject to the linear inequality constraint $\mathbf{A}\hat{\mathbf{x}}_{CLS} \geq b$, where b = [0 0] which means that both range and TEC estimates are forced to be positive. In order to avoid the computationally heavy approach of CLS, a new method, called Brute Force Constraint (BFC) was proposed in [156]. The main idea of BFC is that within only two iterations we are able to estimate TEC and true range subject to the constraint of non-negative TEC. Detailed description of the above-mentioned algorithms and explanation on the constraint choice can be found in [V] and [156].

The ionosphere-free combination usually relies on the assumption of zero or very small measurement errors. In reality, we cannot ignore the potential presence of measurement errors due to multipath propagation. Motivated by this, the performance analysis of dual-frequency range estimation methods in the presence of ionosphere error and multipath propagation was shown in this thesis and specifically in publication [V]. It is based on our previous work in [156], but the multipath channel was generated within a parameterized artificial urban canyon scenario with house fronts, lamppost and so on [157]. The multipath errors were obtained from Galileo E1 and E5 signal Simulink simulators [158]. The studies in [V] show that the performance of three dual-frequency range estimation methods are significantly related to the multipath error. Among the studies methods, BFC shows in average better accuracy in range estimation in the presence of strong multipath error.

4.5 Development of Simulink link-level simulators

As the receiver is a decisive block for the performance of the positioning systems, it must be of high standard to ensure accurate and reliable positioning. In view of this, the algorithm development procedure requires special attention and it needs to be based on solid and comprehensive testing. In the initial algorithm design stage, a simulator is a superior method for testing, due to its low cost and flexibility; it provides full control of the simulated satellite signals and the environment conditions. This means that researchers can readily generate and run a large amount of test scenarios to evaluate the signal processing algorithms holistically based on the simulated system performance before implementing a prototype device.

The Galileo E1 and E5 signal simulators are developed in a Simulink-based platform at Tampere University of Technology (TUT), Finland [158]. The basic version of the Simulink model was created by a former researcher in the department Xuan Hu in early 2009 (and he is gratefully acknowledged). Since then, the Simulink model has been extended by the author by adding several signal processing blocks and algorithms, such as the multipath mitigation algorithms, interference and mitigation blocks, and especially the whole E5a signal acquisition and tracking blocks in the E5 signal simulator, according to the nature and objective of the research. Part of the simulation results reported in [I] − [V] were carried out with these E1 and E5 simulators. The E1 and E5 simulators are created within EU FP project GRAMMAR and they are available under open-access license terms

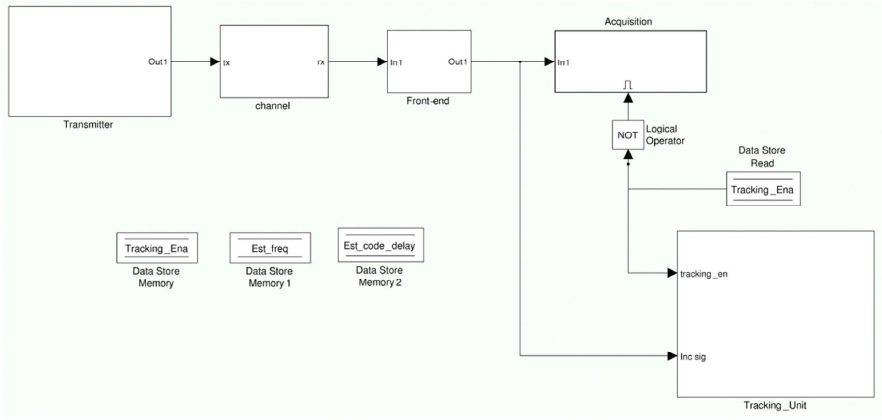

Figure 4.6: Generic TUT Galileo E1/E5 signal simulator structure

for the research community [158].

The Galileo E1 and E5 signal simulators have similar structures. Both of them consist of five main blocks as shown in Figure 4.6. A brief overview of these blocks is presented in the following.

Transmitter

The E1 and E5 signals generated in the transmitters are in the accordance with the Galileo OS SIS ICD [30]. The E1 signal transmitter block is implemented based on CBOC modulation, including primary code and secondary code. The E1B signal is CBOC('+') modulated with navigation data and E1C signal is CBOC('−') modulated with a predefined bit sequences CS25. The E1 signal is formed as the difference between the E1B and E1C signals. The signal at the output of the transmitter is at IF. The transmitter in E5 signal simulator generates the whole E5 signal by using AltBOC(15,10) modulation. The generated signal is then transmitted at IF at the output of the transmitter. The IF for E5 signal and E1 signal can be different.

Channel blocks

The channel blocks in both simulators generate the multipath signals and complex noise using a user-defined C/N_0, multipath delays, powers and phases as input parameters. Two channel configurations can be used: one static channel and one dynamic channel. In the static channel, the multipath signal and the complex Additive White Gaussian Noise (AWGN) are modeled according to the following equation:

$$r(t) = \sum_{l=1}^{L} a_l s(t - \tau_l) + n(t) \tag{22}$$

where $r(t)$ is the signal at the output of the channel block; a_l and τ_l are the path gain and path delay for the l^{th} path, respectively; and $n(t)$ is the complex AWGN.

In the dynamic channel, the multipath profile is generated within a parameterized artificial urban canyon scenario with house fronts, lampposts and so on. The dynamic channel also takes the position of satellite and receiver movement into account. Figure 4.7 gives an example of the channel realization of the dynamic channel. More details of this dynamic channel can be found in [157]. The possible external interference, such as narrowband interference used in [I] and CWI used in [146] can be also generated in an optional block in the channel block.

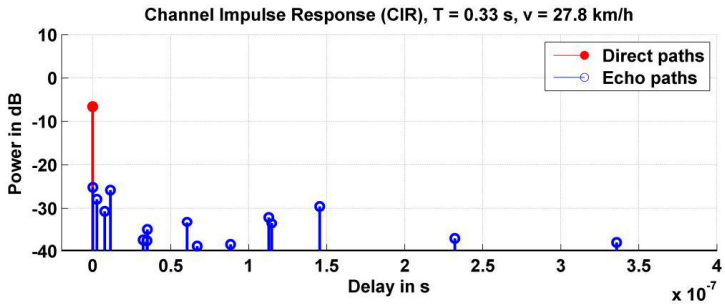

Figure 4.7: Exemplary channel realization (urban channel model)

Front-end filters

The 'Digital Filter Design' toolbox in Simulink is used to design the front-end filter. Commonly, a Chebyshev type I band-pass filter with various bandwidth configurations is used in the simulation, for example, 4 MHz for E1 signal and 20.46 MHz for covering the E5a lobe in [II], 13 MHz for both E1 and E5 signal for a fair performance comparison between E1 and E5 signal in the multipath channels [131].

Interference mitigation block

One frequency excision interference mitigation method is also implemented in the E1 signal simulator for the research in [146]. This technique takes a block of time domain data samples and converts them into the frequency domain. By comparing the magnitude of each frequency component with a pre-defined threshold, the interference components are detected and mitigated.

Acquisition blocks

When the signal is passed through the channel, the 'Acquisition' block is first activated. In both simulators, the acquisition is based on FFT technique. The acquisition detection is implemented according to the Constant False Alarm Rate (CFAR) as described in [159]. The frequency and the code phase are roughly estimated and stored in the memory, which will be used in the tracking block to generate the local replica. In the E1 signal simulator, both SinBOC(1,1) and CBOC modulated local replicas can be used. Since the E5 signal simulator only processes the E5a signal, the BPSK(10) modulated E5a signal is used as the local replica in the acquisition block in E5 simulator. Figure 4.8 shows an example of time-frequency mesh built in E5a signal acquisition process with 1 ms and 10 ms non-coherent time, respectively.

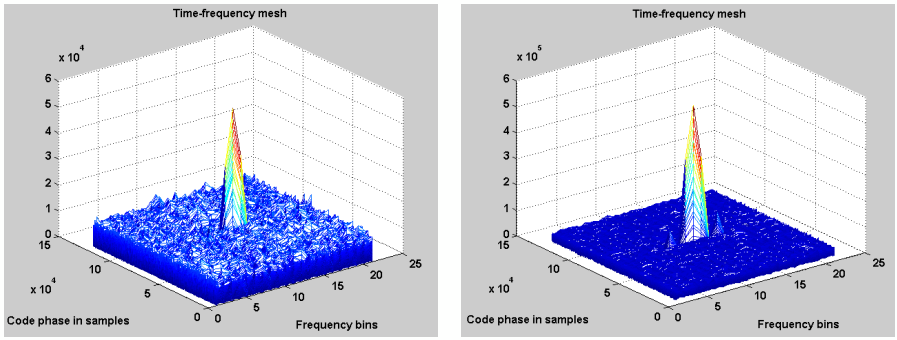

Figure 4.8: Time-frequency meshes in the E5a acquisition processing; left with 1ms non-coherent integration, right with 10 ms non-coherent integration

Tracking blocks

In both of the simulators, the tracking units consist of three main blocks: carrier wipe-off, code NCO block and correlation & discriminator block as described in [131]. The incoming signal is down-converted in the 'carrier wipe-off' block. After the carrier wipe-off, the real part and the imaginary part of the complex signal are separated as the in-phase and quadrature phase channels in the baseband. The 'code NCO' block is used to generate the local replica, which is shifted by the estimated code phase from DLL. Both code and carrier NCOs are implemented using a C-language based S-Function, the details of which are not addressed here for the sake of compactness. In the correlation & discriminator block, FLLs, PLLs and DLLs are included. In the DLL discriminator, various DLL discriminator functions are implemented, such as Narrow Correlator, optimized MGD [IV], Two-stage correlator [III][128]. In E1 signal simulator, the E1B and E1C are implemented as two separate channels. However, these two channels are approximately the same, except the replicas, which either CBOC('+')/CBOC('−') modulated, or SinBOC(1,1) modulated, according to the type of receiver for the research in [I]-[V][131][146] and [160]. The code tracking error is calculated after the simulation is finished. An example of the calculated E5a signal code tracking error versus simulation time in a single path channel is shown in Figure 4.9.

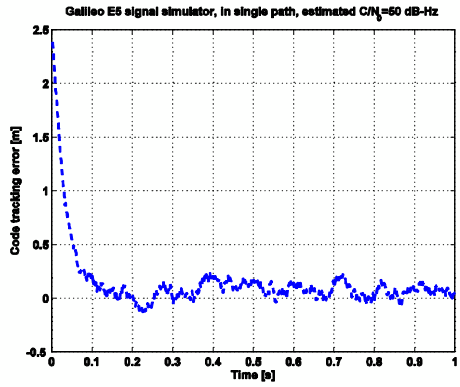

Figure 4.9: Code tracking error versus simulation time of E5a signal at estimated C/N_0=50 dB-Hz with non-coherent integration over 1 ms

4.6 Flexible power-controlled multi-frequency architecture

The multi-frequency receiver has the potential to enhance the positioning performance in terms of, for example, ionosphere delay correction and interference mitigation. However, the architecture of the receiver becomes more complex since it needs to process the signals from two or more frequencies [161][162][163]. Moreover, adding the capability of receiving additional signals will potentially increase the power consumption of a receiver. This constitutes a particular challenge in the mass-market GNSS receivers that depend on a battery as a power source. In order to reduce power consumption, some single-frequency receivers shut down the power in front-end for a fraction of time, but in a continuous manner, so the baseband can keep track of the present signals [164]. The off-time duration is less than the correlation period of the signal in order to ensure that the useful information within each correlation period is not completely lost. This technique, which has been patented in [164] may reduce the power in RF section while the receiver continues to correlate GPS satellite signals and to provide a location fix for the user. This concept of power reduction can be utilized in multi-frequency receiver as well. In multi-frequency receiver, the front-ends are usually separated for receiving signals from different frequency bands and navigation systems. The receiver can reduce the power consumption by activating only one of the front-ends at a time. In addition, the on/off time duration needs to be chosen to ensure that there is enough information for each signal for baseband processing. Figure 4.10 illustrates the idea of flexible power-controlled front-end in a multi-frequency receiver. The figure shows a multi-frequency receiver with overlay structure,

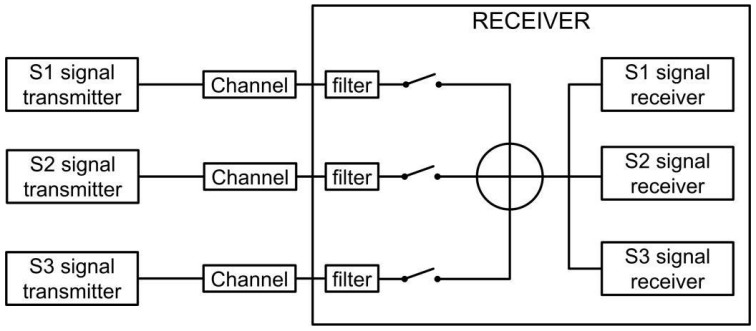

Figure 4.10: Generic block diagram of an overlay structure multi-frequency receiver with power-controlled front-ends

which has separated front-ends. The power on/off modulators can be implemented in each front-end and are assumed to be synchronized. The on/off modulated signals from each front-end may be combined before the baseband receivers. The combined signal is processed separately in each baseband receiver.

With the power-controlled front-end implementation, the signals will be powered off for a short time. Therefore, the signal power will be smaller than that without power modulators and the noise is increased due to the existence of other GNSS signals. Consequently, the C/N_0 in the acquisition and tracking stage may be below the required threshold at some point. This particular phenomenon introduces a new challenge to the receiver as they now require much more sophisticated algorithms to compensate for the loss in C/N_0. For example, MGD [IV] and Two-stage correlator [III] [128], are able to provide higher code tracking accuracy than Narrow Correlator at the same C/N_0 level.

On the other hand, the power modulator intrinsically offers the opportunity for interference mitigation, for example, the pulsed interference originated from the system such as Tactical Air Navigation System (TACAN) and Distance Measuring Equipment (DME). Depending on the length of the interference on/off cycle, the power modulator could blank the pulsed interference by adjusting the off time duration. Moreover, in the multi-mode multi-frequency receiver, an adaptive power on/off modulator can be adjusted to power on the channel, which has the best individual C/N_0 or geometry to compute the navigation solutions.

5 Conclusions and open issues

Location-based services and applications are currently playing a significant role in people's life. There is a growing demand for better positioning performance, especially under poor signal conditions. With the advent of new GNSS systems and the raising growth of indoor positioning technologies, this need has brought out the multi-mode multi-frequency receiver into the center of attention in both academic and business fields. Specifically, a substantial amount of effort is put into investigating the capability of multi-mode multi-frequency receivers on overcoming the known challenges in order to improve positioning performance.

This thesis including the publication part presents the analysis and development of new algorithms in multi-mode multi-frequency receivers for processing the new signals, modulations and frequencies introduced by the modern navigation systems. Combining with the use of link level simulators, the results presented in this thesis provide valuable knowledge for future research and practice and can be applicable in solving relevant problems.

Among various error sources, the multipath and NLOS propagation in urban area and indoor environments are one of the main dominant errors. In this thesis, one multipath mitigation algorithm using multiple correlator structure has been optimized for the new CBOC-modulated signal, taking into account the modulation type and bandwidth in the receiver [IV]. Comparing with two conventional multipath mitigation algorithms, Narrow Correlator and HRC, the optimized MGD gives significantly better multipath mitigation performance in short delay scenarios with wide front-end bandwidth at middle to high C/N_0. The observations in [IV] have also motivated the work on a joint solution of Narrow Correlator and MGD in [128] that tries to combine the robustness of Narrow Correlator to noise with the good multipath performance of MGD. In addition, most multipath mitigation algorithms in the literature are often based on optimistic channel assumptions. Therefore, this thesis includes a performance comparison of four multipath mitigation techniques in realistic measurement-based channel models [III].

The author also proposes a new method for NLOS identification for indoor positioning [VI] based on MIMO signals in a WLAN system. Unlike the kurtosis-based NLOS identification used in UWB systems, the proposed method uses a different form of channel impulse response for kurtosis calculation. In this way, the kurtosis value is insensitive to the system parameters and shows more consistent and clearer separation for LOS and

NLOS conditions. In [VI], the author also discovers that if multi-antennas are available, the average kurtosis gives even better indication of LOS/NLOS conditions than that with single antenna. This new kurtosis-based NLOS identification could help to improve the accuracy of indoor positioning based on path-loss modeling.

This thesis also includes an interference impact assessment in the context of global navigation based on the new modulation CBOC that will be used for Galileo E1 civil signal [I]. Specifically, the author develops a theoretical expression predicting the performance of a Galileo E1 signal receiver in the presence of narrowband interference, taking into account the modulation types in the receiver. The results show that CBOC signal is working better against the narrowband interference than the GPS BPSK signal. The modulation type used in the receiver has impact on the code tracking performance in the presence of narrowband interference. The results also indicate that if the front-end bandwidth is wide enough, CBOC receiver is more prosperous against narrowband interference than SinBOC receiver. This analysis in [I] gives quantitative comparison between GNSS signals against narrowband interference and may help the receiver designer to choose the signals and modulations in their designs.

In addition to the interference analysis on the CBOC modulated signals, this thesis presents an analysis of interference effect in a dual-frequency receiver with overlay front-end structure in [II]. The results show that the overlapping of two signals in the baseband was not a significant problem in terms of RMS of code tracking error, but significantly increased the noise on the signal, which had narrower bandwidth. The author also presents in [II] the impact analysis of external narrowband interference. In the cases where two signals are overlapping in the baseband and the interference introduced by the wideband signal is not located in the narrowband signal, the code tracking performance of the signal with narrow bandwidth is still affected by the interference. The results also indicate that the wideband Galileo E5a signal is more robust against the interference than Galileo E1 signal.

Multiple frequencies enable the ionosphere-free combination, but the combination usually relies on the assumption of zero or very low measurement errors. In reality, we cannot ignore the potential presence of measurement errors due to multipath propagation. This thesis also provides the analysis of three dual-frequency range estimation methods under ionosphere delay and strong multipath errors [V]. The measurement errors were obtained from the Simulink simulators with parameterized artificial urban canyon channels. The results indicate that the dual-frequency range estimation performance of ionosphere correction methods deteriorates significantly in the presence of multipath propagation errors. Among the three methods, LS, CLS and BFC, there is no single solution that performed the best among all test scenarios. The LS method has consistent performance with different TEC. The range estimation error of LS depends on the measurement error. The performance of CLS and BFC are dependent on both TEC and measurement errors. The CLS performs slightly better than LS at the expense of complexity. Based on the

observation, we would suggest that BFC should be used in the dual-frequency receiver, since BFC offers on the average the best performance among the conventional methods in urban area.

Overall, the presented analysis provides necessary perceptions on the robustness of new signals introduced in the new positioning systems against multipath, interference and ionosphere error. The proposed signal processing algorithms achieve improved performance in applications where the conventional algorithms do not perform well. It is the author's belief that her publications are significant paving blocks to the road of the future multi-mode multi-frequency receivers and making them ubiquitous.

As the multi-mode multi-frequency receiver is an awareness raising concept, developing low-cost flexible architectures for combining GNSS and non-GNSS techniques remains a challenging topic. The author believes that in the future, it is also important to design devices that sense the environment and evaluate the affecting parameters. For example, using the input from detectors between LOS/NLOS cases and between indoor/outdoor cases in order to select the best localization techniques or using cognitive spectrum sensing in the context of wireless navigation that can detect all (or best) signals of opportunity available in the environment and then astutely combine them through advanced hybridization engines. In that way, the multi-mode multi-frequency could switch seamlessly among existing methods and achieve optimal performance.

Bibliography

[1] D. Kim, A. Saa-Kortsak, J. Purdham, R. Dales, J. Brook, "Sources of personal exposure to fine particles in Toronto, Ontario, Canada," *Journal of Air & Waste Management*, vol. 88, no. 8, pp. 1134-1146, 2005.

[2] F. Wu, T. Biksey, M. Karol, "Can mold contamination of homes be regulated? Lessons learned from radon and lead policies," *Environment Science & Technology*, vol. 41, no. 12, pp. 4861-4867, 2011.

[3] H. Kuusniemi, J. Liu, L. Pei, Y. Chen, L. Chen, R. Chen, "Reliability considerations of multi-sensor multi-network pedestrian navigation," *IET Radar, Sonar & Navigation*, vol. 6, issue 3, pp. 157-164, March 2012.

[4] H. Kuusniemi, L. Chen, L. Ruotsalainen, L. Pei, Y. Chen, R. Chen, "Multi-sensor multi-network seamless positioning with visual aiding," *Proc. of 2011 International Conference on Localization and GNSS (ICL-GNSS)*, pp. 146-151, June 2011, Tampere, Finland.

[5] T. Hall, C. Counselman, P. Misra, "Radiolocation using AM broadcast signals: positioning performance" *Proc. of the 15th International Technical Meeting of the Satellite Division of The Institute of Navigation (ION GPS)*, pp. 921-932, September 2002, Portland, OR, USA.

[6] T. Hall, C. Counselman, P. Misra, "Instantaneous radiolocation using AM Broadcast signals," *Proc. of the 2001 National Technical Meeting of The Institute of Navigation*, pp. 93-99, January 2001, Long Beach, CA, USA.

[7] P. Misra, B. P. Burke, M. M. Pratt, "GPS performance in navigation," *Proc. of the IEEE*, vol. 87, no.1, pp. 65-85, January 1999.

[8] T. Hall, B. Burke, M. Pratt, P. Misra, "Comparison of GPS and GPS+GLONASS positioning performance," *Proc. ION GPS*, pp. 1543-1550, September 1997, Kansas City, Missouri, US.

[9] A. Rusu-Casandra, *Digital Signal Processing in Global Navigation Satellite Systems*, Doctoral dissertation, Politehnica University of Bucharest, November 2012.

[10] A. Rusu-Casandra, E. S. Lohan, “Impact of narrowband interference on unambiguous acquisition approaches in Galileo,” *Proc. of International Conference on Localization and GNSS (ICL-GNSS)*, pp. 127-132, June 2011, Tampere, Finland.

[11] H. Kuusniemi, E. Airos, M. Z. H. Bhuiyan, T. Kröger, “GNSS jammers: how vulnerable are consumer grade satellite navigation receivers?” *European Journal of Navigation*, vol. 10, issue 2, pp. 14-21, August 2012.

[12] W. Jia, J. Wen, M. Yao, “Unambiguous S-curve shaping technique for multipath mitigation in Cosine-BOC signals,” *IEEE Communications Letter*, vol. 16, pp. 1725-1728, November 2012.

[13] W. Zhao, Y. Zhou, H. Hu, “MIMO-OFDM NLOS identification algorithm based on hypothesis test,” *Proc. of the 2nd International Conference on Computer Science and Electronics Engineering (ICCSEE)*, pp. 1289-1292, March 2013, Hang Zhou, China.

[14] V. Cipov, L. Dobos, J. Papaj, “TOA node distance estimation enhancement in MANET localization algorithm based on cooperative trilateration,” *Advances in Electrical and Electronics Engineering*, vol. 10, no. 4, pp. 211-217, 2012.

[15] P. Tamellini, *Interfaces gráficas de usuario destinadas al studio de señales Radar y GNSS*, Bachelor Thesis, Universitat Oberta de Catalunya, June 2011.

[16] P. Misra, P. Enge, *Global positioning system: signals, measurements, and performance*, Second Edition, Ganga-Jamuna Press, 2006.

[17] Space Segment, http://www.gps.gov/systems/gps/space/.

[18] GPS World, http://www.gpsworld.com/gps-block-iif-4-launch-set-may-15/.

[19] E. Kaplan, *Understanding GPS: principle and applications*, Artech House, 1996.

[20] R. L. Peterson, R. E. Ziemer, D. E. Borth. *Introduction to Spread Spectrum Communications*, Prentice Hall, 1995.

[21] New Civil Signals, http://www.gps.gov/systems/gps/modernization/civilsignals/.

[22] V. Davydov, S. Revinvykh, “Direction 2013: GLONASS today and tomorrow,” *GPS World*, December 2012.

[23] ESA, “Galileo: The European programme for global navigation services.” *ESA Publication Division (ESTEC)*, March 2003.

[24] European Space Agency, http://www.esa.int/Our_Activities/Navigation/The_future_-_Galileo/What_is_Galileo.

[25] Europe’s satellite navigation systems. http://www.satellite-navigation.eu.

[26] S. Wallner, J. A. Avila-Rodriguez, G. W. Hein, "Interference computation between several GNSS systems", *Proc. of 3rd Workshop on Satellite Navigation Technologies (Navitec)*, December 2006, Noordwijk, The Netherland.

[27] Galileo ground segment, http://navipedia.net/index.php/GALILEO_Ground_Segment.

[28] Galileo Services, http://www.gsa.europa.eu/galileo/services.

[29] R. Prasad, M. Ruggieri, *Applied satellite navigation using GPS, Galileo, and augmentation systems*, Artech House, 2005.

[30] *Galileo open service signal in space interface control document OS SIS ICS*, available via: http://ec.europa.eu/enterprise/policies/satnav/galileo/open-service/index_en.htm, September 2010.

[31] C. J. Hegarty, E. Chatre, "Evolution of the Global Navigation SatelliteSystem (GNSS)," *Proceedings of the IEEE* , vol. 96, no. 12, pp. 1902-1917, December 2008.

[32] Navipedia, COMPASS general introduction, http://www.navipedia.net/index.php/COMPASS_General_Introduction

[33] C. Cao, G. Jing, M. Luo "COMPASS satellite navigation system development," *PNT Challenges and Opportunities Symposium*, Stanford University, November 2008.

[34] *BeiDou navigation satellite system signal in space interface control document*, Available via: http://www.beidou.gov.cn/2012/12/27/20121227f5fd4206a9b3415881b125281e819bd4.html.

[35] K. Borre, *A Software-defined GPS and Galileo Receiver: A single-frequency approach*, Birkhäuser, 2007.

[36] U. Engel, "A theoretical performance analysis of the modernized GPS signals," *Proc. of IEEE/ION Position, Location and Navigation Symposium*, pp. 1067-1078, May 2008.

[37] J. W. Betz, "Binary offset carrier modulations for radionavigation," *NAVIGATION*, vol. 48, no. 4, pp. 227-246, Winter 2001/02.

[38] G. Hein, M. Irsigler, J. A. Avila-Rodriguez, T. Pany, "Performance of Galileo L1 signal candidates," *Proc. of European Navigation Conference GNSS (ENC-GNSS)*, May 2004, Rotterdam, The Netherland.

[39] J. A. Rodriguez, M. Irsigler, G. Hein, T. Pany, "Combined Galileo/GPS frequency and signal performance analysis," *Proc. of ION GNSS*, September 2004, Long Beach, California, USA.

[40] E. S. Lohan, A. Burian, M. Renfors, "Low-complexity acquisition methods for split-spectrum CDMA signals," *Wiley International Journal of Satellite Communications*, vol. 26, pp. 503-52, 2008.

[41] E. S. Lohan, A. Lakhzouri, M. Renfors, "Binary-Offset-Carrier modulation techniques with applications in satellite navigation systems," *Wiley Journal of Wireless Communications and Mobile Computing*, July 2006.

[42] J. W. Betz, "The offset carrier modulation for GPS modernization," *Proc. of ION Technical meeting,* pp. 639-648, January 1999, San Diego, CA, USA.

[43] E. Rebeyrol, C. Macabiau, L. Lestarquit, M. L. Boucheret, M. Bousquet, "BOC power spectrum densities," *Proc. of the 2005 National Technical Meeting of the Institute of Navigation*, pp. 769-788, January 2005, San Diego, CA, USA.

[44] G. W. Hein, J. A. Avila-Rodriguez, S. Wallner, A. R. Pratt, J. Owen, J. Issler, J. W. Betz, C. J. Hegarty, S. Lenahan, J. J. Rushanan, A. L. Kraay, T. A. Stansell, "MBOC: The new optimized spreading modulation recommended for GALILEO L1 OS and GPS L1C," *Proc. of IEEE/ION PLANS*, pp. 883- 892, April 2006, San Diego, CA, USA.

[45] J. A. Avila-Rodriguez, S. Wallner, G. Hein, E. Rebeyrol, O. Julien, C. Macabiau, L. Ries, A. DeLatour, L. Lestarquit, J. Issler, "CBOC - An implementation of MBOC," *Proc. of First CNES Workshop on Galileo Signals and Signal Processing*, October 2006, Toulouse, France.

[46] "Galileo Joint Undertaking - GPS-Galileo Working Group A (WGA) Recommendations on L1 OS/L1C optimization."
Available via: http://www.galileoju.com/page3.cfm.

[47] E. S. Lohan, M. Renfors, "Correlation properties of multiplexed-BOC (MBOC) modulation for future GNSS signal," *Proc. of European Wireless Conference*, April 2007, Paris, France.

[48] N. C. Shivaramaiah, A. G. Dempster, "The Galileo E5 AltBOC: Understanding the signal structure," *Proc. of the International Global Navigation Satellite Systems Society, IGNSS Symposium*, December 2009, Holiday Inn Surfers Paradise, Old, Australia.

[49] E. Rebeyrol, C. Macabiau, L. Lestarquit, L. Ries, J. L. Issler, M. L. Boucheret, M. Bousquet, "BOC power spectrum densities," *Proc. of the National Technical Meeting of The Institute of Navigation, (ION-NTM)*, pp. 769-778, January 2005, Long Beach, California, USA.

[50] E. Rebeyrol, O. Julien, C. Macabiau, L. Ries, A. Delatour, L. Lestarquit, "Galileo civil signal modulations," *GPS Solutions*, vol. 11, Issue 3, pp.159-171, July 2007.

[51] L. Ries, F. Legrand, L. Lestarquit, W. Vigneau, J. L. Issler, "Tracking and multipath performance assessments of BOC signals using a bit-Level signal processing Simulator," *Proc. of the International Technical Meeting of the Institute of Navigation, (ION-GNSS)*, September, 2003, Oregon Convention Center, Portland, Oregon, USA.

[52] W. De Wilde, M. Hollreiser, "Galileo ALTBOC receiver," *Proc. of the European Navigation Conference (ENC GNSS)*, May 2004, Rotterdam, The Netherland.

[53] M. Soellner, P. Erhard, "Comparison of AWGN code tracking accuracy for alternative-BOC, complex-LOC and complex-BOC modulation options in Galileo E5-band," *Proc. of the European Navigation Conference (ENC GNSS)*, April 2003, Graz, Austria.

[54] E. S. Lohan, A. Lakhzouri, M. Renfors, "Complex double-binary-offset-carrier modulation for a unitary characterization of Galileo and GPS signals," *IEE Proceedings-Radar, Sonar and Navigation*, vol. 153, no. 5, pp. 403-408, October 2006.

[55] J. B. Y. Tsui, *Fundamentals of global positioning system receivers: A software approach*, Second Edition, Wiley Interscience, 2005.

[56] E. S. Lohan, "Statistical analysis of BPSK-like techniques for the acquisition of Galileo signals," *Proc. of AIAA International Communications Satellite System Conference (ISCC)*, September 2005, Rome, Italy.

[57] D. Skournetou, *Mitigation of dominant channel propagation effects in GNSS-based positioning*, Doctoral dissertation, Tampere University of Technology, 2011.

[58] S. Turunen, *Weak signal acquisition in satellite positioning*, Doctoral dissertation, Tampere University of Technology, September 2010.

[59] D. P. Taylor, "Introduction to "Synchronous communications," *Proc. of the IEEE*, vol. 90, issue. 8, pp. 1459- 1460, August 2002.

[60] C. H. Yinger, W. A. Feess, V. Nuth, R. N. Haddad, "GPS accuracy versus number of NIMA stations," *Proc. of the 16th International Technical Meeting of the Satellite Division of The Institute of Navigation (ION GPS/GNSS)*, pp. 1526-1533, September 2003, Portland, OR, USA.

[61] B. Parkinson, J. J. Spilker, *Global positioning system: theory and applications volume 1*, American Institute of Aeronautics and Astronautics, 2006.

[62] G. X. Gao, S. Datta-Barua, T. Walter, P. Enge, "Ionosphere effects for wideband GNSS signals," *Proc. of the 63rd Annual Meeting of the Institute of Navigation*, pp. 147-155, April 2007, Cambridge, Massachusetts, US.

[63] A. J. Mannucci, “Ionosphere and ionospheric delay,” available via: http://www.cosmic.ucar.edu/summercamp_2005/presentations/Mannucci_Anthony_20050602.pdf.

[64] B. Hofmann-Wellenhof, H. Lichtenegger, J. Collins, *GPS theory and practice*, New York: Springer-Verlag, 1993.

[65] M. Kaur, S. Kakar, D. Mandal, “Electromagnetic interference,” *Electronics Computer Technology (ICECT), 2011 3rd International Conference on* , vol. 4, pp.1-5, April 2011.

[66] J. A. Lázaro, *GNSS array-based acquisition: theory and implementation*, Doctoral dissertation, Universitat Politècnica de Catalunya, 2012.

[67] P. Boulton, R. Borsato, B. Butler, “GPS interference testing: lab, live and LightSquared,” Technical Article, *InsideGNSS*, July/August, 2011.

[68] J. W. Betz, “Effect of narrowband interference on GPS code tracking accuracy,” *Proc. of the 2000 National Technical Meeting of The Institute of Navigation*, pp. 16-27, January 2000, Anaheim, CA, USA.

[69] J. W. Betz, “Effect of partial-band interference on receiver estimation of C/N0: theory,” *Proc. of the National Technical Meeting of The Institute of Navigation*, pp. 817-828, January 2001, Long Beach, CA, USA.

[70] D. Cummings, “Aggregate ultra wideband impact on global positioning system receivers,” *Proc. of IEEE Radio and Wireless Conference (RAWCON)*, pp. 101-104, August 2001, Waltham, MA, USA.

[71] R. Giuliano, F. Mazzenga, “On the coexistence of power-controlled ultrawideband systems with UMTS, GPS, DCS1800, and fixed wireless systems,” *IEEE Transactions on Vehicular Technology*, vol. 1, pp. 62-81, January 2005.

[72] M. Hamalainen, V. Hovinen, R. Tesi, J. Iinatti, M. Latva-aho, “On the UWB system coexistence with GSM900, UMTS/WCDMA, and GPS,” *IEEE Journal on Selected Areas*, vol. 20, pp. 1712-1721, December 2002.

[73] J. P. Cabrera-Plaza, T. Burger, “Inter-system interference experiments for Galileo and GPS in L1 (1575.42 MHz),” *Proc. of the European Navigation Conference (ENC GNSS)*, Graz, Austria, April 2003.

[74] J. W. Betz, and B. M. Titus, “Intersystem and intrasystem interference with signal imperfections,” *Proc. of IEEE Position Location and Navigation Symposium (PLANS)*, pp. 558-565, April 2004, Monterey, CA, USA.

[75] H. Kuusniemi, M. Z. H. Bhuiyan, “Signal Barred,” *Geospatial World, The Geospatial Industry Magazine*, pp. 31-33, November 2012.

[76] J. P. Keith, “Multipath Errors Induced by Electronic Components in Receiver Hardware,” *Proc. of the 2000 National Technical Meeting of The Institute of Navigation*, pp. 706-715, January 2000, Anaheim, CA, USA.

[77] N. Samama, *Global Positioning, Technology and Performance*, Wiley, 2008.

[78] R. Mautz, *Indoor Positioning Technologies*, Swiss Geodetic Commission, Geodetic-Geophysical Reports of Switzerland, no. 86, 2012.

[79] M. Bouet, A. L. dos Santos, “RFID tags: Positioning principles and localization techniques,” *Wireless Days, 2008. WD '08. 1st IFIP*, pp. 1-5, November 2008.

[80] Y. Qi, H. Kobayashi, H. Suda, “On time-of-arrival positioning in a multipath environment,” *IEEE Transactions on Vehicular Technology*, vol. 55, no. 5, September 2006.

[81] H. C. Chen, T. H. Lin, H. T. Kung, C. K. Lin, Y. Gwon, “Determining RF angle of arrival using COTS antenna arrays: A field evaluation,” *Proc. of Military Communications Conference*, pp. 1-6, October/November 2012.

[82] H. Liu, H. Darabi, P. Banerhee, J. Liu, “Survey of wireless indoor positioning techniques and systems,” *IEEE Transaction on Systems, Man, and Cybernetics-part C: Applications and Reviews*, vol. 37, no. 6, November 2007.

[83] S. Hellan, O. Stengel, “CC1020/1021 Received signal strength indicator,” *Chipcon Products from Texas Instruments, Application Note AN303*, January 2005.

[84] S. Nikitaki, G. Tsagkatakis, P. Tsakalides, “Efficient training for fingerprint based positioning using matrix completion,” *Proc. of the 20th European Signal Processing Conference (EUSIPCO)*, pp. 195-199, August 2012, Bucharest, Romania.

[85] V. Moghtadaiee, A. G. Dempster, B. Li, “Accuracy indicator for fingerprinting localization systems,” *Proc. of IEEE/ION Position Location and Navigation Symposium (PLANS)*, pp. 1204-1208, April 2012, Myrtle Beach, SC, USA.

[86] H. Nurminen, J. Talvitie, S. Ali-Loytty, P. Muller, E. S. Lohan, R. Piche, M. Renfors, “Statistical path loss parameter estimation and positioning using RSS measurements,” *Proc. of Ubiquitous Positioning, Indoor Navigation, and Location Based Service (UPINLBS)*, pp. 1-8, October 2012, Helsinki, Finland.

[87] S. Shrestha, *RSS-based position estimation in cellular and WLAN networks*, Master’s Thesis, Tampere University of Technology, 2012.

[88] R. Mautz, “Overview of current indoor positioning systems,” *Geodesy and Cartography*, vol. 35, no. 1, pp. 18-22, 2009.

[89] G. Lopez-Risueño, G. Seco-Granados, A. Garcia, "Evaluation of GPS indoor positioning using real measurements and a One-Shot software receiver," *Proc. of the European Navigation Conference (ENC GNSS)*, July 2005, Munich, Germany.

[90] G. P. Mattos, "Solutions to the cross-correlation and oscillator stability problems for indoor C/A code GPS," *Proc. of the 16th International Technical Meeting of the Satellite Division of The Institute of Navigation*, pages 654–659, September 2003, Portland, OR, USA.

[91] F. A. Diggelen, *A-GPS: Assisted GPS, GNSS, and SBAS*, Artech House, 2009.

[92] J. Zhang, B. Li, A. Dempster, C. Rizos, "Evaluation of high Sensitivity GPS receivers," *Coordinates – Positioning, Navigation and Beyond*, vol. 7, no. 3, pp. 7-12, 2011.

[93] G. Lachapelle, "GNSS indoor location technologies," *Journal of Global Positioning Systems*, vol. 3, no. 1-2, pp. 2-11, 2004.

[94] M. Kjærgaard, H. Blunck, T. Godsk, T. Toftkjær, D. Christensen, K. Grønbæk, "Indoor positioning using GPS revisited," *Pervasive Computing*, Lecture Notes in Computer Science, vol. 6030, pp. 38–56, 2010.

[95] C. Pfeffer, S. Scheiblhofer, R. feger, A. Stelzer, "An S-FSCW based multi-channel reader system for beamforming applications using surface acoustic wave sensor," *Radioengineering*, vol. 20, no. 4, December 2011.

[96] E. Laitinen, E. S. Lohan, J. Talvitie, S. Shrestha, "Access point significance measures in WLAN-based location," *Proc. of 9th Workshop on Positioning Navigation and Communication (WPNC)*, pp. 24-29, March 2012, Dresden, Germany.

[97] S. Shrestha, E. Laitinen, J. Talvitie, E. S. Lohan, "RSSI channel effects in cellular and WLAN positioning," *Proc. of 9th Workshop on Positioning Navigation and Communication (WPNC)*, pp. 187-192, March 2012, Dresden, Germany.

[98] L. Pei J. Liu, R. Guinness, Y. Chen, T. Kroger, R. Chen, L. Chen, "The evaluation of WiFi positioning in a Bluetooth and WiFi coexistence environment," *Proc. of Ubiquitous Positioning, Indoor Navigation, and Location Based Service (UPINLBS)*, pp. 1-6, October 2012, Helsinki, Finland.

[99] A. Molisch, "Ultrawideband propagation channels theory, measurement and modeling," *IEEE Transactions on Vehicular Technology*, vol. 54, no. 5, pp. 1528−1545, September 2005.

[100] M. R. Mahfouz, M. J. Kuhn, Y. Wang, J. Turnmire, A. E. Fathy, "Towards sub-millimeter accuracy in UWB positioning for indoor medical environments," *Proc. of*

IEEE Topical Conference on Biomedical Wireless Technologies, Networks, and Sensing Systems (BioWireleSS), pp. 83-86, January 2011, Phoenix, AZ, USA.

[101] S. Gezici, H. V. Poor, "Position estimation via ultra-wide-band Signals," *Proc. of the IEEE* , vol. 97, no. 2, pp. 386-403, February 2009, doi:10.1109/JPROC.2008.2008840.

[102] W. Liu, H. Ding, X. Huang, X. Li, J. Yuan, "Preliminary study on noncooperative positioning using UWB impulse radio," *Proc. of IEEE International Conference on Ultra-Wideband (ICUWB)*, pp. 279-283, September 2012.

[103] B. W. Parkinson, P. Axelrad, "Autonomous GPS integrity monitoring using the pseudorange residual," *Navigation: Journal of the Institute of Navigation*, vol. 35, no. 2, pp. 255-274, 1988.

[104] M. Irsigler, *Multipath propagation, mitigation and monitoring in the light of Galileo and the modernized GPS*, Doctoral dissertation, University FAF Munich, Munich, Germany, 2008.

[105] K. A. Fisher, *The navigation potential of signals of opportunity-based time difference of arrival measurements*, Doctoral dissertation, Air University, USA, March 2005.

[106] C. Yang, T. Nguyen, D. Venable, M. White, R. Siegel, "Cooperative position location with signal of opportunity," *Proc. of the IEEE 2009 National Aerospace & Electronics Conference (NAECON)*, pp. 18-25, July 2009, Fairborn, Ohio, USA.

[107] M. A. Enright, C. N. Kurby, "A signals of opportunity based cooperative navigation network," *Proc. of the IEEE 2009 National Aerospace & Electronics Conference (NAECON)*, pp.213-218, July 2009, Ohio, USA.

[108] M. Robinson, R. Ghrist, "Topological Localization Via Signals of Opportunity," *IEEE Transactions on Signal Processing*, vol. 60, no. 5, pp. 2362-2373, May 2012 doi: 10.1109/TSP.2012.2187518.

[109] V. Moghtadaiee, A. G. Dempster, S. Lim, "Indoor localization using FM radio signals: A fingerprinting approach," *Proc. of 2011 International Conference on Indoor Positioning and Indoor Navigation (IPIN)*, pp. 1-7, September 2011, Guimarães, Portugal.

[110] P. Nelapati, *An intelligent SOP navigation system with two mobile receivers*, Master's Thesis, University of Toledo, 2011.

[111] L. Zheng, R. Xue, "Signals of opportunity navigation methods for complex lower airspace flight," *Proc. of IEEE 5th International Conference on Cybernetics and Intelligent Systems (CIS)*, pp. 272-276, September 2011, Qindao, China.

[112] H. D. Whyte, T. Bailey, "Simultaneous localization and mapping: part I," *IEEE Robotic & automation Magazine*, vol. 13, no. 2, pp. 99-110, June 2006.

[113] R. E. Phelts, P. Enge, "The multipath invariance approach for code multipath mitigation," *Proc. of the 13th International Technical Meeting of the Satellite Division of The institute of Navigation (ION GPS)*, September 2000, Portland, OR, USA.

[114] R. L. Fante, J. J. Vaccaro, "Multipath and reduction of multipath-induced bias on GPS time-of-arrival," *IEEE Transactions on Aerospace and Electronic Systems*, vol. 39, no. 3, July 2003.

[115] P. fine, W. Wilson, "Tracking algorithms for GPS offset carrier signals," *Proc. of The 1999 National Technical Meeting of The Institute of Navigation (ION NTM)*, pp. 671-676, January 1999, San Diego, CA, USA.

[116] L. L. Hagerman, "Effects of multipath on coherent and non-coherent PRN ranging receiver," *Aerospace Report TOR-0073 (3020-03)-3*, Development Planning Division, The Aerospace Corporation.

[117] A. J. V. Dierendonck, P. C. Fenton, T. Ford, "Theory and performance of narrow correlator spacing in a GPS receiver," *Navigation: Journal of The Institute of Navigation*, vol. 39, no. 3, pp. 265-284, Fall 1992.

[118] P. Fenton, "Pseudorandom noise ranging receiver which compensates for multipath distortion by making use of multiple correlator time delay spacing," *Novatel Patent*, US 5414729, May 1995.

[119] P. Fenton, A. J. V. Dierendonck, "Pseudorandom noise ranging receiver which compensates for multipath distortion by dynamically adjusting the time delay spacing between early and late correlators," *Novatel Patent*, US 5495499, February 1996.

[120] J. W. Betz, K. R. Kolodziejski, "Extended theory of early-late code tracking for a bandlimited GPS receiver," *Navigation: Journal of the Institute of Navigation*, vol. 47, no. 3, pp. 211-226, 2000.

[121] M. S. Braasch, "Performance comparison of multipath mitigating receiver architecture," *Proc. of IEEE Aerospace Conference*, vol. 3, pp. 1309-1315, March 2001, Big sky, Montana, USA.

[122] M. Irsigler, B. Eissfeller, "Comparison of multipath mitigation techniques with consideration of future signal structures," *Proc. of the 16th International Technical Meeting of the Satellite Division of The Institute of Navigation (ION GPS/GNSS)*, pp. 2584-2592, September 2003, Portland, OR. USA.

[123] L. Garin, J. M. Rousseau, "Enhanced Strobe Correlator multipath rejection for code and carrier," *Proc. of the 10th International Technical Meeting of the Satellite Division of The Institute of Navigation (ION GPS)*, pp. 559-568, September 1997, Kansas City, MO, USA,.

[124] G. A. McGraw, Rockwell Collins, M. S. Braasch, "GNSS Multipath Mitigation Using Gated and High Resolution Correlator Concepts," *Proc. of the 1999 National Technical Meeting of The Institute of Navigation (ION NTM)*, pp. 333-342, January 1999, San Diego, CA, USA.

[125] H. Hurskainnen, E. S. Lohan, X. Hu, J. Raasakka, J. Nurmi, "Multipath gate delay tracking structure for GNSS signals and their evaluation with Simulink, SystemC, and VHDL," *International Journal of Navigation and Observation,* vol. 2008, Article ID 785695, 2008. *DOI: 10.1155/2008/785695*.

[126] D. Skournetou, E. S. Lohan, "Non-coherent multiple correlator delay structures and their tracking performance for Galileo signals," *Proc. of European Navigation Conference in GNSS (ENC-GNSS)*, pp. 247-258, May-June 2007.

[127] X. Hu, E. S. Lohan, "GRANADA validation of optimized Multiple Gate Delay structures for Galileo SinBOC(1,1) signal tracking," *Proc. of 7th International Conference on ITS Telecommunications (ITST)*, pp. 1-5, June 2007, Sophia Antipolis, France.

[128] M. Z. H. Bhuiyan, J. Zhang, E. S. Lohan, "Enhanced Delay Tracking Performance of a C/N_0-based Two-Stage Tracker for GNSS receivers," *Proc. of the European Navigation Conference on GNSS (ENC-GNSS)*, October 2010, Braunschweig, Germany.

[129] F. Dovis, L. L. Presti, M. Fantino, P. Mulassano, J. Godet, "Comparison between Galileo CBOC candidates and BOC(1,1) in terms of detection performance," *International Journal of Navigation and Observation*, vol. 2008, Article ID 793868, 9 pages, 2008.

[130] H. T. Diessongo, H. Bock, T. Schüler, S. Junker, A. Kiroe, "Exploiting the Galileo E5 wideband Signal," *Inside GNSS*, pp. 64-73, September/October 2012.

[131] J. Zhang, E. S. Lohan, "Galileo E1 and E5a link-level performances in single and multipath channels," *Proc. of the Third international ICST Conference (PSATS)*, pp. 378-390, February 2011, Malaga, Spain.

[132] Y. Tawk, C. Botteron, A. Jovanovic, P. A. Farine, "Analysis of Galileo E5 and E5ab code tracking," *GPS Solution,* online First, Springer, May 2011.

[133] S. Maranò, W. M. Gifford, H. Wymeersch, M. Z. Win, "NLOS identification and mitigation for localization based on UWB experimental data," *IEEE Journal on Selected Areas in Communications*, vol. 28, no. 7, pp. 1026-1035, September 2010.

[134] J. Borras, P. Hatrack, N. B. Mandayam, "Decision theoretic framework for NLOS identification," *Proc. of the 48th IEEE Vehicular Technology Conference (VTC)*, vol. 2, pp. 1583-1587, May 1998, Ottawa, Canada.

[135] N. Alsindi, C. Duan. J. Zhang, T. Tsuboi, "NLOS Channel Identification and Mitigation in Ultra Wideband TOA-based Wireless Sensor Networks," *Proc. of the 6th Workshop on Positioning, Navigation and Communication (WPNC)*, pp. 59-66, March 2009, Hannover, Germany.

[136] S. Venkatesh, R. M. Buehrer, "Non-line-of-sight identification in ultra-wideband systems based on received signal statistic," *IET, Microwaves, Antennas & Propagation*, vol. 1, issue 6, pp. 1120–1130, 2007

[137] K. Yu, Y. J. Guo, "Non-line-of-sight detection based on TOA and signal strength," *Proc. of IEEE 19th International Symposium on Personal, Indoor and Mobile Radio Communications (PIMRC)*, pp. 1-5, September 2008, Cannes, France.

[138] S. Al-Jazzar and J. Caffery, Jr., "New algorithms for NLOS identification," *Proc. of IST Mobile and Wireless Communications Summit*, June 2005, Dresden, Germany.

[139] A. Maali, H. Mimoun, G. Baudoin, A. Ouldali, "Joint TOA estimation and NLOS identification based on UWB energy detection," *Proc. of European Microwave Conference (EuMC)*, pp. 1508-1511, September 2010, Paris, France.

[140] I. Güvenç, C. C. Chong, F. Watanabe, H. Inamura, "NLOS identification and weighted least-squares localization for UWB systems using multipath channel statistics," *EURASIP Journal on Advances in Signal Processing*, vol. 2008, Article no. 36, January 2008.

[141] L. Mucchi, P. Marcocci, "A new UWB indoor channel identification method," *Proc. of* the *2nd International Conference on Cognitive Radio Oriented Wireless Networks and Communications (CrownCom)*, pp. 58-62, August 2007, Orlando, Florida, USA.

[142] I. Guvenc, C. C. Chong, F. Watanabe, "NLOS identification and mitigation for UWB localization systems," *Proc. of IEEE Wireless Communications and Networking Conference (WCNC)*, pp. 1571–1576, 2007, Hong Kong, China.

[143] R. L. Fate, J. J. Vaccaro, "Wideband cancellation of interference in a GPS receiver array," *IEEE Transactions on Aerospace and Electronic Systems*, vol. 2, no. 2, pp. 549-564, 2000.

[144] I. J. Gupta, T. D. Moor, "Space-Frequency Adaptive Processing (SFAP) for Interference Suppression in GPS receiver," *Proc. of the 2001 National Technical Meeting of The Institute of Navigation*, pp. 377-385, January 2001, Long Beach, CA, USA.

[145] D. S. De Lorenzo, *Navigation accuracy and interference rejection for adaptive antenna array*, Doctoral dissertation, Stanford University, August 2007.

[146] J. Zhang, E. S. Lohan, "Effect and mitigation of narrowband interference on Galileo E1 signal acquisition and tracking accuracy," Proc. of *International Conference on Localization and GNSS (ICL-GNSS)*, pp. 36-41, June 2011, Tampere, Finland.

[147] National Academy of Engineering, *Global navigation satellite systems: report of a joint workshop of the national academy of engineering and the Chinese academy of engineering*. National Academies Press, 2012.

[148] A. Rügamer, C. Mongrédian, S. Urquijo, G. Rohmer, "Optimal path-control for dual-frequency overlay GNSS receivers," *Proc. of International Conference on Localization and GNSS (ICL-GNSS)*, pp. 158-163, June 2011, Tampere, Finland.

[149] D. Skournetou, E. S. Lohan, "Ionosphere-corrected range estimation in dual-frequency GNSS receivers," *IET Radar, Sonar and Navigation*, vol. 5, no. 3, pp. 215-224, March 2011.

[150] H. Hurskainen, E. S. Lohan, J. Nurmi, S. Sand, C. Mensing, M. Detratti, "Optimal dual frequency combination for Galileo mass market receiver baseband," *Proc. of IEEE Workshop on Signal Processing Systems (SiPS)*, pp. 261-266, October 2009, Tampere, Finland.

[151] J. A. Klobuchar, "Ionosphere effects on GPS," *GPS World*, pp. 48-51, April 1991.

[152] J. A. Klobuchar, "Ionospheric time-delay algorithms for single-frequency GPS users," *IEEE Transactions on Aerospace and Electronic Systems*, vol. AES-23, no. 3, pp. 325-331, May 1987.

[153] S. M. Radicella, "The NeQuick model genesis, use and evolution," *Annals of geophysics*, vol. 52 (3-4), pp. 417-422, 2009.

[154] B. Nava, P. Coïsson and S.M. Radicella, "A new version of the NeQuick ionosphere electron density model," *Journal of Atmospheric and Solar Terrestrial Physics*, vol. 70, Issue 15, pp. 1856-1862, December 2008.

[155] P. de O. Camargo, J. F. G. Monico, L. D. D. Ferreira, "Application of ionospheric corrections in the equatorial region for L1 GPS users," *Earth, Planet Space*, vol. 52, no. 11, pp. 1083-1089, 2000.

[156] D. Skournetou, E. S. Lohan, "Ionosphere-corrected range estimation in dual-frequency GNSS receivers," in *IET Radar, Sonar and Navigation*, vol. 52, no. 3, pp. 215-224, March 2011.

[157] W. Wang, T. Jost, A. Lehner, F. Perez-Diaz, U. C. Fiebig, "Towards a channel model for joint GNSS and mobile radio based positioning," *Proc. of COST Action IC1004,*

Cooperative Radio Communications for Green Smart Environments, 2011, Lisbon, Portugal.

[158] Simulink open-source software for Galileo E1 and E5 signals, *http://www.cs.tut.fi/tlt/pos/Software.htm*, Tampere University of Technology, accessed Mar 2013.

[159] E. Pajala, E. S. Lohan, M. Renfors, "CFAR detectors for hybrid-search acquisition for Galileo signals," *Proc. of European Navigation Conference (ENC-GNSS)*, July 2005. Munich, Germany.

[160] B. A. Siddiqui, J. Zhang, M. Z. H. Bhuiyan, E. S. Lohan, "Joint data-pilot acquisition and tracking of Galileo E1 open service signal," *Proc. of Ubiquitous Positioning Indoor Navigation and Location Based Services (UPINLBS)*, pp. 1-7, October 2010, Helsinki, Finland.

[161] T. Hekmat, D. Heinrichs, "Dual-frequency receiver technology for mass-market applications," *Proc. of the 14th International Technical Meeting of the Satellite Division of The Institute of Navigation (ION GPS)*, pp. 844-849, September 2001, Salt Lake City, UT, USA.

[162] E. R. Parada, F. Chastellain, C. Botteron, Y. Tawk, P. A. Farine, "Design of a GPS and Galileo multi-frequency front-end," *Proc. of IEEE 69th Vehicular Technology Conference (VTC)*, pp. 1-5, April 2009, Barcelona, Spain.

[163] D. M. Akos, A. Ene, J. Thor, "A prototyping platform for multi-frequency GNSS receivers," *Proc. of the 16th International Technical Meeting of the Satellite Division of The Institute of Navigation (ION GPS/GNSS)*, pp. 117-128, September 2003, Portland, OR, USA.

[164] E. B. Rodal, "Low power GPS receiver," United States Patent, 5650785, June 1997.

Publication I

J. Zhang, E. S. Lohan, “Effect of narrowband interference on Galileo E1 signal receiver performance,” *International Journal of Navigation and Observation*, vol. 2011, Article ID 959871, 10 pages, 2011. DOI:10.1155/2011/959871.

Hindawi Publishing Corporation
International Journal of Navigation and Observation
Volume 2011, Article ID 959871, 10 pages
doi:10.1155/2011/959871

Research Article

Effect of Narrowband Interference on Galileo E1 Signal Receiver Performance

Jie Zhang and Elena-Simona Lohan

Department of Communications Engineering, Tampere University of Technology, 33720 Tampere, Finland

Correspondence should be addressed to Jie Zhang, jie.zhang@tut.fi

Received 19 August 2011; Revised 9 November 2011; Accepted 13 December 2011

Academic Editor: Gyu-In Jee

Satellite navigation technology is becoming essential for civil application. The high-accuracy navigation service is demanded. However, the satellite signal may be exposed to the signal from other systems, which are sharing the same frequency band. This is a potential threat for the performance of navigation devices. The aim of this paper is to present an interference impact assessment in the context of global navigation based on the new modulation Composite Binary Offset Carrier (CBOC) that will be used for Galileo E1 civil signal. The focus is on the analysis of the Galileo CBOC-modulated signal robustness against narrowband interference.

1. Introduction

Satellite navigation is a process of providing autonomous global geospatial position with coverage all over the world. The navigation technology is essential for several civil applications, such as in the transportation field (e.g., road, rail, and aviation). Other applications, such as precision agriculture, wildlife behavior monitoring, surveying, and time-based applications are also based on the estimation of users' Position, Velocity, and Time (PVT) [1]. These applications, especially the ones dealing with safety, require high accuracy of users' PVT estimation.

The Global Navigation Satellite Systems (GNSSs) signals are allocated to Radio Navigation Satellite Services (RNSSs) and Aeronautical Radio Navigation Services (ARNSs) on a worldwide coprimary basis. However, the Global Navigation Satellite Systems (GNSSs) signals may be exposed to potential interference from other services that are sharing the similar frequency band. They could likely represent potential threats for GNSS devices. The interference may degrade the GNSS receivers' performance and compromise the safety.

Potential interferences are largely emanated from unintentional source or intentional jamming and spoofing of GNSS signal. Radio frequency interference (RFI) is one of the unintentional interference sources, whose frequency might be located in the satellite signal bands. RFI is normally classified as either wideband or narrowband, depending on whether its bandwidth is large or small relative to the bandwidth of the desired GNSS signal. Wideband interference can be a Gaussian waveform as in the case of Ultra-Wideband (UWB) systems or harmonic from television transmission overcoming the front-end filter of a GNSS receiver [2]. Narrowband interference could originate from Amplitude Modulation (AM) or Frequency Modulation (FM) station.

The interference represents an impairing factor in GNSS application mainly due to the low power of the GNSS signal at the earth surface. The GNSS receiver may fail to acquire and track the satellite signals in the present of interference. Reports of measurement campaigns like [3] have shown that unaided GNSS receiver could experience loss of lock near FM and TV broadcast transmitter. Thus, it is important to have better understanding of the effects of RFI on GNSS receiver, in order to improve mitigation solutions.

The effect of narrowband interference has been assessed in the context of Global Positioning System (GPS) C/A signal in both theory and experiments [4–7]. However, the effect of narrowband interference on Galileo E1 signal, which is

sharing the same frequency band with GPS C/A signal, has not been studied much. The code tracking performance in the presence of narrowband interference in Galileo E1 signal receiver may differ from that in the GPS signal due to different modulation used in Galileo E1 band [8, 9]. Moreover, the modulation type of local replica used in a receiver could be different than that used in the transmitter [10, 11]. Therefore, the theoretical equation developed by Betz [4] for evaluating the effect of narrowband interference on GPS C/A signal cannot be directly applied to the Galileo E1 signal. This is because it does not consider the aspect of receiver modulation type. The mathematical model needs to be modified in order to consider the modulation used in the receiver.

To summarize the above discussion, the effect of narrowband interference on Galileo E1 signal receiver, where the receiver type is also taken into account from both theory and simulations has not been evaluated. The goal of this paper is to present an analytical code tracking model of Galileo E1 signal in the presence of narrowband interference and evaluate the robustness of E1 signal towards the narrowband interference, taking into account the impact of different modulation types in the receiver. The code tracking accuracy of two tracking loops is compared: noncoherent early-minus-late correlator (NELP) and coherent early-minus-late processing (CELP). The Cramér-Rao Lower Bound (CRLB) is used as reference in the delay tracking error studies. The results are also compared with simulations, which have been done with an open source Simulink simulator, Galileo E1 signal Tx-Rx chain built at Tampere University of Technology [12]. The details of this simulator will be introduced in the following section.

The rest of the paper will be organized as follows: Section 2 presents the overview on the research of narrowband interference effects on GPS C/A signal. Section 3 compares the difference between Galileo E1 signal and GPS L1 signal and presents the modified analytical expression for Galileo E1 signal and numerical results, which takes the receiver modulation type into account. Section 4 summarizes the setup of the simulator. Simulation results are presented and discussed in Section 5, and finally, the conclusions are drawn in Section 6.

2. Effect of Narrowband Interference on GPS Signal

It is well known that a GNSS receiver can be exposed to many classes of undesired signals. Much research on effects of narrowband interference on GPS C/A signal has been conducted [4–6]. One of the most popular analytical models of GPS C/A signal code tracking in the presence of narrowband interference is introduced in [4, 6]. This analysis uses complex baseband representations of signal and noise, and lowpass equivalent models of filtering and processing. From the mathematic point of view, it shows that the variance of the code tracking error (in chip) for CELP and equivalent expression for NELP are shown in (1) and (2) [4, 6],

$$(\sigma^2)_{\mathrm{CELP}} = B_L(1-0.5B_LT)\times\left[\frac{\int_{-\beta_r/2}^{\beta_r/2} G_W(f)G_S(f)\sin^2(\pi f\Delta)df}{(2\pi)^2C_S\left(\int_{-\beta_r/2}^{\beta_r/2} fG_S(f)\sin(\pi f\Delta)df\right)^2}\right], \tag{1}$$

$$(\sigma^2)_{\mathrm{NELP}} = B_LT(1-0.5B_LT)\times\left[\frac{\int_{-\beta_r/2}^{\beta_r/2} G_W(f)G_S(f)\sin^2(\pi f\Delta)df}{(2\pi)^2C_S\left(\int_{-\beta_r/2}^{\beta_r/2} fG_S(f)\sin(\pi f\Delta)df\right)^2} + \frac{\left(\int_{-\beta_r/2}^{\beta_r/2} G_W(f)G_S(f)df\right)^2 - \left|\int_{-\beta_r/2}^{\beta_r/2} G_W(f)G_S(f)e^{i2\pi f\Delta}df\right|}{4(2\pi)^2TC_S^2\left(\int_{-\beta_r/2}^{\beta_r/2} fG_S(f)\sin(\pi f\Delta)df\int_{-\beta_r/2}^{\beta_r/2} fG_S(f)\cos(\pi f\Delta)df\right)^2}\right], \tag{2}$$

where $G_S(f)$: normalized GPS C/A BPSK signal spectrum $G_S(f) = T_C\mathrm{sinc}^2(\pi fT_C)$ with $\int_{-\infty}^{\infty} G_S(f) = 1$, where $\mathrm{sinc}(y) = \sin(y)/y$ and T_C is the chip period; $G_W(f)$: $G_W(f) = N_0 + C_lG_l(f)$; N_0 is power density of the noise; $G_l(f)$ is normalized power spectrum density of interference with $\int_{-\infty}^{\infty} G_l(f) = 1$; C_l is the interference carrier power over infinite bandwidth; the noise and interference are each represented as zero mean, wide sense stationary stochastic process, independent of the signal, and statistically uncorrelated with each other; C_S: power of the signal; β_r: receiver front-end double-sided bandwidth; Δ: early-late spacing in second; B_L: one-sided equivalent rectangular bandwidth of the code tracking loop in Hz; T: Integration time in seconds used in the discriminator.

The Cramér-Rao lower bound of time-of-arrival estimation for integration time T, then assuming the estimates are smoothed with the code tracking loop:

$$(\sigma^2)_{\mathrm{LB}} = \frac{B_L(1 - 0.5B_LT)}{(2\pi)^2 C_S \int_{-\beta_r/2}^{\beta_r/2} f^2 (G_S(f)/G_W(f))\,df}. \quad (3)$$

These theoretical expressions predict the performance of a GPS receiver in narrowband interference. They show that the interference near the carrier frequency has little effect on code tracking error, interference at a frequency midway between the carrier frequency, and first null has greater effect [4].

3. Effect of Narrowband Interference on Galileo Signal

The equations above are derived for GPS L1 Binary Phase Shift Keying (BPSK) modulated signal. In order to check if above equations are applicable to Galileo E1 CBOC-modulated signal, we need to first have the knowledge of what is new in the CBOC modulation.

Galileo E1 signal and GPS L1 signal are allocated at the same carrier frequency. In order to minimize the interference between two signals, a new type of modulation, named "Multiplex Binary Offset Carrier (MBOC)" will be used on the Galileo E1 signal. The main idea behind MBOC is to minimize the interference with GPS L1 signal and to put a small amount of power on higher frequency, which could improve the code tracking performance [8, 9]. In the latest Galileo Open Service Signal In Space Interface Control Document (OS SIS ICD) [13], Composite Binary Offset Carrier (CBOC) modulation, which is one of the implementation of MBOC is assigned for Galileo E1 band. This implementation is the sum (or difference) of two weighted Sine-Binary Offset Carrier (SinBOC) subcarrier waves [8]. The one used in E1 band is denoted via CBOC(6,1,1/11). It is the sum (or difference) of a SinBOC(1,1)-modulated code and a SinBOC(6,1)-modulated code, which includes 1/11 power from SinBOC(6,1) component (and 10/11 power from SinBOC(1,1) component). Mathematically, the power spectral density (PSD) of CBOC(6,1,1/11) is

$$G_{\mathrm{CBOC}(6,1,1/11)}(f) = \frac{10}{11} G_{\mathrm{SinBOC}(1,1)}(f) + \frac{1}{11} G_{\mathrm{SinBOC}(6,1)}(f), \quad (4)$$

where $G_{\mathrm{SinBOC}(m,n)}(f)$ is the normalized PSD of a Sine-BOC(m,n)-modulation, given by [10, 14]:

$$G_{\mathrm{SinBOC}(m,n)}(f) = \frac{1}{T_c}\left(\frac{\sin(\pi(T_c/N_B))\sin(\pi f T_c)}{\pi f \cos(\pi(T_c/N_B))}\right)^2. \quad (5)$$

Here $T_c = 1/fc$, fc is chip rate (1.023 MHz for E1 signal); the BOC modulation order (N_B) is defined as $N_B = 2 * (m/n)$. In time domain, CBOC(6,1,1/11) has several variables. The variables CBOC(+), which are the sum of two SinBOC signal, will be used in the data channel of E1 signal, and CBOC(−), where two SinBOC waves are subtracted, will be used in the pilot channel in E1 signal.

Normalized PSD of CBOC(6,1,1/11), SinBOC(1,1)- and BPSK-modulated signals are shown in Figure 2. Compared with the PSD of BPSK, there are two main lobes located symmetrically around the center frequency in PSD of CBOC(6,1,1/11)- and SinBOC(1,1)-modulated signals. The CBOC(6,1,1/11) has additional power at about ±6 MHz away from the center frequency.

As seen from (4), the transmitted E1 CBOC-modulated signal consists of two SinBOC signals, and more than 90% of signal power is from SinBOC(1,1) component. Therefore, the CBOC signal receiver could use either the CBOC modulated local replica in the receiver or SinBOC(1,1) modulated replica [10, 11, 15]. However, using difference modulation at the receiver side may cause the change on the signal power spectrum in the receiver. In order to check the impact of the modulation type in the receiver, we can model the transmitter-receiver chain for Galileo E1 signal as shown in Figure 1. The modulation at the transmitter is characterized by the transfer function $H_{\mathrm{Tx}}(f)$, which is the CBOC modulation transfer function. The Additive White Gaussian Noise and narrowband interference are then added in the transmitted signal. The front-end filter is used to limit the signal bandwidth, which is characterized by $B(f)$. After the front-end filter, the local replica $H_{\mathrm{Rx}}(f)$ at the receiver side is modulated with modulation whose transfer function is either $H_{\mathrm{CBOC}}(f)$ or $H_{\mathrm{BOC}}(f)$. The $G(f)$ is the signal part in the correlation between the received signal and modulated local replica. Depending on the modulation type used in the receiver, it can be expressed as:

$$G(f) = C_S \left| H_{\mathrm{Tx}}(f) H_{\mathrm{Rx}} * (f) \right|. \quad (6)$$

When the transmitter and receiver both have CBOC modulation type, (6) becomes

$$G(f) = C_S \left| H_{\mathrm{CBOC}}(f) H_{\mathrm{CBOC}} * (f) \right|. \quad (7)$$

When the receiver uses SinBOC(1,1)-modulated local replica, the PSD will be:

$$G(f) = C_S \left| H_{\mathrm{CBOC}}(f) H_{\mathrm{SinBOC}(1,1)} * (f) \right|. \quad (8)$$

Above, $H_{\mathrm{CBOC}}(f)$ and $H_{\mathrm{BOC}}(f)$ are the transfer function of CBOC and SinBOC modulations as shown in (9) [10]:

$$\begin{aligned} H_{\mathrm{CBOC}}(f) &= e^{-j\pi f T_C} \frac{\sin(\pi f T_C)}{\pi f} \\ &\quad \times \left(w_1 e^{-j\pi f (T_C/2)} \tan\left(\frac{\pi f T_C}{2}\right) + a w_2 \tan\left(\frac{\pi f T_C}{12}\right)\right), \\ H_{\mathrm{BOC}(1,1)}(f) &= e^{-j\pi f (3T_C/2)} \frac{\sin(\pi f T_C)}{\pi f} \tan\left(\frac{\pi f T_C}{2}\right), \end{aligned} \quad (9)$$

where T_C is chip rate; w_1, w_2 are weighting factor satisfying $w_1^2 + w_2^2 = 1$ (e.g., $w_1 = \sqrt{10/11}$, $w_2 = \sqrt{1/11}$ for CBOC(6,1,1/11)) and $a = \pm 1$ is a weight factor that used

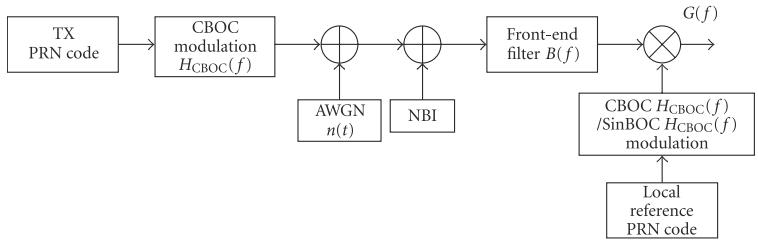

Figure 1: Block diagram of CBOC transmitter with reference CBOC- or SinBOC-modulated code at receiver.

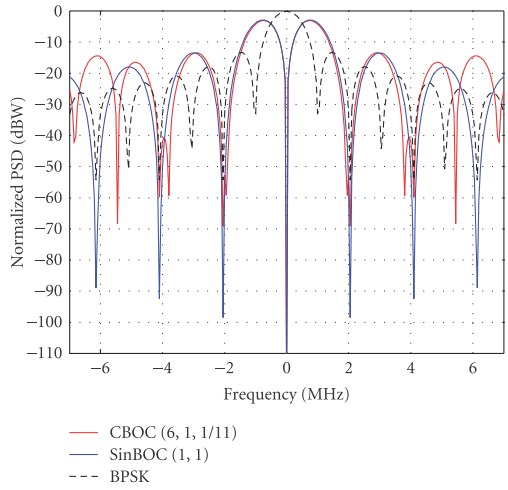

Figure 2: Normalized PSD of CBOC-, SinBOC(1,1)-, and BPSK-modulated signal.

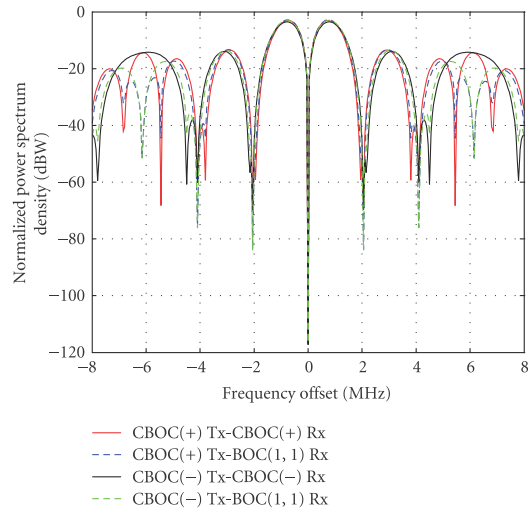

Figure 3: Normalized PSDs of CBOC-modulated signal receiver with CBOC reference code or SinBOC(1,1) reference code.

for data channels (for CBOC(+), $a = 1$) and pilot channel (for CBOC(−), $a = -1$).

Usually the normalized PSDs are used [16] instead of the expression given above. The normalization is done in such a way that the signal has unit power over infinite bandwidth [10]. The normalized PSD for the two different receiver type are then:

(A) *Rx with CBOC reference code*:

$$\overline{G(f)} = \frac{C_S \left| H_{\mathrm{CBOC}}(f) H_{\mathrm{CBOC}} * (f) \right|}{\int_{-\infty}^{\infty} C_S \left| H_{\mathrm{CBOC}}(f) H_{\mathrm{CBOC}} * (f) \right| df}, \quad (10)$$

(B) *Rx with SinBOC reference code*:

$$\overline{G(f)} = \frac{C_S \left| H_{\mathrm{CBOC}}(f) H_{\mathrm{SinBOC}(1,1)} * (f) \right|}{\int_{-\infty}^{\infty} C_S \left| H_{\mathrm{CBOC}}(f) H_{\mathrm{SinBOC}(1,1)} * (f) \right| df}. \quad (11)$$

If we plot (10) and (11) as shown in Figure 3, there is almost no difference between the two transmitter-receiver modulation combinations within the main lobe (between ±2 MHz). However, outside the main lobe, difference between the power spectrums can be observed. When the BOC modulation is used in the receiver, the power spectrum from $4fc$ to $6fc$ has changed compared with the spectrum shown in Figure 2. The additional power is attenuated in the receiver. It means that the effect of narrowband interference will be changed. These changes on code tracking performance are analyzed in the next section.

4. Code Tracking Error Variances

After we derive the signal power spectrum in the receiver, the code tracking error variance shown in (2) needs to be modified accordingly. The $G_S(f)$ needs to be replace by the new derived $\overline{G(f)}$. Equation (2) will then become as follows:

$$(\sigma^2)_{\text{NELP\_E1}} = B_L T(1-0.5B_L T)\times\left[\frac{\int_{-\beta_r/2}^{\beta_r/2} G_W(f)\overline{G(f)}\sin^2(\pi f\Delta)df}{(2\pi)^2 C_S\left(\int_{-\beta_r/2}^{\beta_r/2} f\overline{G(f)}\sin(\pi f\Delta)df\right)^2}\right.$$
$$\left.+\frac{\left(\int_{-\beta_r/2}^{\beta_r/2} G_W(f)\overline{G(f)}df\right)^2-\left|\int_{-\beta_r/2}^{\beta_r/2} G_W(f)\overline{G(f)}e^{i2\pi f\Delta}df\right|}{4(2\pi)^2 TC_S^2\left(\int_{-\beta_r/2}^{\beta_r/2} f\overline{G(f)}\sin(\pi f\Delta)df\int_{-\beta_r/2}^{\beta_r/2} f\overline{G(f)}\cos(\pi f\Delta)df\right)^2}\right]. \tag{12}$$

The tracking error variance for a coherent early-minus-late processing (CELP) in the presence of narrowband interference then becomes

$$(\sigma^2)_{\text{CELP\_E1}} = B_L(1-0.5B_L T)\times\left[\frac{\int_{-\beta_r/2}^{\beta_r/2} G_W(f)\overline{G(f)}\sin^2(\pi f\Delta)df}{(2\pi)^2 C_S\left(\int_{-\beta_r/2}^{\beta_r/2} f\overline{G(f)}\sin(\pi f\Delta)df\right)^2}\right]. \tag{13}$$

Accordingly, the Cramér-Rao Lower Bound (CRLB) in the presence of narrowband interference is then:

$$(\sigma^2)_{\text{LB\_E1}} = \frac{B_L(1-0.5B_L T)}{(2\pi)^2 C_S\int_{-\beta_r/2}^{\beta_r/2} f^2\left(\overline{G(f)}/G_W(f)\right)df}. \tag{14}$$

Based on the theoretical prediction above, we provide numerical results in order to have some insights, which are difficult to obtain from the analytical expression. For all of the following numerical results, the E1 signal power is -164 dBW, and the noise power density is -204 dBW/Hz, yielding a signal carrier to noise density ratio (C/N_0) of 40 dB-Hz. The integration time used to compute the code tracking variance is 4 ms. The front-end filter of the receiver has two different bandwidths: 4 MHz, which covers the main lobe of E1 signal power spectrum, and 14 MHz, which also includes the power allocated in the higher frequency component.

The interference used for these numerical results is the band limited Gaussian noise with 10 kHz bandwidth and varying center frequency and power. The standard deviation of code tracking, which is the square root of code tracking variance, is analyzed as a function of the interference center frequency. It shows the effect of different placement of the interference relative to E1 signal band center. The effect of narrowband interference with varying power at fixed frequency is also studied below.

Figure 4 gives the standard deviation of code tracking error comparison between BPSK signal and CBOC-modulated signal in the presence of narrowband interference. Here, for both signals, the receiver uses the same modulation as in transmitter. As we can see that, the CBOC signal has better overall performance against the narrowband interference than the BPSK signal. This is because of the additional power on the high frequency in CBOC modulation and the narrower peak in the autocorrelation function of CBOC modulation compared with that of BPSK. For both BPSK- and CBOC-modulated signals, when the interference center frequency matches the E1 carrier, the interference does not affect the useful signal. This is because the interference is eliminated by the downconversion from Intermediate Frequency (IF) to baseband. The biggest effect of narrowband interference on CBOC signal happens at $\pm 1fc$, $\pm 3fc$, $\pm 5fc$ away from the carrier. However, these points are the frequencies at where the interference in GPS BPSK signal has the minimum effect. This would be very useful in dual-system receiver, which is using GPS L1 and Galileo E1 signal, since the receiver can switch between tracking Galileo E1 signal and GPS L1 signal based on the detected interference frequency to avoid the big effect on the tracking performance.

The relative performance of the three considered discriminators (NELP, CELP, and CRLB) versus the interference frequency offset when the receiver utilizes the same modulation as in the transmitter is shown in Figure 5. It can be observed that the narrowband interference has the biggest effect when the interference is allocated at $1fc$ (1.023 MHz) away from the carrier. The effect is decreasing when the interference is moving away from the carrier. At $6fc$, the degradation in the tracking performance is increased.

If we compare the tracking performance in presence of narrowband interference when the receiver uses difference modulation as shown in Figure 6, the CBOC(−) Tx-BOC(1,1) Rx combination is more robust towards the narrowband interference than other combinations. In general, if the front-end bandwidth is wide enough, using BOC modulation in the receiver has worse tracking performance than using CBOC modulation in the receiver due to the loss of signal power. However, it gives better performance if the interference is at $6fc$ away from the carrier.

As shown in Figure 7, when the receiver front-end bandwidth is getting narrower, there is no big difference in the code tracking performance of the different transmitter-receiver modulation combinations in the presence of narrowband interference.

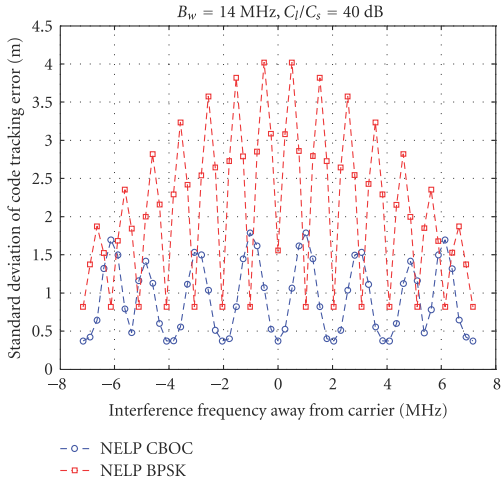

Figure 4: Standard deviation of code tracking error versus the center frequency of narrowband interference with CBOC and BPSK signal.

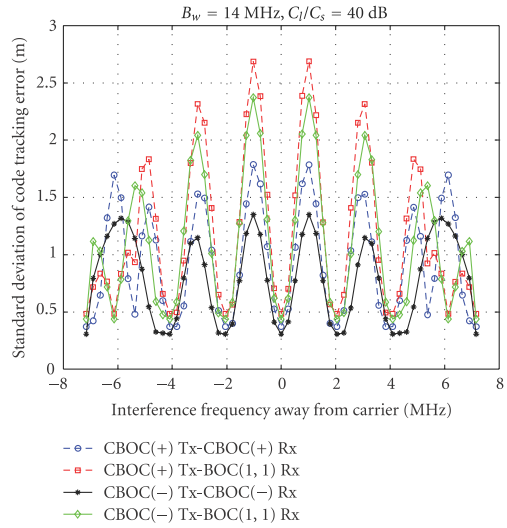

Figure 6: Standard deviation of code tracking error versus narrowband interference center offset for different Tx-Rx modulation combinations for 14 MHz front-end bandwidth.

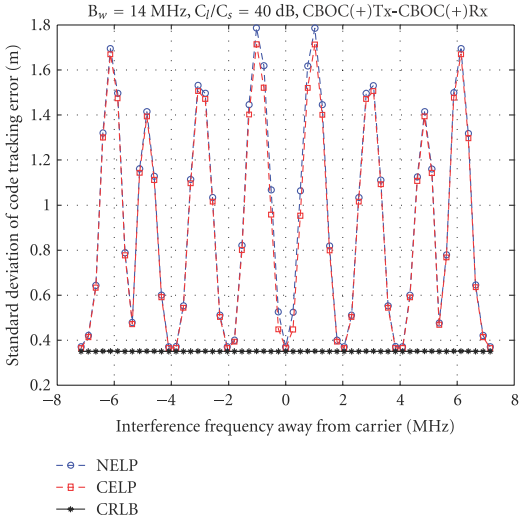

Figure 5: Standard deviation of code tracking error versus the center frequency of narrowband interference with CBOC signal.

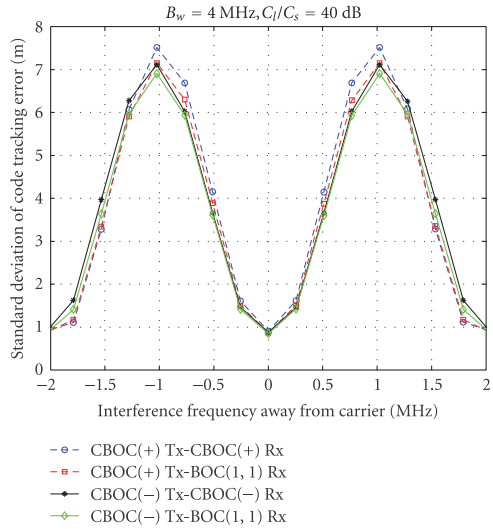

Figure 7: Standard deviation of code tracking error versus narrowband interference center offset for different Tx-Rx modulation combinations for 4 MHz front-end bandwidth.

Figure 8 shows the code tracking standard deviation for different interference power when the interference is placed at 1*fc* away from the carrier. The CBOC(−) modulation in the transmitter with CBOC(−) modulation in the receiver again shows the best resistance against the narrowband interference.

For the −105 dBW interference power, which is 60 dB higher than the signal, the CBOC(−)-CBOC(−) combination has up to 12 meters less error than the CBOC(+)-BOC(1,1) combination. On the other hand, if the narrowband interference is located at 6*fc* away from the carrier, the CBOC modulation in the transmitter with BOC modulation

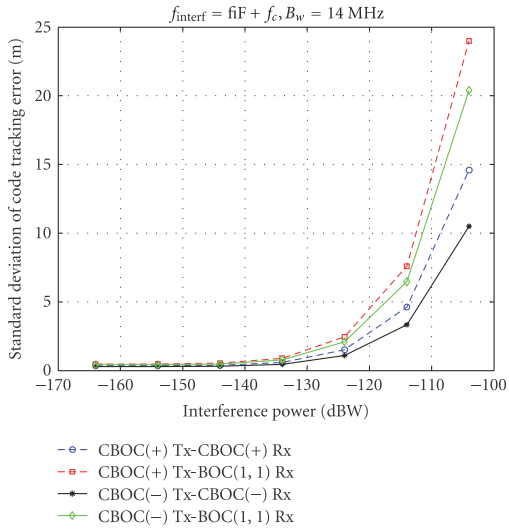

Figure 8: Standard deviation of code tracking error versus interference power when the interference is located at 1fc away from the carrier.

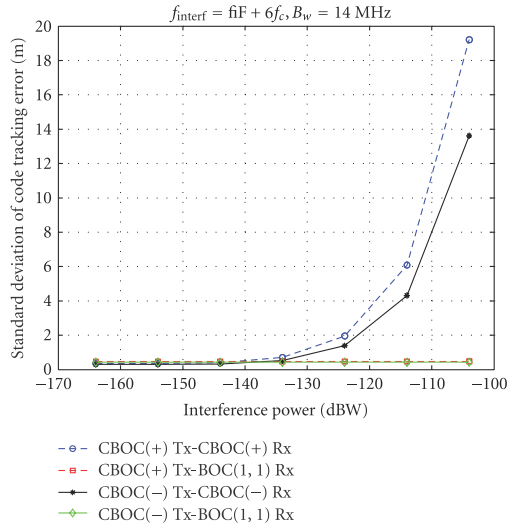

Figure 9: Standard deviation of code tracking error versus interference power when the interference is located at 6fc away from the carrier.

in the receiver has big advantage that the code tracking performance does not degrade with the incensement of interference power as shown in Figure 9.

5. Simulation Setup

In order to validate the analytical expression derived in the previous section, the effect of narrowband interference is also evaluated in a link-level simulator [12]. This link-level simulator is an open source Galileo E1 signal Simulink simulator build at Department of Communications Engineering at Tampere University of Technology. The block diagram of this simulator is shown in Figure 10.

The transmitter block is implemented based on CBOC modulation, including primary code and secondary code, in accordance with the latest Galileo OS SIS ICD [13]. The transmitter consists of two channels, E1B and E1C. E1B is CBOC(+)-modulated signal with navigation data and E1C is CBOC(−)-modulated signal with a predefined bit sequence of CS25 (i.e., pilot channel). The E1 signal is formed as the difference between those two signals. The signal at the output of the transmitter is at IF. The channel generates multipath and complex Additive White Gaussian Noise (AWGN) according to user-defined C/N_0. In this paper, we only consider single-path scenarios in order to focus on the narrowband interference effects. The receiver's front-end filter is a Chebyshev type I filter. The tracking is implemented separately for E1B channel and E1C channel. The reference code can be either CBOC-modulated (i.e., CBOC(+) for E1B channel and CBOC(−) for E1C channel), or SinBOC(1,1)-modulated code for both E1B and E1C channels. The synchronization in the receiver is done

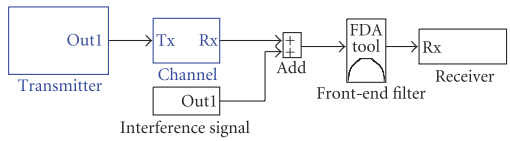

Figure 10: Galileo E1 Tx-Rx chain Simulink simulator.

Table 1: Simulation parameters.

Simulation parameters	Value
Sampling frequency (MHz)	26
Front-end bandwidth (double-sided) (MHz)	4/13
B_L (Hz)	1
Integration time T (ms)	4
Desired signal C_S/N_0 (dB-Hz)	45
Interference signal C_I/N_0	85
Interference signal BW (kHz)	10

based on a Delay Lock Loop (DLL). In the discriminator, the Narrow Correlator (NCORR) [17] is used. The equivalent rectangular bandwidth of the code tracking loop is set to 1 Hz (double-sided).

Power levels of the desired signal and thermal noise were set to produce a signal with C/N_0 of 45 dB-Hz. The narrowband interference is generated as that the white Gaussian noise passes through a bandpass filter (see Figure 11). The center frequency of the bandpass filter defines the interference center frequency. The simulation parameters are summarized in Table 1.

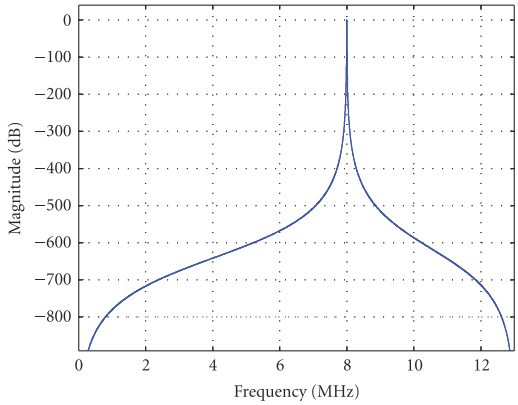

Figure 11: Example of bandpass filter use for generating narrowband interference.

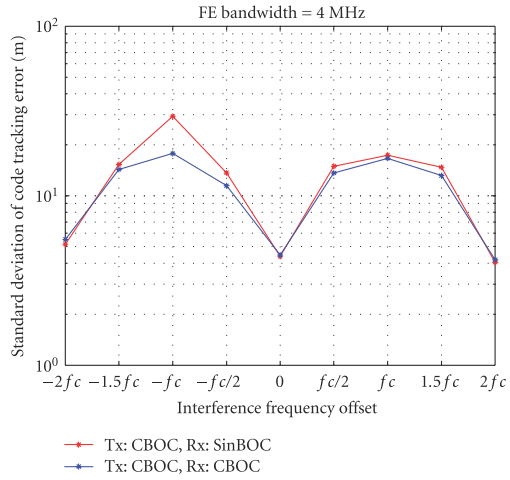

Figure 12: Code tracking error versus interference frequency offset related to carrier when front-end bandwidth is 4 MHz.

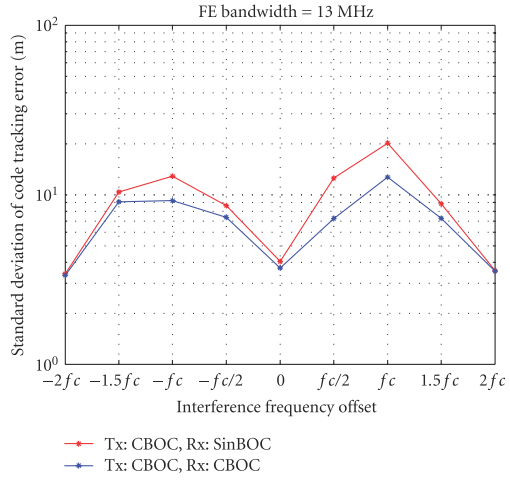

Figure 13: Code tracking error versus interference frequency offset related to carrier when front-end bandwidth is 13 MHz.

6. Simulation Results

In this section, the simulation results of code tracking performance in the presence of narrowband interference are presented along with the discussion. The performance criteria are based on standard deviation of code tracking error, which is obtained from the Simulink model. One thing need to be mentioned here is that the results from Simulink simulation cannot be directly compared with the theoretical results. It is because the simulator tracks the CBOC(+) and CBOC(−) signals at the same time, and the code tracking output is the average of tracking output from both signals.

Figure 12 shows the standard deviation of code tracking error for different interference location. It can be observed that the biggest effect happens at $\pm fc$ away from the carrier for both receiver types. The CBOC receiver has a little better performance than SinBOC receiver against the narrowband interference within the front-end bandwidth. This is because of the narrower peak in the CBOC autocorrelation function than that in the SinBOC correlation function. The same simulations have also been done with wider front-end bandwidth as shown in Figure 13. Compared with the results in Figure 12, the tracking error is smaller regardless of receiver type. The difference between the code tracking with CBOC and SinBOC receiver is bigger, because the additional power is located at high frequency.

Figures 14 and 15 show the code tracking performance for the incensement of interference power when the interference is located at $1fc$ and $6fc$ away from the carrier, respectively. As can be seen, for both CBOC receiver and SinBOC receiver, when the interference is placed at $1fc$, the code tracking performance is getting worse with the incensement of interference power and CBOC receiver is more robust towards the interference when the interference to signal power ratio is very high. This is consistent with the results shown in Figure 8. When the interference is located at $6fc$ away from the carrier, the receiver which uses SinBOC modulation has much better code tracking performance than the receiver uses CBOC modulation. This is because that there is a null in the PSD of SinBOC-modulated signal at $6fc$ from carrier frequency. The interference will not affect the useful signal.

7. Conclusions

This paper has evaluated the robustness of CBOC signal towards the narrowband interference, taking into count the impact of modulation type in receiver. This paper has first overviewed the analytical model for tracking GPS BPSK signal in the presence of narrowband interference. Then

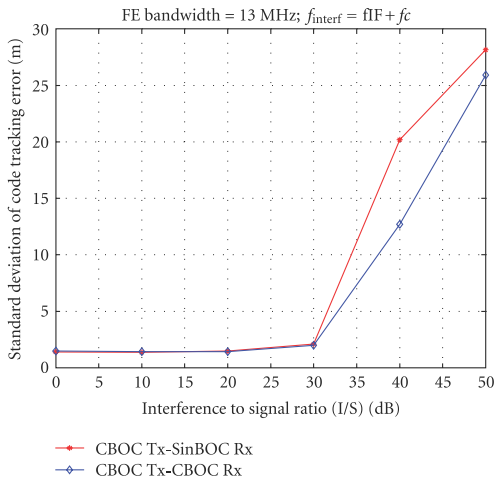

Figure 14: Code tracking error versus interference to signal power ratio when the interference is located at 1fc away from the carrier.

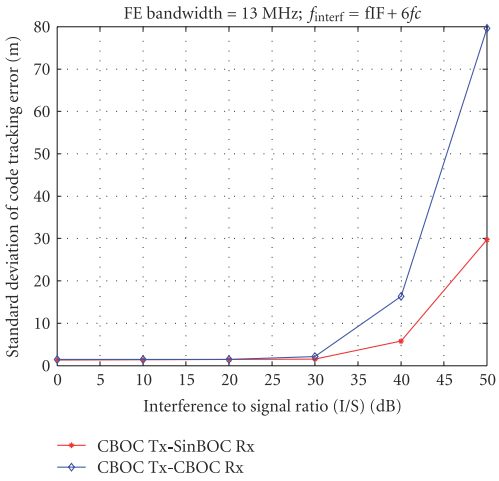

Figure 15: Code tracking error versus interference to signal power ratio when the interference is located at 6fc away from the carrier.

the difference between the BPSK and CBOC modulation has been discussed and the impact of the modulation type in the receiver is analyzed theoretically. The analytical model for code tracking of Galileo CBOC signal in the presence of narrowband interference is presented according to the discussion of modulation type impact. The results are shown based on both derived mathematical equation and simulation in a link-level Simulink simulator.

The results obtained from the theoretical expression show that CBOC signal is more robust than the GPS BPSK signal towards the narrowband interference. For CBOC signal, regardless of the modulation type in the receiver, the narrowband interference has little effect on the carrier frequency and has the most effect when the interference is placed at one chip rate away from the carrier. The modulation used in the receiver has impact on the code tracking performance in the presence of narrowband interference of CBOC signal. In general, the CBOC receiver has better performance against the narrowband interference than the SinBOC receiver. However, if the interference is located at 6fc away from the carrier, the CBOC receive does not give any benefit against strong interference.

For future work, the theoretical and simulation results presented here regarding the performance of E1 CBOC signal in the presence of narrowband interference will be confirmed in a hardware setup.

Acknowledgments

The research leading to these results has received funding from the European Union's Seven Framework Programme (FP7/2007–2013) under the Grant Agreement n227890 (GRAMMAR project) and from Academy of Finland, which are gratefully acknowledged. The authors would also like to thank Nokia Foundation and Tekniikan edistämissäätiö (TES) for their support.

References

[1] B. Motella, S. Savasta, D. Margaria, and F. Dovis, "A method to assess robustness of GPS C/A code in presence of CW interferences," *Hindawi International Journal of Navigation and Observation*, vol. 2010, Article ID 294525, 8 pages, 2010.

[2] E. D. Kaplan and C. Hegarty, *Understanding GPS: Principles and Applications*, Artech House Publishers, 2nd edition, 2005.

[3] F. Klinker and O. B. M. Piestersem, *Interference of GPS signal, Influence of Licensed Transmitter on GPS signal Quality in the Netherlands' Airspace*, National Aerospace Laboratory, 2000.

[4] J. W. Betz, "Effect of narrowband interference on GPS code tracking accuracy," in *Proceedings of the 2000 National Technical Meeting of The Institute of Navigation*, pp. 16–27, Anaheim, Calif, USA, January 2000.

[5] J. W. Betz, "Effect of partial-band interference on receiver estimation of C/N0: theory," in *Proceedings of the National Technical Meeting of The Institute of Navigation*, pp. 817–828, Long Beach, Calif, USA, January 2001.

[6] K. R. Kolodziejski and J. W. Betz, "Effect of non-white gaussian interference on GPS code tracking accuracy," The MITRE Corporation Technical Report MTR99B21R1, 1999.

[7] H. Chris, T. Michael, and L. Young, "Simplified techniques for analyzing the effects of non-white interference on GPS receivers," in *Proceedings of the 15th International Technical Meeting of the Satellite Division of The Institute of Navigation (ION GPS '02)*, pp. 620–629, Portland, Ore, USA, September 2002.

[8] J. A. Avila-Rodriguez, S. Wallner, and G.W. Hein, "CBOC—an implementation of MBOC," in *Proceedings of the 1st CNES Workshop on Galileo Signals and Signal Processing*, Tolouse, France, October 2006.

[9] G. W. Hein, J. A. Avila-Rodriguez, S. Wallner et al., "MBOC: the new optimized spreading modulation recommended for

GALILEO L1 OS and GPS L1C," in *Proceedings of the IEEE/ION Position, Location, and Navigation Symposium*, pp. 883–892, April 2006.

[10] E. S. Lohan, "Analytical performance of CBOC-modulated Galileo E1 signal using sine BOC(1,1) receiver for massmarket applications," in *Proceedings of the IEEE PLANS, Position Location and Navigation Symposium*, pp. 245–253, Indian Wells, Calif, USA, May 2010.

[11] J. Zhang and E. S. Lohan, "Multi-correlator structures for tracking Galileo signals with CBOC and SinBOC(1,1) reference receivers and limited front-end bandwidths," in *Proceedings of the 7th Workshop on Positioning, Navigation and Communication (WPNC '10)*, pp. 179–186, Dresden, Germany, March 2010.

[12] Simulink open-source software for Galileo E1 signals, Tampere University of Technology, http://www.cs.tut.fi/tlt/pos/Software.htm.

[13] Galileo Open Service Signal In Space Interface Control Document, (SIS-ICD08), http://www.gsa.europa.eu/go/galileo/os-sis-icd/galileo-open-service-signal-in-space-interface-control-document.

[14] J. W. Betz, "The Offset Carrier Modulation for GPS modernization," in *Proceedings of the National Technical Meeting of The Institute of Navigation*, pp. 639–648, 1999.

[15] B. A. Siddiqui, J. Zhang, M. Z. H. Bhuiyan, and E. S. Lohan, "Joint Data-Pilot acquisition and tracking of Galileo e 1 Open Service signal," in *Proceedings of the Ubiquitous Positioning Indoor Navigation and Location Based Service (UPINLBS '10)*, pp. 1–7, October 2010.

[16] G. Artaud, L. Ries, J. Dantepal, J. Issler, T. Grelier, and A. Delatour, "CBOC performances using software receiver," in *Proceedings of the 2nd Workshop on GNSS Signals & Signal Processing (GNSS SIGNALS '07)*, Nordwijk, Netherlands, October 2007.

[17] J. W. Betz and K. R. Kolodziejski, "Extended theory of early-late code tracking for a bandlimited GPS receiver," *Journal of the Institute of Navigation*, vol. 47, no. 3, pp. 211–226, 2000.

Publication II

J. Zhang, E. S. Lohan, “Galileo E1 and E5a link-level performance for dual frequency overlay structure,” *ICST Transactions on Ubiquitous Environments journal*, 2012.
DOI: 10.4108/trans.ubienv.2012.e3.

ICST Transactions
on Ubiquitous Environments

Research Article ICST.ORG

Galileo E1 and E5a Link-level Performance for Dual Frequency Overlay Structure

Jie Zhang*, Elena-Simona Lohan

Tampere University of Technology, Korkeakoulunkatu 10, FI-33720 Tampere, Finland

Abstract

The emerging European global satellite system Galileo has gained much public interest regarding location and position services. Two Galileo Open Service signals, namely E1 and E5, will provide the frequency diversity. The dual-frequency receiver will greatly enhance the performance of satellite navigation. However, the dual-frequency receiver becomes more complex since it needs to process two signals. Using common front-end components and common baseband for all the signals is a popular concept in literature in order to decrease the complexity. In this concept, two signals will be combined before the common baseband. The signals will then interfere with each other and the radio frequency (RF) interference in one signal band may also appear in other signal bands after the signal superposition. This article investigates the impact of interference due to the signal superposition on code tracking.

Keywords: Galileo, E1/E5a, dual frequency receiver, common baseband, signal superposition, interference, code tracking, Simulink, simulators.

Received on 30 September 2011; accepted on 5 January 2012; published on 29 March 2012

doi: 10.4108/trans.ubienv.2012.e3

1. Introduction

Satellite navigation is a process of providing autonomous global geo-spatial position with coverage all over the world. The navigation technology is essential for several civil applications, such as in the transportation field (e.g., road, rail and aviation). Other applications, such as precision agriculture, wildlife behaviour monitoring, surveying and time based applications are also based on the estimation of users' Position, Velocity and Time (PVT) [1]. These applications, especially the ones dedicate to safety, require high accuracy of users PVT estimation.

The increasing demands for navigation services have also accelerated the advent of new navigation systems. By 2020 there will probably be at least three independent Global Navigation Satellite Systems (GNSS) available: GPS, GLONASS and Galileo. However, conventional navigation devices usually receive only a single frequency satellite signal coming from only one system and the receivers may suffer from sever performance degradation in GNSS-challenged environment, such as urban areas. Moreover, various sources of radio-frequency interferences (RFI), both wideband and narrowband, interfere with the received satellite signal. Despite the growing need for accurate and reliable satellite positioning, the above-mentioned issue still severely limits the achievable system performance.

Utilizing dual frequencies could greatly enhance the performance of satellite navigation. For example, one of the error sources for satellite navigation, the RFI, either intentional or unintentional, represents an impairing factor in GNSS application mainly due to the low power of the GNSS signal at the earth surface. This RFI is likely to

*Corresponding author, Email:jie.zhang@tut.fi

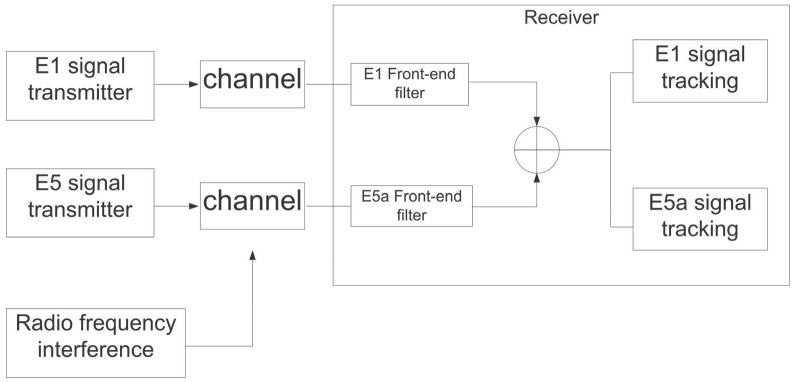

Figure 1. Block diagram of simulator

affect only one of the two frequencies, thus receiving the signal through dual frequency may enhance the results. Indeed, the frequency diversity will provide better robustness against interference since one signal band may still be used while the other is jammed [2]. In addition, two frequencies can be used to correct the ionosphere error if the higher order effects are ignored, so that a higher positioning accuracy can be provided. Moreover, a dual-frequency receiver could have a better performance in multipath mitigation, through different phases of the reflections of the difference frequencies [3]. For the reason above, we believe that the dual-frequency receiver implementation will be the main trend in the next generation receivers as soon as the signals become available.

The dual-frequency receiver, however, becomes more complex since it needs to process the signals from two frequencies. One well-known concept to reduce the complexity is to share the same front-end components and to use one common baseband stage [2][4]. In this method, two signals will be combined before the common baseband stage as shown in [2]. However, the superposition of signals may bring some problems. For example, if the Intermediate Frequencies (IF) of signals are close to each other in the baseband, the signals may interfere with each other. This will affect the accuracy of code tracking on both signals. In addition, if there is RFI within one signal band, it might also appear in other signal bands after signals' superposition. The RFI may degrade the tracking performance of both signals. To the author's knowledge, these two problems have not been evaluated much in the literature so far. The goal of this article is to investigate the impact of signal superposition on code tracking accuracy in a dual frequency receiver from two aspects: 1) choice of relative IF for two signals in a dual frequency receiver; 2) the impact of RFI. The signals considered in this article are Galileo E1 and E5a signals. This is because the E1/E5a combination is the optimal solution for mass-market dual frequency receivers from the hardware implementation point of view [4]. The characteristics of E1 and E5 signals are summarized in Table 1 [5]. CBOC here stands for Composite Binary Offset Carrier modulation [6] and AltBOC for Alternate Binary Offset Carrier modulation [7]. The investigation has been conducted with two Simulink Tx-Rx chain simulators for Galileo E1 and E5 signals [8], respectively. These two simulators are built at Tampere University of Technology (TUT) in Finland.

The rest of the paper will be organized as follows: next section introduces the simulator used in this article and some details of the main blocks in the simulator. Then, the simulation setup and results will be presented in Section 3; finally, the conclusions are drawn in Section 4.

Table 1. Parameters of E1 and E5 signal

	E1 signal	E5 signal
Modulation type	CBOC(6,1)	AltBOC(15,10)
Chip rate (MHz)	1.023	10.23
Carrier frequency (MHz)	1575.42	E5: 1191.795 E5a:1176.45 E5b:1207.12
Reference BW (MHz)	24.552	E5: 51.15 E5a: 20.46 E5b: 20.46

2. Simulink model overview

2.1 Generic simulator structure

Simulation is a powerful method in the analysis and design of communication devices. The research on new signals, which are not available in the sky, can be done through simulations [9]. The simulators for E1 and E5a signals used in this article for evaluating the tracking performance were created at TUT, under Simulink from Mathworks. Two simulators were combined in order to conduct the simulations in this article. The block diagram of this modified simulator is as shown in Figure 1.

2.2 Before the signals superposition

As shown in Figure 1, the E1 and E5 signals are first generated separately in two transmitter blocks. The transmitters generate the whole band E1 and E5 signals. The two signals may be passing through common or different wireless channels, depending on the relative location of the transmitters (satellites). Here, we assume E1 and E5 signals are coming from the same satellite, so the channel power-delay profiles are identical to E1 and E5 signals. However, it is to be mentioned that these common channel profile will affect differently the E1 and E5a signals, since they operate at different chip rates and different IF. After passing through the channel, the signals are captured by the receiver and filtered by the front-end filters. The main details about each block are introduced in the text as followed.

2.2.1 E1 signal transmitter

The E1 signal transmitter block is implemented based on CBOC modulation, including primary code and secondary code, in the accordance with the latest Galileo OS SIS ICD [5]. In the E1 signal transmitter block, E1B channel uses a CBOC(+)- modulated signal with navigation data and E1C channel uses a CBOC(−)-modulated signal with a pre-defined bit sequence of CS25[10]. The E1 signal is formed as the difference between those two signals. The signal at the output of the transmitter is at IF.

2.2.2 E5 signal Transmitter

The E5 signal transmitter generates the whole E5 signal. The E5aI, E5aQ, E5bI and E5bQ are modulated by using AltBOC(15,10) 8-PSK modulation, as described in [5]. The whole E5 signal is transmitted at IF at the output of the E5 signal transmitter. The IF for E5 signal may be different than the IF for E1 signal.

2.2.3 Channel blocks

The channel block generates the multipath signals and complex noise for a user-defined Carrier to Noise density ratio (C/N_0), multipath delay and power. In this article, we only consider the single path scenario in order to focus on the effect of RFI.

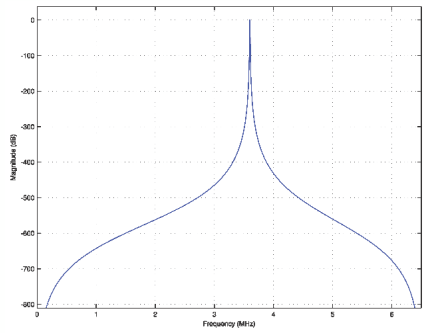

Figure 2. Example of bandpass filter use for generating narrowband interference

2.2.4 Front-end filters

The front-end blocks are used for receiver front-end filtering. They are Chebyshev type I bandpass filters with order 6. There are several front-end bandwidths can be used, e.g., infinite bandwidth for the ideal case, 4 MHz which can cover the main lobe of E1 signal power spectrum and 20.46 MHz for E5a signal.

2.3 Radio frequency interference

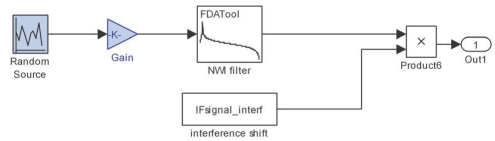

Figure 3. Interference generation

The possible external interference is generated separately. In this article, we assume the external interference is narrowband radio frequency interference. This interference is generated in such a way that the white Gaussian noise passes through a bandpass filter (see Figure 2 and Figure 3). The filtered noise can be shifted to different carrier frequencies.

2.4 Tracking stage

The filtered E1 and E5a signals are combined before the tracking stages. Since the common baseband structure

contains a number of tracking channels and each channel is capable of processing one signal at a time, therefore, the tracking stages in this simulator are implemented separately for E1 and E5a signals. The E5a signal tracking stage processes only E5a signal. The function of blocks including in the tracking stage will be introduced next.

In both E1 and E5a tracking channel, the tracking stage consists of three main blocks: carrier wipe-off block, code Numerically Controlled Oscillator (NCO) block and dual channel correlation and discriminator block.

In the carrier wipe-off block, the received signal is down-converted to the baseband with the estimated frequency and phase from Phase Lock Loop (PLL) and Frequency Lock Loop (FLL) in the tracking loop.

The "code NCO" block generates the local Pseudorandom Noise (PRN) reference code, which is shifted by the estimated code phase from Delay Lock Loop (DLL). According to the correlator offset and the status of phase holding shifter, the local reference codes are determined. In E1 signal receiver, the local reference codes are generated separately for E1B and E1C channel, respectively. In E5a signal receiver, only In-phase E5a signal is generated.

Table 2. Signal simulator parameters

Parameters	Typical value
Sampling frequency in E1 transmitter	52
Sampling frequency in E1 tracking (MHz)	52
Intermediate frequency IF for E1 signal (MHz)	3.42
Early-Late correlator spacing in E1 tracking (chips)	Bandwidth dependent $\Delta_{E\ L} \geq fc\_{E1}/Bw$
Reference code in E1 tracking	SinBOC(1,1) modulated E1B and E1C
Sampling frequency *fs* in transmitter (MHz)	104
Sampling frequency *in tracking* (MHz)	52
IF for whole E5 signal (MHz)	15.34
IE5a frequency f_{E5a} (MHz)	10.23
Early-Late correlator spacing in E5a tracking (chips)	Bandwidth dependent $\Delta_{E\ L} \geq fc\_{E5}/Bw$
Reference code in E5a tracking	E5aI code

In the dual channel correlation and discriminator block, FLL and PLL and DLL are included. In the DLL discriminator block, various conventional discriminator functions are implemented, such as narrow correlator [11], Multiple Gate Delay (MGD) [12][13] and two-stage estimator [14]. In the simulation, only the narrow correlator is used. The main parameters used in the E1 and E5a signal Simulink model are summarized in Table 2.

3. Simulations

The simulations have been done with the simulator introduced above. In all the simulations, the power level of the desired signal and thermal noise were set to produce a signal with C/N_0 of 55 dB-Hz. The narrow correlator was used in the discriminator in both E1 and E5a tracking stage. The impact of different IF values and narrowband interference was investigated. The details of the simulation setup and results are shown in the next section. The simulation parameters are summarized in Table 3.

Table 3. Simulation parameters

Simulation parameters	Value
C/N_0	55 dB-Hz
Front-end bandwidth	E1: 4MHz E5a: 20.46 MHz
Discriminator	Narrow Correlator
Impact on IF on code tracking simulations	
E5a IF	10.23 MHz
E1 PSD IF shift relative to E5a PSD	0:1.023:10.23MHz
Impact of Narrowband interference simulations	
Narrowband interference bandwidth	10 kHz

3.1 Impact of IF on code tracking

3.1.1 Simulation setup

In order to find the effect of the choice of IF value for E1 and E5a signals, we configured the simulator as follows: as shown in Figure 4, the E5a signal stays at a fixed IF, 10.23 MHz and the E1 signal is shifted to different IF. Since the signals will not interfere with each other when the E1 and E5a signal spectrums are not overlapping, therefore, we only evaluate the effect on code tracking when the E1 and E5s spectrum are overlapped. The effect on code tracking for E1 and E5a signals are evaluated separately.

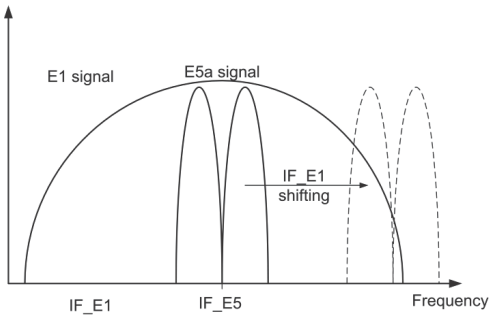

Figure 4. Illustration of IF shifting in simulation

3.1.2 Simulation results

The simulation results for evaluating the effect of IF for E1 and E5a signals are shown in Figure 5 and Figure 6. As can be seen from the Figure 5, the signal superposition degrades a little the code tracking performance compared with of the performance without signal superposition. For both E1 and E5a tracking, the code tracking error increases about 0.2 m. The relative position of IF for E1 and E5a signals does not have significant effect on the code tracking. On the other hand, the variance of E1 code tracking error is doubled after the signal superposition, as seen in Figure 6. The variance of E5a tracking error does not increase much. This is because of the fact that the bandwidth of E1 signal is much smaller than the bandwidth of E5a signal. The E1 signal interferes only in a part of the E5a signal.

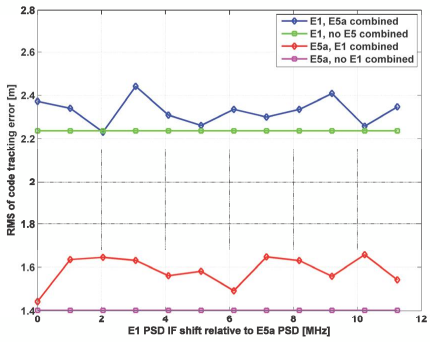

Figure 5. RMS of code tracking error for E1 and E5a signal

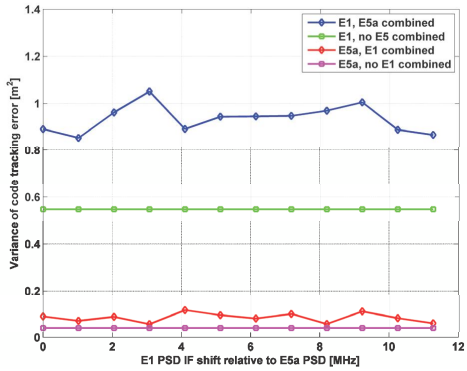

Figure 6. Variance of code tracking error for E1 and E5a signal

3.2 Impact of narrowband interference

3.2.1 Simulation setup

In order to evaluate the impact of the RFI introduced by the signals' superposition, we fixed the IF for the E5a signal at 10.23 MHz, and IF for the E1 signal at 12.25 MHz. This value was chosen from the local minimum value in E1 tracking as shown in Figure 5.

In the evaluation on code tracking of both signals, we are interested in finding out what is interference level introduced by one signal band into another signal band. As shown in Figure 7, when the interference is originally within E1 signal band, the interference will also appear in E5s signal band after superposition. However, if the interfere exists only within the E5a signal band before superposition, the interference may not appear in the band of E1 signal after superposition, as shown in lower diagram in Figure 7. Since the interference cannot be filtered out in the tracking stage, the interference may still have some impact on the code tracking accuracy. Therefore, the simulations for E1 signal tracking were done with interference located within the whole E5a band. The aim is to see the differences between the tracking with and without signal superposition in the presence of narrowband interference. The narrowband interference was generated as described in Section 2. The simulation parameters were summarized in Table 3.

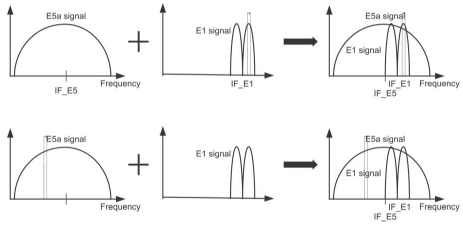

Figure 7. Illustration of signal superposition in the presence of narrowband interference

3.2.2 Simulation results

Figure 8 presents the results of E1 signal code tracking error after signal superposition when the interference is brought in E1 signal band from E5a signal band. As it can be seen in the figure, the interference in E5a band has a significant effect on E1 signal tracking accuracy, no matter whether the interference is within the E1 signal band after the superposition or not. If the interference is located at 1**fc* away from the IF of E1 signal, the RMS of E1 code tracking error is up to 400 meters when the interference is located within the E1 signal band and when the interference to signal power ratio (ISR) is 40 dB. The effect on code tracking is getting smaller when the interference is moving far away from the E1 band. We also found that, when the ISR is getting higher, the degradation on code tracking is getting bigger. The ISR threshold is between 25 dB and 30 dB, which means that, when the interference is below this threshold, the narrowband interference effect on code tracking is negligible.

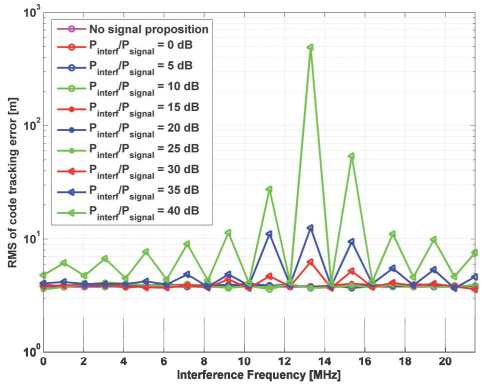

Figure 8. RMS of E1 code tracking error when the E5a signal introduces RFI to E1 signal

Figure 9 shows that the RMS of E5a code tracking error when the E1 signal introduces RFI to E5a signal band. As it can be seen from the figure, compared with the situation of without signal superposition (no RFI introduced to E5a), we can observe that the interference introduced by the E1 signal have very little effect on tracking E5a signal if the ISR is less than 25 dB. When the ISR is up to 40 dB, the E5a signal code tracking performance is significantly degraded. We also found that, E5a signal is much more robust against narrowband interference than E1 signal. It is because of the high chip rate and wideband width.

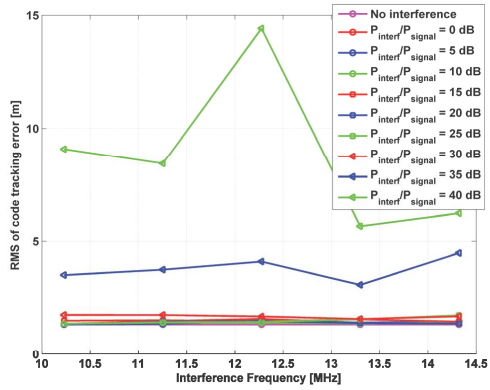

Figure 9. RMS of E5a code tracking error when the E1 signal introduces RFI to E5a signal

4. Conclusions

In this article, we analyzed the effect of signal superposition on code tracking. The evaluation was conducted with a Simulink simulator, including signal transmitters, propagation channels, front-end filter and signal tracking stages. The simulation results showed that the overlapping of two signal bands did not have much effect on either signal' s code tracking. However, the noise level was increased much, especially on E1 signal.

We also evaluated the effect of interference, which is introduced from one signal band to another signal band. The results showed that there were significantly effects on code tracking accuracy. If the interference introduced by E5a signal was not located in the E1 signal band after the superposition, the code tracking performance was still affected by the interference. The results also indicated that the E5a signal was more robust against the interference than E1 signal.

For future work, taking advantage of common baseband structure in the dual frequency receiver to avoid interference and improve the tracking performance will be conducted.

Acknowledgements

The research leading to these results has received funding from the European Union's Seven Framework Programme (FP7/2007-2013) under the grant agreement n227890 (GRAMMAR project) and from Academy of Finland, which are gratefully acknowledged. The author would also like to thank Nokia Foundation and Tekniikan edistämissäätiö (TES) for their support.

References

[1] B. Motella, S. Savasta, D. Margaria, F. Dovis, A Method to Assess Robustness of GPS C/A Code in Presence od CW Interference, Hindawi International Journal of Navigation and Oberservation, "Special Issue: Integrating Radio Positioning and Communications: New Synergies",Vol.2010, pp1-8, ISSN;1687-5990, June1, 2010

[2] Rugamer, A., Mongredian, C., Urquijo, S.; Rohmer, G.; (2011) Optimal path-control for dual-frequency overlay GNSS receivers, *International Conference on Localization and GNSS (ICL-GNSS)*, vol., no., pp.158-163

[3] Akos, D.M., Ene, A., Thor, J., (2003) A Prototyping Platform for Multi-Frequency GNSS Receivers, *Proceedings of the 16th International Technical Meeting of the Satellite Division of The Institute of Navigation (ION GPS/GNSS)*, Portland, OR, pp. 117-128.

[4] Hurskainen, H.; Lohan, E.-S.; Nurmi, J.; Sand, S.; Mensing, C.; Detratti, M.; (2009) Optimal dual frequency superposition for Galileo mass market receiver baseband, *Signal Processing Systems, SiPS. IEEE Workshop on* , vol., no., pp.261-266

[5] Galileo Open Service Signal In Space Interface Control Document, OD SIS ICD, Issue 1 (2010)

[6] G. W. Hein, J. A. Avila-Rodriguez, S. Wallner, A.R. Pratter, J. Owen, J. L. Issler, J. W, "MBOC, The new oprtimized spreading modulation recommended for Galileo L1 OS and GPS L1C", in Position, Location, And Navigation Symposium, 2006, IEE/ION, pp. 883-892, April 2006

[7] Sleewaegen, J.M., De Wilde, W., Hollreiser, M., "Galileo AltBOC Receiver", in Proc. Of ENC-GNSS, May 17, 2004, Rotterdam

[8] Simulink open source software for Galileo E1 signals, Http;//www.cs.tut.fi/tlt/pos/Software.htm,Tampere Univeristy of Technology, accessed March 2011.

[9] Borre, K., Akos, D.M., Bertelsen, N., Rinder, P. and Jensen. S.H.,, A Software-Defined GPS and Galileo Receiver: A single-Frequency Approch. Birhkhäuser Boston, 2007.

[10] Hein, G.W., Godet, J., Issler, J.L., Martin, J.C., Erhard, P., Rodridus, R.L., Pratt, T. (2002) Status of Galileo Frequency and Signal Design. In Processing of ION GPS, Oregon Convention Center - Portland, Oregon

[11] Dierendonck, A.V., Fenton, P. And Ford, T. (1992) Theory and performance of narrow correlator spacing in a GPS receiver, Journal of the Institute of navigation, vol. 39, pp. 265-283

[12] Zhang, J. and Lohan, E.S.; , Multi-correlator structures for tracking Galileo signals with CBOC and SinBOC(1,1) reference receivers and limited front-end bandwidths (2010), In *Proceedings of Positioning Navigation and Communication (WPNC),* Dresden, 11-12 March, pp.179-186

[13] Hurskainen, H., Lohan, E.S., Hu, X., Raasakka, J. and Nurmi, J. (2008) Multiple Gate Delay Tracking Structures for GNSS Signals and Their Evaluation with Simulink, SystemC, and VHDL," International Journal of Navigation and Observation, vol. 2008, Article ID 785695, 17 pages, 2008.

[14] Bhuiyan, M. Z. H., Zhang J., and Lohan, E. S. (2010) Enhanced Delay Tracking Performance of a C/N0-based Two-Stage Tracker for GNSS Receivers, European Navigation Conference on Global Navigation Satellite Systems, ENC GNSS 2010, 19 - 21 October, 2010, Braunschweig, Germany

Publication III

M. Z. H. Bhuiyan, J. Zhang, E. S. Lohan, W. Wang, S. Sand, "Analysis of multipath mitigation techniques with land mobile satellite channel model," *Radioengineering*, vol. 21, no. 4, December 2012.

Analysis of Multipath Mitigation Techniques with Land Mobile Satellite Channel Model

Mohammad Zahidul H. BHUIYAN[1,2], Jie ZHANG[3], Elena Simona LOHAN[3], Wei WANG[4], Stephan SAND[4]

[1]Dept. of Navigation and Positioning, Finnish Geodetic Institute, Finland
[2]Visiting Researcher, Dept. of Computer Systems, Tampere University of Technology, Finland
[3]Dept. of Communications Engineering, Tampere University of Technology, Finland
[4]Inst. of Communications and Navigation, German Aerospace Center, Germany

zahidul.bhuiyan@fgi.fi, jie.zhang@tut.fi, elena-simona.lohan@tut.fi, wei.wang@dlr.de, stephan.sand@dlr.de

Abstract. *Multipath is undesirable for Global Navigation Satellite System (GNSS) receivers, since the reception of multipath can create a significant distortion to the shape of the correlation function leading to an error in the receivers' position estimate. Many multipath mitigation techniques exist in the literature to deal with the multipath propagation problem in the context of GNSS. The multipath studies in the literature are often based on optimistic assumptions, for example, assuming a static two-path channel or a fading channel with a Rayleigh or a Nakagami distribution. But, in reality, there are a lot of channel modeling issues, for example, satellite-to-user geometry, variable number of paths, variable path delays and gains, Non Line-Of-Sight (NLOS) path condition, receiver movements, etc. that are kept out of consideration when analyzing the performance of these techniques. Therefore, this is of utmost importance to analyze the performance of different multipath mitigation techniques in some realistic measurement-based channel models, for example, the Land Mobile Satellite (LMS) channel model [1]-[4], developed at the German Aerospace Center (DLR). The DLR LMS channel model is widely used for simulating the positioning accuracy of mobile satellite navigation receivers in urban outdoor scenarios. The main objective of this paper is to present a comprehensive analysis of some of the most promising techniques with the DLR LMS channel model in varying multipath scenarios. Four multipath mitigation techniques are chosen herein for performance comparison, namely, the narrow Early-Minus-Late (nEML), the High Resolution Correlator, the C/N_0-based two stage delay tracking technique, and the Reduced Search Space Maximum Likelihood (RSSML) delay estimator. The first two techniques are the most popular and traditional ones used in nowadays GNSS receivers, whereas the later two techniques are comparatively new and are advanced techniques, recently proposed by the authors. In addition, the implementation of the RSSML is optimized here for a narrow-bandwidth receiver configuration in the sense that it now requires a significantly less number of correlators and memory than its original implementation. The simulation results show that the reduced-complexity RSSML achieves the best multipath mitigation performance in moderate-to-good carrier-to-noise density ratio with the DLR LMS channel model in varying multipath scenarios.*

Keywords

Multipath mitigation technique, GNSS receiver, channel model, performance analysis.

1. Introduction

Multipath is still considered as a dominant source of ranging errors in Global Navigation Satellite Systems (GNSS), such as the Global Positioning System (GPS) or the developing European satellite navigation system Galileo. Multipath is undesirable in the context of GNSS, since the reception of multipath can create a significant distortion to the shape of the correlation function used in the time delay estimate of a Delay Locked Loop (DLL) of a navigation receiver, leading to an error in the receiver's position estimate. Therefore, in order to mitigate the impact of multipath on a navigation receiver, the multipath problem has been approached from several directions. Among them, the use of special multipath limiting antennas (i.e., choke ring or multi-beam antennas), the post-processing techniques to reduce carrier multipath, the carrier smoothing to reduce code multipath, and the code tracking algorithms based on receiver internal correlation technique are the most prominent approaches [5] - [7]. The use of special multipath limiting antenna may incur extra hardware cost, and the post-processing techniques cannot be utilized in real-time positioning. Hence, the focus in this paper is mainly limited to the correlation-based multipath mitigation techniques as being the most widely used option for multipath mitigation in GNSS receivers.

The most conventional correlation-based code tracking structure is based on a feedback delay estimator known as Early-Minus-Late (EML) technique. In the classical

EML, two correlators are spaced at one chip apart from each other in order to form a discriminator function, whose zero crossings determine the path delays of the received signal [8], [9]. Unfortunately, the classical EML fails to cope with multipath propagation [5], [10]. Therefore, a number of enhanced EML-based techniques have been introduced in the literature for last two decades to mitigate the impact of multipath. One class of these enhanced EML techniques is based on the idea of narrowing the spacing between the early and late correlators, i.e., the narrow EML (nEML) or the narrow correlator [5], [11], [12]. The choice of correlator spacing usually depends on the receiver's available front-end bandwidth along with the associated sampling frequency [13]. A correlator spacing in the range of 0.05 to 0.2 chips is commercially available for the nEML-based GPS receivers [14].

Another class of discriminator-based DLL variants proposed for GNSS receivers is the so-called Double-Delta ($\Delta\Delta$) technique, which uses more than three correlators in the tracking loop (typically, five correlators: two early, one in-prompt and two late) [12]. The $\Delta\Delta$ technique offers better multipath rejection in medium-to-long delay multipath [11], [15] in good Carrier-to-Noise density ratio (C/N_0). Couple of well-known particular cases of $\Delta\Delta$ technique are the High Resolution Correlator (HRC) [12], the Strobe Correlator (SC) [12], [16], the Pulse Aperture Correlator (PAC) [17] and the modified correlator reference waveform [12], [18]. One other similar tracking structure is the Multiple Gate Delay (MGD) correlator [19] – [22], where the number of early and late gates and the weighting factors used to combine them in the discriminator are the parameters of the model, and can be optimized according to the multipath profile as illustrated in [15]. While coping better with the ambiguities of Binary Offset Carrier (BOC) correlation function, the MGD provides slightly better performance than the nEML at the expense of higher complexity and it is sensitive to the parameters chosen in the discriminator function (i.e., weights, number of correlators and correlator spacing) [15], [22].

Another tracking structure closely related to the $\Delta\Delta$ technique is the Early1/Early2 (E1/E2) tracker, initially proposed in [23], and later described in [12]. In E1/E2 tracker, the main purpose is to find a tracking point on the correlation function that is not distorted by multipath. As reported in [12], E1/E2 tracker shows some performance improvement over the $\Delta\Delta$ technique only for very short delay multipath for GPS L1 Coarse/Acquisition (C/A) signal.

Another feedback tracking structure is the Early-Late-Slope (ELS) technique [12], which is also known as Multipath Elimination Technique (MET) [24]. The simulation results performed in [12] showed that the ELS is outperformed by the HRC with respect to Multipath Error Envelopes (MEEs), for both Binary Phase Shift Keying (BPSK) and Sine Binary Offset Carrier (SinBOC) modulated signals.

A new multipath estimation technique, named as A-Posteriori Multipath Estimation (APME), is proposed in [25], which relies on a-posteriori estimation of the multipath error tracking. Multipath error is estimated independently in a multipath estimator module on the basis of the correlation values from the prompt and very late correlators. According to [25], the multipath performance of GPS L1 C/A signal is comparable with that of the Strobe Correlator: slight improvement for very short delays (i.e., delays less than 20 meters), but rather significant deterioration for medium delays. A similar slope-based multipath mitigation strategy, named as Slope-based Multipath Estimator (SBME), was proposed in [26]. SBME first derives a multipath estimation equation by utilizing the correlation shape of the ideal normalized correlation function, which is then used to compensate for the multipath bias of a nEML tracking loop. SBME requires an additional correlator at the late side of the correlation function, which is then used in conjunction with a nEML tracking loop. It is reported in [26] that SBME has superior multipath mitigation performance than the nEML, and has slightly worse performance than the HRC in closely spaced two-path channel model.

In [27], a fundamentally different approach is adopted to solve the multipath problem for GNSS receivers. The proposed technique, named as Tracking Error Compensator (TrEC), utilizes the multipath invariant properties of the received correlation function in order to provide significant performance benefits over the nEML for narrow-band GPS receivers [27], [28]. However, the performance of the TrEC has not yet been tested for BOC or Composite BOC (CBOC) signals.

One of the most promising advanced multipath mitigation techniques is the Multipath Estimating Delay Lock Loop (MEDLL) [29] - [31], implemented by NovAtel for GPS receivers. MEDLL is considered as a significant evolutionary step in the receiver-based attempt to mitigate multipath. It uses many correlators in order to determine accurately the shape of the multipath corrupted correlation function. According to [31], MEDLL provides superior medium to long delay multipath mitigation performance than nEML at the cost of multi-correlator based tracking structure.

A completely different approach to mitigate multipath error is used in NovAtel's recently developed Vision Correlator [32]. The Vision Correlator (VC) is based on the concept of Multipath Mitigation Technique (MMT) developed in [33]. It can provide a significant improvement in detecting and removing multipath signals as compared to other standard multipath resistant code tracking algorithms (for example, the PAC of NovAtel). However, the only shortcoming of the VC is that it requires a reference function shape to be used to fit the incoming data with the direct path and the secondary path reference signals. The reference function generation has to be accomplished a-priori, and it must incorporate the issues related to Radio Frequency (RF) distortions introduced by the front-end.

Several advanced multipath mitigation techniques were also proposed in [34]-[36]. While improving the delay estimation accuracy, these techniques require a higher number of correlators than the traditional DLL, and they are also sensitive to the noise-dependent threshold choice [35].

The multipath studies presented in the literature are often based on optimistic assumptions, for example, assuming a static two-path channel [12], [37] or a fading channel with a Rayleigh or a Nakagami distribution [36], [38]. But, in reality, there are a lot of channel modeling issues, for example, satellite-to-user geometry, variable number of paths, variable path delays and gains, Non Line-Of-Sight (NLOS) path condition, receiver movements, etc. that are kept out of consideration when analyzing the performance of these techniques. Therefore, this is of utmost importance to analyze the performance of different multipath mitigation techniques in some realistic measurement-based channel models, for example, the Land Mobile Satellite (LMS) channel model [1]-[4], developed at the German Aerospace Center (DLR). The main motive of this research is to present a comprehensive analysis of some of the most promising techniques in the DLR LMS channel model in varying multipath scenarios. Four multipath mitigation techniques are chosen herein for performance comparison, namely, the nEML, the HRC, the C/N_0-based two stage delay tracking technique, and the Reduced Search Space Maximum Likelihood (RSSML) delay estimator. The first two techniques are the most popular and traditional ones used in nowadays GNSS receivers, whereas the later two techniques are comparatively new and modified techniques, recently proposed by the authors in [39] and [34], respectively. These two new techniques are considered here, since they offer better multipath mitigation performance than some other techniques, as mentioned in [35]. A brief description of these techniques is presented in Section 4. A Simulink-based open source software simulator, developed at the Tampere University of Technology (TUT) for Galileo E1 signal [40], is used here to carry out the simulations.

The rest of the paper is organized as follows. Section 2 provides a brief description on the land mobile satellite channel model developed by German Aerospace Center (DLR). Section 3 describes the Simulink-based simulation model for Galileo E1 signal developed in Tampere University of Technology (TUT), Finland. A brief overview of the analyzed multipath mitigation techniques is presented in Section 4. The simulation results in DLR channel model are presented in Section 5 with an illustrative comparison of the analyzed techniques. At the end, some general remarks are drawn in Section 6 based on findings of this research. In brief, the novelty of this work lies in algorithm testing with a realistic DLR LMS channel model, in complexity-reduced RSSML proposal, and in the discussion of the design issues on the multipath mitigation unit of a Galileo receiver. Some part of this work is also available to the research community via an open-access simulator [40] and an open-access DLR LMS channel model [41].

2. Land Mobile Satellite Channel Model

The DLR Land Mobile Satellite (LMS) channel model is an open access model, and it can be freely downloaded from the DLR website [41]. The channel model used in this study is the GNSS channel part in a joint channel model for joint GNSS and mobile radio based positioning [4]. This joint model, as shown in Fig. 1, coherently combines the DLR LMS [1]-[3] channel model and an extended WINNER model, which is used for positioning in mobile radio communications. In the GNSS channel model, a combination of a deterministic and statistic modeling approach is considered. The direct path component is determined by physical deterministic effects within a parameterized artificial urban canyon scenario with house fronts, lamppost and trees, which are stochastically generated. These are diffractions caused by house front or a lamp-post which is calculated using Knife Edge. Shadowing effect caused by trees is incorporated by a tree top model having attenuation proportional to the path length through the canopy accomplished by a stochastic fading process. The multipath components are generated with the DLR LMS channel model, which is widely used for the

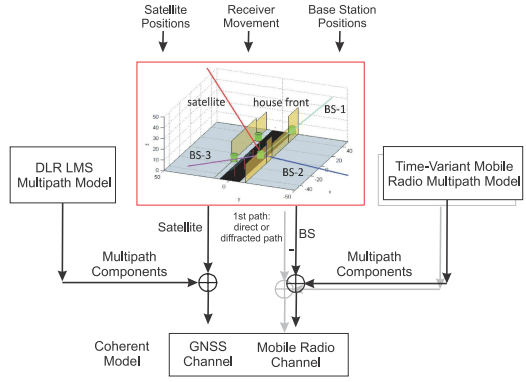

Fig. 1. Flow chart of the combined model for joint GNSS and mobile radio based positioning.

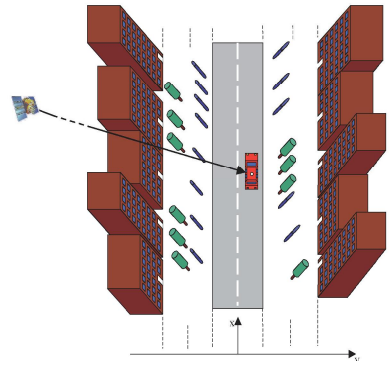

Fig. 2. Satellite model of the artificial scenery with moving receiver.

simulations of the positioning accuracy of mobile satellite navigation receivers in urban outdoor scenarios. Within the DLR LMS channel model, the multipath components are generated by statistical process. For a moving receiver, the delay variance of each path is geometrically determined and the complex amplitude is generated by a stochastic fading process. A typical LMS channel emerges from a constellation depicted in Fig. 2, where the moving receiver is driving through an urban canyon. The obstacles like trees and houses can clearly be seen, and the coordinate system to describe the azimuth and elevation is introduced as explained in [3].

3. Simulation Model

All the simulations have been carried out in an open source Galileo E1 signal simulator [40], which is developed in a Simulink-based platform at Tampere University of Technology (TUT), Finland. The Simulink model used to generate the simulation results is shown in Fig. 3. The Simulink model, as presented here, consists of four parts: i) a transmitter block, ii) a DLR channel block, iii) a Front-end filter block, and iv) a tracking unit (which incorporates a Frequency Locked Loop (FLL), a Phase Locked Loop (PLL) and a Delay Locked Loop).

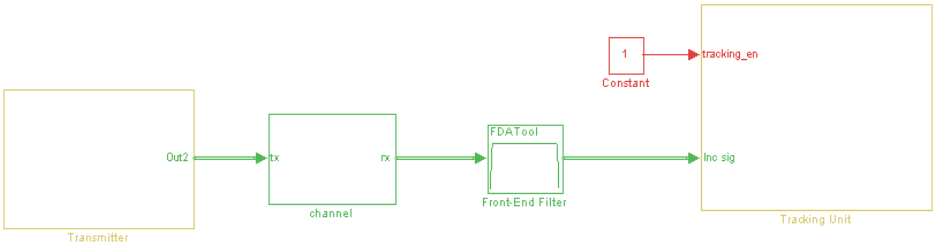

Fig. 3. TUT Galileo E1 signal simulator (upper level block diagram).

3.1 Transmitter Block

The Galileo E1 transmitter block is implemented according to the latest Galileo Open Service (OS) Interface Control Document (ICD) [42]. E1B and E1C channels are modeled according to the following equation [42]:

$$s_{E1}(t)=\frac{1}{\sqrt{2}}(e_{E1B}(t)(\alpha\, sc_{E1B,a}(t)+\beta\, sc_{E1B,b}(t))- e_{E1C}(t)(\alpha\, sc_{E1C,a}(t)-\beta\, sc_{E1C,b}(t))) \quad (1)$$

where $sc_X(t)=\mathrm{sgn}(\sin(2\pi R_{s,X}t))$, $e_{E1B(t)}$ and $e_{E1C(t)}$ are binary signal components and α and β represent weighting factors. Above, $R_{s,X}$ is the sub-carrier rate corresponding to channel X (i.e., either E1B or E1C). As explained in [42], $\alpha=\sqrt{10/11}$ and $\beta=\sqrt{1/11}$.

3.2 DLR Channel Block

In the channel block, the multipath signals and the complex AWGN are generated. The basic function of the channel block can be modeled according to the following equation:

$$r_{E1}(t)=\sum_{i=1}^{l}a_i(t)s_{E1}(t-\tau_i)+\eta(t) \quad (2)$$

Here $r_{E1}(t)$ is the received E1 signal at the output of the channel block; a_i and τ_i are the path gain and path delay for the *i*-th path, respectively, and $\eta(t)$ is the complex AWGN. In the simulations reported later in Section 5, the number of channel paths was fixed to 5 ($l = 5$), but this is simply a parameter of the model that can be varied accordingly. The complex path gains a_i and the corresponding path delays τ_i are taken from a five-path DLR LMS channel model, as mentioned in Section 2.

3.3 Front-end Filter Block

In the simulations, a 6th order Chebyshev type I filter is used with a 3-dB double-sided bandwidth of 3 MHz. Simulink's 'Digital Filter Design' toolbox is used to design the filter with the specified parameters.

3.4 Tracking Unit

The tracking Unit consists of three major blocks: 'Carrier Wipe-Off' block, 'Code NCO' block, and 'Dual Channel Correlation and Discriminators' block, as shown in Fig. 4.

The incoming signal is down converted to the base-band in the 'Carrier Wipe-Off' block. The carrier wipe-off is performed according to the following equation:

$$r_{E1\_BB}(t)=r_{E1}(t)e^{-j\left(2\pi\hat{f}t+\hat{\varphi}\right)} \quad (3)$$

where $\hat{f}$ is the frequency with some initial frequency error ($\hat{f}=f_{IF}+\Delta f$, where $\Delta f <= 125$ Hz, and f_{IF} is the final Intermediate Frequency (IF)); $\hat{\varphi}$ is the estimated phase from the FLL-assisted-PLL. After the carrier wipe-off, the real part and the imaginary part of the complex signal are separated as the in-phase channel and the quadrature chan-

nel (i.e., I and Q channels, respectively as shown in Fig. 4) in baseband. The 'Code NCO' block shifts the code phase based on the estimated delay error coming out from the DLL filter. This block generates four signals as output: the adjusted E1B and E1C replicas, the trigger enabling signal and the shifted NCO phase. The trigger enabling signal is used in conjunction with 'tracking_en' which eventually enables both FLL-assisted-PLL and DLL blocks of E1B and E1C channels (when both the variables are set to 1). Both the code and carrier NCOs are implemented using C-language based S-function, the details of which are not addressed here for the sake of compactness.

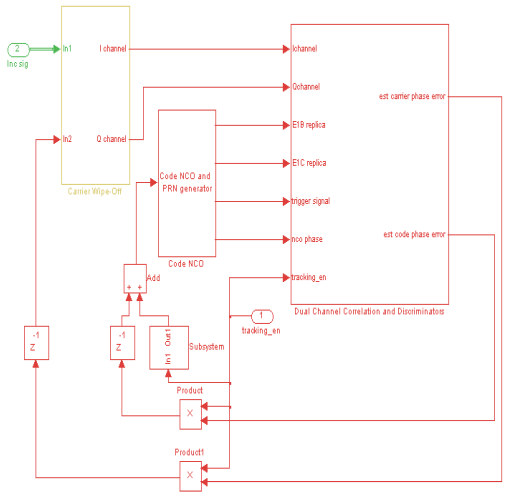

Fig. 4. Tracking unit.

In the 'Dual Channel Correlation and Discriminators' block, E1B and E1C are implemented as two separate channels, as shown in Fig. 5. However, these two channels are approximately the same, except the replicas used for integration and dump, which are either CBOC(+)/CBOC(-) modulated or SinBOC(1,1)-modulated, according to the type of receiver. In the reported simulation, SinBOC(1,1) modulated reference codes are considered for both the channels. It is already shown in [43] that the performance deterioration caused by implementing a SinBOC(1,1) reference receiver is negligible as compared to implementing a CBOC reference receiver.

The C/N_0 estimation is performed based on the ratio of the signal's wideband power to its narrowband power as mentioned in [44]. In this method, the power of the signal is computed over a wide bandwidth with a relatively short coherent integration time and over a narrow bandwidth with a longer coherent integration time. The wideband power is computed after 4 milliseconds (ms) of coherent integration (after each code epoch length), and the narrowband power is computed after 16 ms of coherent integration in order to estimate the carrier-to-noise density ratio for each particular channel.

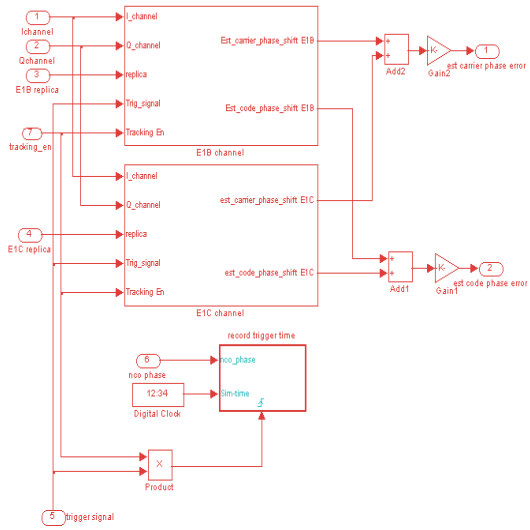

Fig. 5. Dual Channel Correlation and Discriminators block.

4. Multipath Mitigation Techniques

4.1 Conventional Techniques (nEML and HRC)

Several multipath mitigation techniques exist nowadays that reduce the multipath error significantly. Among them, the narrow Early-Minus-Late (nEML) is the most popular technique due to its simpler implementation and robust tracking performance against false locks. The nEML uses a narrower correlator spacing (i.e., usually within 0.05 to 0.2 chips) than the conventional early-minus-late technique which uses 1 chip spacing between early and late correlators. This eventually reduces the tracking error in the presence of noise and multipath [5]. The other conventional technique considered here is the High Resolution Correlator, a variant of the $\Delta\Delta$ technique. The HRC consists of two correlator pairs, where the spacing between the very early and very late correlators is twice the spacing between the early and late correlators. It was shown in [11] that the HRC has better performance than the nEML in case of medium to long delay multipath. However, the HRC cannot reject the short delay multipath effects and it suffers from false lock problem. Additionally, it has severe performance degradation in noisy environment [34].

4.2 C/N_0-based Two Stage Delay Tracking Technique

The C/N_0-based two stage delay tracking technique, which is first proposed in [39], is a combination of two individual tracking techniques, namely the nEML and the HRC), the two stage delay tracker always starts with a nEML tracking loop, since it begins to track the signal

with a coarsely estimated code delay as obtained from the acquisition stage. At the second or final stage of tracking (i.e., when the DLL tracking error is around zero), the two stage delay tracking technique switches its DLL discriminator from the nEML to the HRC, since the HRC offers better multipath mitigation capability than the nEML. While doing so, it also has to ensure that the estimated C/N_0 level meets a certain threshold set by the two stage tracking technique. This is mainly because of the fact that the HRC cannot perform as well as nEML in weak signal condition due to its smaller uncertainty region around the actual zero crossing. It has been empirically found that a C/N_0 threshold of 33 dB-Hz can be a good choice to switch between the techniques. Therefore, at the fine tracking stage, the two stage delay tracking technique switches from nEML to HRC only when the estimated C/N_0 meets the above criteria (i.e., C/N_0 greater than 33 dB-Hz).

4.3 Reduced Search Space Maximum Likelihood Delay Estimator

A Reduced Search Space Maximum Likelihood (RSSML) delay estimator is a maximum likelihood based approach, which mitigates the multipath effects reasonably well at the expense of increased complexity. The RSSML, as proposed in [34], attempts to compensate the multipath error contribution by performing a nonlinear curve fit on the input correlation function which finds a perfect match from a set of ideal reference correlation functions with certain amplitude(s), phase(s) and delay(s) of the multipath signal. With the presence of multipath signal, the RSSML tries to separate the LOS component from the combined signal by estimating all the signal parameters in a maximum likelihood sense, which consequently achieves the best curve fit on the received input correlation function. As mentioned in [34], the classical RSSML incorporates a threshold-based peak detection method, which reduces the code delay search space significantly.

In the reduced-complexity RSSML implementation, a slightly different approach has been adopted for the selection of competitive delays. Instead of computing the peak detection thresholds based on the estimated noise variance [34], it considers all those code delays as the competitive delays that are within ±0.2 chips away from the prompt correlator, as shown in Fig. 6. This is meaningful in the sense that it is quite likely to have a delay error near the previous delay estimate. By doing so, the reduced-complexity RSSML avoids computing the peak detection thresholds, the estimation of which is often inaccurate in time-varying urban/suburban multipath channel model. In this implementation, a total of 41 correlators have been used with a correlator spacing of 0.05 chips resulting in a code delay window range of ±1 chip with respect to the prompt correlator. This new approach reduces the correlator requirement by around 78.76% in contrast to the classical RSSML that requires 193 correlators to cover a code delay window range of ±2 chips with respect to the prompt correlator.

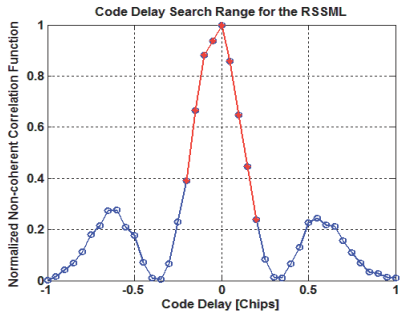

Fig. 6. Competitive code delays (around ±0.2 chips within the prompt correlator) for the RSSML.

The ideal non-coherent correlation functions are generated off-line considering a pre-correlation bandwidth of 3 MHz (double-sided) and those are saved in a look-up table in memory. In real-time, the reduced-complexity RSSML reads the correlation values from the look-up table, translates the ideal reference correlation functions at the middle delay index to the corresponding candidate delay index within the code delay window, and then computes the Minimum Mean Square Error (MMSE) for that specific delay candidate. As mentioned earlier, the search space is reduced to the code delays that are within ±0.2 chips from the prompt correlator. The brief step-by-step procedure for the proposed reduced-complexity RSSML implementation is summarized below:

Step 1: *Generate candidate code delays;*

Step 2: *Read the non-coherent reference correlation functions from the look-up table;*

Step 3: *Translate the non-coherent reference correlation functions which are at the middle delay index to the corresponding candidate delay index for each candidate code delay;*

Step 4: *Compute the MMSE for each candidate code delay;*

Step 5: *Select the candidate code delay with the lowest MMSE value as the LOS code delay.*

5. Simulation Results

Simulations have been carried out in a five-path DLR LMS channel model in varying scenarios (i.e., pedestrian/car navigation, different road widths, different satellite elevations, etc.). Tab. 1 summarizes the key simulation parameters for Fig. 7. The simulations have been carried out for 10 seconds (s) for each particular C/N_0 level, generating 10000/4=2500 observations per C/N_0. The tracking errors are computed after each coherent integration period (i.e., 4 ms for Galileo E1 signal). In the final statistics, the tracking errors for the first two seconds are ignored in order to remove the initial error bias that may come from the delay difference between the received signal and the

locally generated reference code. Therefore, the left-over tracking errors after two seconds are mostly due to the effect of multipath and noise. The Root-Mean-Square-Error (RMSE) are computed for 2000 (i.e., 10 – 2 = 8 s of data generates 2000 measurements) tracking measurements in each particular C/N_0 level. The RMSE of delay estimates are plotted in meters (m), by using the relationship $RMSE_m = RMSE_{chips} * c * T_c$; where c is the speed of light, T_c is the chip duration, and $RMSE_{chips}$ is the RMSE in chips. RMSE vs. C/N_0 plots are shown in Fig. 7 for the simulation profile mentioned in Tab. 1 with two different first-path delays (i.e., ~0.04 chips and ~0.16 chips, respectively).

Parameters	Values
Band	E1
fs (MSps)	26
IF (MHz)	3.42
Receiver filter (-3dB filter boundaries) (MHz)	3.42±1.5
C/N_0 (dB-Hz)	[25; 35; 45; 55]
Track number	01
Track type	Car
Road width (m)	5
Maximum speed	10 m/s
Satellite Vehicle (SV) number	35
Satellite Vehicle (SV) elevation (deg.)	45.74
Number of channel paths	5
Data duration (s)	10
Correlator spacing (chips)	0.17 chips for all techniques, except RSSML which has 0.05 chips spacing
First path delay (samples)	1 or 4

Tab. 1. Simulation parameters.

The impact of the first-path delay on the nEML and the HRC techniques is evident from the figure (i.e., high RMSE values for certain C/N_0 levels). It can also be seen that the reduced-complexity RSSML and the two stage delay tracking technique exhibit similar tracking performance no matter what the first path delays are (at least for the first-path delays in the range of ±0.16 chips). There is quite likely to have a delay mismatch between the received signal and the locally generated reference code in the range of ±0.16 chips, which actually depends on the time-bin resolution of the code search space at the acquisition stage. Therefore, it is very important to verify the robustness of a delay tracking technique in terms of first-path delay tolerance, especially in harsh multipath channel conditions where the threat of false locking to any of the close-in paths is quite significant. However, the reduced-complexity RSSML offers the best tracking performance in both the scenarios for moderate-to-good C/N_0 (i.e., C/N_0 higher than 33 dB-Hz), followed by the two stage delay tracking technique being the second best option. The tracking error plots for two different path delays are also shown in Fig. 8. As seen in Fig. 8(b), the HRC locks to a neighboring peak even in a good signal condition in case of ~0.16 chips first-path delay.

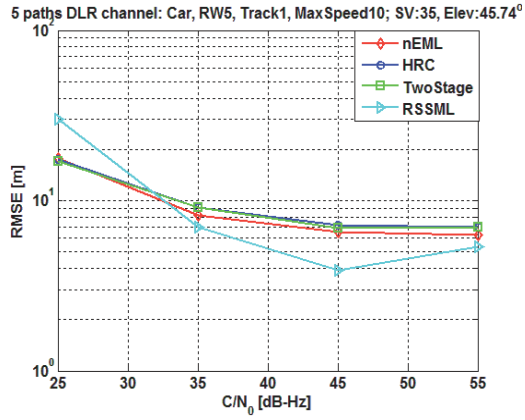

(a) First path delay: ~0.04 chips

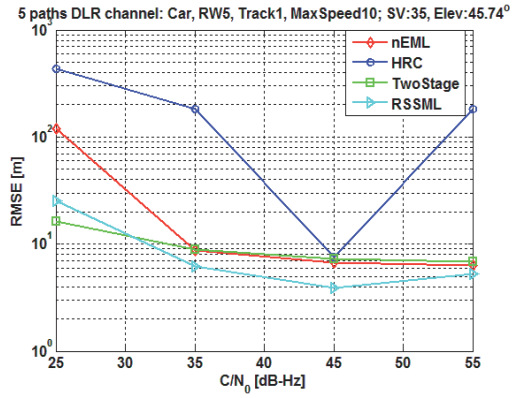

(b) First path delay: ~0.16 chips

Fig. 7. RMSE vs. C/N_0 for SV 35 with different first path delays in an urban environment (maximum speed: 10 m/s) in a five-path DLR channel model.

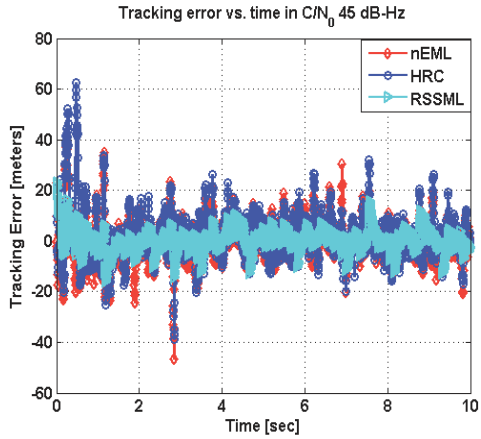

(a) First path delay: ~0.04 chips, C/N_0: 45 dB-Hz

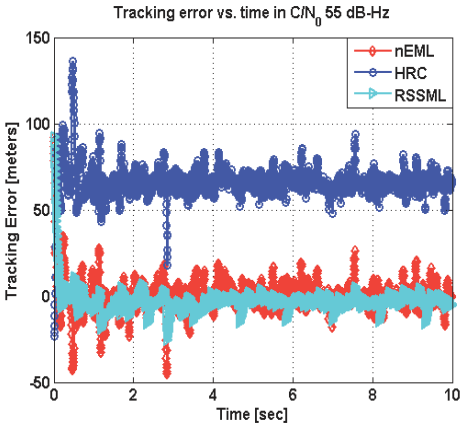

(b) First path delay: ~0.16 chips, C/N_0: 55 dB-Hz

Fig. 8. Tracking error vs. time for SV 35 in an urban environment (maximum speed: 10 m/s) in a five-path DLR channel model.

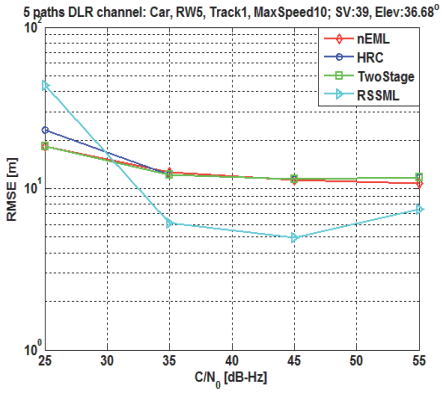

(a) Road width: 5 m

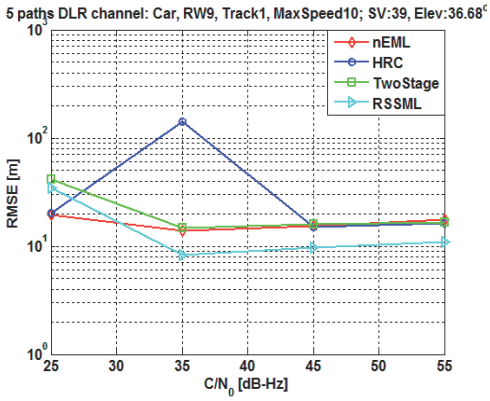

(b) Road width: 9 m

Fig. 9. RMSE vs. C/N_0 for SV 39 with different road widths in an urban environment (maximum speed: 10 m/s) in a five-path DLR channel model, first-path delay: 0 chips.

In Fig. 9, RMSE vs. C/N_0 plots are shown for Satellite Vehicle (SV) 39 with an elevation angle 36.7^0 for two different road widths (i.e., 5 m and 9 m) in an urban environment. The simulation is set for the car users with a maximum speed of 10 m/s, and the first-path delay in this case is assumed to be 0 chips. All other parameters are unchanged from the previous simulation. It can be seen from Fig. 9(b) that the HRC locks to a false neighboring peak at C/N_0 35 dB-Hz in the case of 9 meters road width, even with 0 chips first-path delay. Here also, the reduced-complexity RSSML shows the best multipath mitigation performance from C/N_0 30 dB-Hz and onwards for both the scenarios, followed by the nEML and the two stage delay tracking technique.

In Fig. 10, a RMSE vs. C/N_0 plot is shown for SV 25 having a low elevation angle 5.4^0 for a pedestrian user (maximum speed 1 m/s) in an urban environment. The first-path delay is assumed to be ~0.08 chips, and the road width is 9 m. All other parameters are unchanged from the previous simulation.

As seen from Fig. 10, the nEML and the HRC both suffer from poor tracking robustness. Like the previous simulation results, the reduced-complexity RSSML offers the best tracking performance followed by the two stage delay tracking technique.

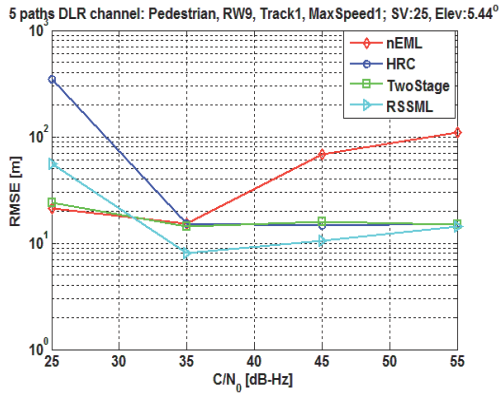

Fig. 10. RMSE vs. C/N_0 for the low-elevated SV 25 with first path delay ~0.08 chips in a pedestrian environment (maximum speed: 1 m/s) in a five-path DLR channel model.

A comparative performance analysis is shown in Tab. 2 for the four different techniques analyzed herein. The analysis is mostly based on tracking robustness, multipath mitigation performance, correlator requirement, memory requirement and implementation complexity. In all the simulations, the reduced-complexity RSSML achieved the best multipath mitigation performance from C/N_0 33 dB-Hz and onwards. In addition, it can also be considered as the most robust technique as it offers steady tracking performance in different channel conditions. After the reduced-complexity RSSML, the two stage delay tracking technique can be the second best choice in terms

of multipath mitigation performance and tracking robustness. The good thing with the two stage delay tracking technique is that it utilizes the inherent advantages of both the techniques (i.e., the nEML and the HRC) in an intelligent way with the help of a C/N_0 estimator. However, the performance of the two stage technique is somehow dependent on the accuracy of the C/N_0 estimation, and therefore, a good C/N_0 estimator should be used for an optimal performance.

The HRC suffers from false locking, especially in noisy environment, or in harsh multipath environment like dense urban canyon, and hence, it is not recommended to use HRC in those channel conditions. On the contrary, the nEML is still an attractive choice for the mass-market receivers for its relatively better tracking robustness, moderate multipath mitigation performance, and above all, simpler implementation.

Techniques / Criteria	nEML	HRC	Two Stage	Reduced – Complexity RSSML
Multipath mitigation performance	Good	Very Good	Very Good	Best
Tracking robustness	Good	Bad	Very Good	Best
Correlator requirement	Few (3)	Few (5)	Few (5)	Many (41)
Memory requirement	No	No	No	Yes
Implementation complexity	Very Low	Very Low	Low	Moderate

Tab. 2. Performance analysis of multipath mitigation techniques.

The implementation complexity of any multipath mitigation technique mainly depends on the correlation structure and the implementation issues concerning channel estimation, correlator requirement, required number of mathematical operations, memory requirement and so on. Among the analyzed techniques, the reduced-complexity RSSML is the most complex one, since it utilizes a moderate number of correlators for channel estimation. Additionally, it requires a moderate set of reference correlation functions which are generated off-line to be used as a-priori information while estimating the LOS code delay. The memory requirement of the reduced-complexity RSSML eventually depends on few factors including the maximum number of paths to be considered, the correlator spacing, the number of correlators and the resolution of each multipath parameter (i.e., path delays, path phases and path amplitudes). In our MATLAB implementation, the complexity-reduced RSSML requires little less than 1 megabytes of memory with maximum number of paths set to 2, the correlator spacing set to 0.05 chips, and the number of correlators for a two-chip window length set to 41. This new approach reduces the memory requirement by 92.86% in contrast to the classical RSSML that requires 14 megabytes of memory.

6. Conclusions

Multipath is a major limiting factor for high precision-oriented GNSS applications. A variety of multipath mitigation techniques exist in the literature to deal with this particular phenomenon. Most of these techniques offer good multipath mitigation performance for medium-to-long delay multipath. However, the multipath studies presented in the literature are often based on optimistic assumptions, for example, assuming a static two-path channel or a fading channel with a Rayleigh or a Nakagami distribution, and so on. This is always very meaningful to analyze the performance of different techniques in some realistic measurement-based channel models, for example, the DLR LMS channel model. In this study, the authors provided a comprehensive analysis of some of the most promising multipath mitigation techniques in the DLR LMS channel model. It was shown that the reduced-complexity RSSML, in general, achieved the best multipath mitigation performance in a realistic DLR channel model in varying multipath scenarios. The implementation complexity of the proposed reduced-complexity RSSML was also reduced from its original implementation. The correlator requirement and the memore requirement are reduced by 78.76% and 92.86%, respectively in contrast to the classical RSSML. Yet, it requires a moderate amount of correlators and memory as compared to the existing tracking techniques, which makes it suitable for high-end receivers. Among the other analyzed techniques, the C/N_0-based two stage delay tracking technique can be a good DLL choice for mass-market receivers as it offers the best trade off between performance and complexity.

Acknowledgements

The research leading to these results has received funding from the European Union's Seventh Framework Programme (FP7/2007-2013) under grant agreement number 227890 (GRAMMAR project). This research work has also been supported by the Academy of Finland and by the TISE Graduate School.

References

[1] LEHNER, A. *Multipath Channel Modelling for Satellite Navigation System*. Ph.D. thesis, 2007, ISBN: 978-3-8322-6651-6.

[2] LEHNER, A., STEINGA, A., SCHUBERT, F. A location and movement dependent GNSS multipath error model for pedestrian applications. *ATTI Journal dell'Istituto Italiano di Navigazione*, 2009, p. 108 – 119, ISSN 1120-6977.

[3] LEHNER, A., STEINGA, A. A novel channel model for land mobile satellite navigation. In *Proceedings of the ION GNSS*. Long Beach (USA), Sep 2005.

[4] WANG, W., JOST, T., LEHNER, A., PEREJ-DIAZ, F., FIEBIG, U.-C. Towards a channel model for joint GNSS and mobile radio based positioning. In *Proceedings of COST Action IC1004, Coop-*

erative Radio Communications for Green Smart Environments. Lisbon (Portugal), 2011.

[5] VAN DIERENDONCK, A. J., FENTON, P., FORD T. Theory and performance of narrow correlator spacing in a GPS receiver. *Navigation: Journal of the Institute of Navigation,* 1992, vol. 39, no. 3, p. 265 - 283.

[6] BROWN, A. Multipath rejection through spatial processing. In *Proceedings of ION GPS 2000*. Utah, USA, Sep 2000.

[7] RAY, J. *Mitigation of GPS Code and Carrier Phase Multipath Effects using a Multi-Antenna System.* Ph.D. thesis, University of Calgary, 2000.

[8] BALTERSEE, J., FOCK, G., SCHULZ-RITTICH, P. Adaptive code-tracking receiver for direct-sequence code division multiple access (CDMA) communications over multipath fading channels and method for signal processing in a RAKE receiver. *US Patent Application Publication, US 2001/0014114 A1* (Lucent Technologies), Aug 2001.

[9] BISCHOFF, R., HB-UMBACH, R., SCHULZ, W., HEINRICHS, G. Employment of a multipath receiver structure in a combined Galileo/UMTS receiver. In *Proceedings of IEEE VTC Spring*, 2002, vol. 4, p. 1844 - 1848.

[10] SIMON, M. K., ALOUINI, M. S. *Digital Communication over Fading Channels*. 1st ed. John Wiley & Sons, 2000.

[11] MCGRAW, G. A., BRAASCH, M. S. GNSS multipath mitigation using gated and high resolution correlator concepts. In *Proceedings of the National Technical Meeting of the Satellite Division of the Institute of Navigation*. San Diego (USA), Jan 1999.

[12] IRSIGLLER, M., EISSFELLER, B. Comparison of multipath mitigation techniques with consideration of future signal structures. In *Proceedings of ION GNSS*, OR, USA, Sep 2003, p. 2584 – 2592.

[13] BETZ, J. W., KOLODZIEJSKI, K. R. Extended theory of early-late code tracking for a bandlimited GPS receiver. *Navigation: Journal of the Institute of Navigation*, 2000, vol. 47, no. 3, p 211 to 226.

[14] BRAASCH, M. S. Performance comparison of multipath mitigating receiver architectures. In *Proceedings of IEEE Aerospace Conference*. Big Sky (Mont, USA), Mar 2001, p. 1309 - 1315.

[15] HURSKAINEN, H., LOHAN, E. S., HU, X., RAASAKKA, J. NURMI, J. Multiple Gate Delay tracking structures for GNSS signals and their evaluation with Simulink, SystemC, and VHDL. *International Journal of Navigation and Observation*, 2008, DOI:10.1155/2008/785695.

[16] GARIN, L., ROUSSEAU, J. M. Enhanced strobe correlator multipath rejection for code and carrier. In *Proceedings of ION GPS.* Kansas City (USA), Sep 1997, p. 559 - 568.

[17] JONES, J., FENTON, P., SMITH, B. Theory and performance of the pulse aperture correlator. *Tech. Report*, NovAtel, Canada, Sep 2004.

[18] WEILL, L. R. Multipath mitigation - How good can it get with new signals? *GPS World*, 2003, vol. 16, no. 6, p. 106 – 113.

[19] BELLO, P. A., FANTE, R. L. Code tracking performance for novel unambiguous M-code time discriminators. In *Proceedings of ION NTM.* San Diego (USA), Jan 2005.

[20] FANTE, R. Unambiguous tracker for GPS binary-offset carrier signals. In *Proc. of ION NTM.* Albuquerque (USA), 2003.

[21] FANTE, R. Unambiguous first-order tracking loop M-code. *MITRE Technical Paper*, 2004.

[22] BHUIYAN, M. Z. H. *Analyzing Code Tracking Algorithms for Galileo Open Service Signal*. M.Sc. Thesis, 2006, Tampere University of Technology, Finland.

[23] VAN DIRENDONCK, A. J., BRAASCH, M. S. Evaluation of GNSS receiver correlation processing techniques for multipath and noise mitigation. In *Proceedings of ION NTM.* CA, USA, Jan 1997, p. 207 - 215.

[24] TOWNSEND, B., FENTON, P. A practical approach to the reduction of pseudorange multipath errors in a L1 GPS receiver. In *Proceedings of ION GPS*. UT, USA, Sep 1994, p. 143 - 148.

[25] SLEEWAEGEN, J. M., BOON, F. Mitigating short-delay multipath: A promising new technique. In *Proceedings of ION GPS.* UT, USA, Sep 2001, p. 204 - 213.

[26] BHUIYAN, M. Z. H., LOHAN, E. S., RENFORS, M. A Slope-based multipath estimation technique for mitigating short delay multipath in GNSS receivers. In *Proceedings of the IEEE International Symposium on Circuits and Systems*. Paris (France), 2010, p. 3573–3576.

[27] PHELTS, R. E., ENGE, P. The multipath invariance approach for code multipath mitigation. In *Proceedings of ION GPS.* UT, USA, Sep 2000, p. 2376 - 2384.

[28] PHELTS, R. E., ENGE, P. Multipath mitigation for narrowband receivers. In *Proceedings of the IEEE PLANS*. CA, USA, Mar 2000, p. 30 - 36.

[29] VAN NEE, R. D. J. The multipath estimating delay lock loop. In *Proceedings of IEEE Second International Symposium on Spread Spectrum Techniques and Applications*. Yokohama (Japan), 1992, p. 39 - 42.

[30] VAN NEE, R. D. J., SIERVELD, J., FENTON, P. C., TOWNSEND, B. R. The multipath estimating delay lock loop: approaching theoretical accuracy limits. In *Proceedings of IEEE Position Location and Navigation Symposium*, 1994, vol. 1, p. 246 - 251.

[31] TOWNSEND, B. R., VAN NEE, R. D. J., FENTON, P. C., VAN DIERENDONCK, A. J. Performance evaluation of the multipath estimating delay lock loop. In *Proceedings of ION NTM.* Anaheim (USA), Jan 1995.

[32] FENTON, P. C., JONES, J. The theory and performance of NovAtel Inc.'s vision correlator. In *Proceedings of ION GNSS.* Long Beach (USA), Sep 2005, p. 2178 - 2186.

[33] WEILL, L. R. Multipath mitigation using modernized GPS signals: How good can it get? In *Proceedings of ION GPS*. CA, USA, Sep 2002, p. 493 - 505.

[34] BHUIYAN, M. Z. H., LOHAN, E. S. Advanced Multipath Mitigation Techniques for Satellite-Based Positioning Applications. *International Journal of Navigation and Observation*, 2010, DOI:10.1155/2010/412393.

[35] BHUIYAN, M. Z. H. *Analysis of Multipath Mitigation Techniques for satellite-based Positioning Applications*. Ph.D. thesis, 2011, Tampere University of Technology, Finland.

[36] LOHAN, E. S., LAKHZOURI, A., RENFORS, M. Feedforward delay estimators in adverse multipath propagation for Galileo and modernized GPS signals. *EURASIP Journal of Advances in Signal Processing*, 2006, Article ID 50971.

[37] WU, J., DEMPSTER, A. G. Validation of carrier multipath mitigation for BOC-GPRN discriminator. In *Proceedings of ENC-GNSS*. Naples (Italy), May 2009.

[38] BHUIYAN, M. Z. H, LOHAN, E. S., RENFORS, M. Code tracking algorithms for mitigating multipath effects in fading channels for satellite-based positioning. *EURASIP Journal on Advances in Signal Processing*, 2008, Article ID 863629.

[39] BHUIYAN, M. Z. H., ZHANG, J., LOHAN, E. S. Enhanced delay tracking performance of a C/N_0-based two-stage tracker for GNSS receivers. In *Proceedings of the European Navigation Conference on Global Navigation Satellite System.* Braunschweig (Germany), Oct 2010.

[40] Tampere University of Technology. *Simulink-based open source Galileo E1 signal simulator.* [Online] Cited 2012-04-23. Available at: http://www.cs.tut.fi/tlt/pos/Software.htm.

[41] German Aerospace Center. *Land Mobile Multipath Channel Model V3.0.* [Online] Cited 2012-04-23. Available at: http://www.kn-s.dlr.de/satnav/LandMobile.html.

[42] European Space Agency. *Galileo Open Service Signal In Space Interface Control Document*. Issue 1, Revision 1, European Space Agency, Sep 2010.

[43] SIDDIQUI, B. A., ZHANG, J., BHUIYAN, M. Z. H., LOHAN, E. S. Joint data-pilot acquisition and tracking of Galileo E1 open service signal. In *Proceedings of UPINLBS'2010*. Helsinki (Finland), Oct 2010.

[44] PARKINSON, B. W., SPILKER, J. J. Global positioning system: Theory and applications. *American Institute of Aeronautics*, vol. 1, 1996, p. 390 - 392.

About Authors

Mohammad Zahidul H. BHUIYAN received his M.Sc. degree in 2006 and Ph.D. degree in 2011 from the Department of Communications Engineering, Tampere University of Technology, Finland. During his Ph.D., he visited Positioning, Location and Navigation research group in University of Calgary, Canada for about ten months. He had also been actively involved in several EU, TEKES and Academy of Finland funded research projects. He joined the Department of Navigation and Positioning at the Finnish Geodetic Institute in October 2011 as a senior research scientist with research interests covering various aspects of GNSS receiver design and sensor fusion algorithms for seamless outdoor/indoor positioning.

Jie ZHANG received her B.Sc. degree in Communications Engineering from Beijing University of Technology, China and M.Sc. degree in RF Electronics from Tampere University of Technology, Finland in 2010. Currently, she is a PhD candidate and researcher in the Dept. of Communications Engineering at Tampere University of Technology, Finland. Her research interests include signal processing for multi-mode multi-frequency operation in navigation devices and path-loss modeling for indoor positioning.

Elena Simona LOHAN completed the M.Sc. degree in Electrical Engineering from the Politehnica University of Bucharest, Romania, in 1997, the D.E.A. degree in Econometrics, at Ecole Polytechnique, Paris, France, in 1998, and the Ph.D. degree in Telecommunications from Tampere University of Technology. Since December 2003, she has been working as an Adjunct Professor at TUT and she has been acting as a group leader for the mobile and satellite-based positioning activities at the Department of Communications Engineering. Her research interests include wireless positioning techniques, GNSS receiver architectures, CDMA signal processing, and wireless channel modelling and estimation. She was also involved with the EU FP6 project GREAT and EU FP7 project GRAMMAR as a technical team leader and working package leader, respectively.

Wei WANG received the Bachelor degree in the field of Communications Engineering from University of Wuhan, China, in 2003 and the Master degree from University of Kiel, Germany, in 2006. Since 2007, he has been working as a scientific staff member at the Institute of Communications and Navigation of German Aerospace Center (DLR), Oberpfaffenhofen, Germany. His research interests are channel characteristics analysis and modeling for localization/navigation based on channel measurements, positioning/navigation and related topics.

Stephan SAND (M.Sc. EE 2001, Dipl.-Ing 2002, Dr.Sc. ETH Zurich 2010) is currently managing and working on multi-sensor navigation research projects at the Institute of Communications and Navigation, German Aerospace Center (DLR), Oberpfaffenhofen, Germany. He was visiting researcher at NTT DoCoMo R&D Yokosuka, Japan in 2004 and at the Swiss Federal Institute of Technology (ETH) Zurich, Switzerland in 2007 working in the area of wireless communications. Stephan has authored and co-authored more than 80 technical and scientific publications in conferences and journals in the areas of wireless communication and multi-sensor navigation. He has been involved in several research projects on mobile radio funded by the European Commission (4MORE, NEWCOM, COST289, PLUTO) and by international industry cooperation. In the GJU/GSA project GREAT and the EU FP7-ICT collaborative project WHERE, he has been leading the work on hybrid location determination. He was the coordinator of the recent EU FP7 project GRAMMAR on Galileo mass-market receivers. He is a member of the International Conference on Localization and GNSS (ICL-GNSS) steering committee and was the general chair of ICL-GNSS 2012.

Publication IV

J. Zhang, E. S. Lohan, "Multi-correlator structures for tracking Galileo signals with CBOC and SinBOC(1,1) reference receivers and limited front-end bandwidths," *Proc. of The 7th IEEE Workshop on Positioning, Navigation and Communication 2010 WPNC*, pp. 179-186, March 2010, Dresden, Germany.

Multi-correlator structures for tracking Galileo signals with CBOC and SinBOC(1,1) reference receivers and limited front-end bandwidths

Jie Zhang and Elena Simona Lohan
Department of Communication Engineering, Tampere University of Technology
Tampere, Finland
Email: jie.zhang, elena-simona.lohan@tut.fi

***Abstract*—Multipath is one of the paramount error sources in code tracking. Optimized Multiple Gate Delay structures have been proposed before for SinBOC(1,1)-modulated signal and infinite receiver bandwidth, in order to cope better with multipath. The new modulation, Composite Binary Offset Carrier (CBOC) modulation, used in Galileo E1 band makes it possible that either SinBOC(1,1) or CBOC reference code could be used in receiver design. In this paper, we describe the MGD optimization steps and optimized parameters for Galileo CBOC signals processed with SinBOC(1,1) and CBOC reference codes, respectively, and with limited front-end receiver bandwidth, that is usually employed in mass-market GNSS receivers. The performance of the proposed MGD structure is verified in a Galileo E1 Open Service (OS) Simulink-based software receiver. The performance evaluation criteria are based on Multipath Error Envelope (MEE) and Root Mean Square Error (RMSE) in multipath channels.**

I. Introduction

As one of the emerging Global Navigation Satellite Systems (GNSSs), Galileo is going to provide more services, higher availability and higher accuracy than the only fully operational GNSS nowadays, Global Positioning System (GPS). In order to inter-operate with GPS, Galileo E1 band has the same carrier frequency as GPS L1 band. In order to avoid the interference from GPS, a new modulation compared to GPS was proposed to be used. In the latest Galileo Open Service, Signal In Space Interface Control Document (OS SIS ICD) [1], Composite Binary Offset Carrier (CBOC) modulation was assigned for Galileo E1 band. This new modulation is the sum (or difference) of two weighted Sine-Binary Offset Carrier (SinBOC) sub-carrier waves. The one used in E1 band is denoted via CBOC(6,1,1/11), which is the sum (or difference) of a SinBOC(1,1)-modulated code and a SinBOC(6,1)-modulated code, which includes $1/11$ power from SinBOC(6,1) component (and $10/11$ power from SinBOC(1,1) component). The two variants of CBOC(6,1,1/11) used in [1] are: CBOC(+), which is formed as the sum of the two sub-carrier waveforms SinBOC(1,1) and SinBOC(6,1), and CBOC(-), which is formed as the difference of the two sub-carrier waveforms. CBOC(+) is assigned for use in E1-B data channel and CBOC(-) is employed by the E1-C pilot (or dataless) channel. From the GNSS receiver point of view, it is realized that the conventional receiver implementation may be not the optimum solution for this modern signal in some heavy interference environment because of the ambiguity problem in the natural autocorrelation function of BOC or MBOC signal. Moreover, the CBOC modulation combines two sub-carrier wave component, the tracking can be done either with CBOC modulated reference codes (i.e., CBOC(+) for data channel and CBOC(-) for pilot channel), or with SinBOC(1,1)-modulated reference code for both E1-B and E1-C channels, since more than 90 percent power is on SinBOC(1,1) component.

In GNSS receiver, one of the main error sources is the multipath propagation. Several code delay tracking algorithms exists nowadays that try to mitigate the multipath problem. For example, Narrow Correlator (NCORR) proposed a narrower correlator spacing than the conventional early minus late code tracking (i.e.,$<$ 1 chip) [2]. Another class of enhanced algorithms is given by the so-called double-delta correlator. This class of delay tracking algorithms has gained more and more attention lately and it consists of an additional correlator pair, containing a Very Early(VE) correlator and a Very Late(VL) correlator, with which the tracking performance may be improved. On example in this class is the High Resolution Correlator (HRC)[3]. The spacing between VE and VL is twice the spacing between E (Early) and L (Late) correlators. Several papers showed that HRC has better performance than Narrow Correlator with medium and long path delays [5], [7], [6], and [8]. However, HRC cannot reject the short delay multipath effects and suffers from severe performance degradation in noisy environments. HRC is also under patent protection [3]. In [4], a so-called Multiple Gate Delay (MGD) was introduced, which is conceptually close to HRC, but it has more correlator pairs and flexible weighting factor. However, the tracking performance of the MGD proposed in [4] was significantly worse than Narrow Correlator. The main reason for that was that the weighting factor and correlator spacing were not optimized. An enhanced MGD structure was introduced in [5] and [6], where optimization of its parameters (correlator spacings and weighting coefficients) was done for SinBOC(1,1) modulation signal and for infinite receiver bandwidth only. The results in [5] and [6] showed that the optimized MGD for SinBOC(1,1) modulated signal has promising tracking performance in short delay multipath scenarios. However, the impact of limited front-end filter bandwidth and the impact of

CBOC modulation were not analyzed. In this paper, we present the MGD optimization for CBOC modulated signals with two types of receivers: one using a reference CBOC waveform, and the other one, more suited to mass-market applications, using reference SinBOC(1,1) waveform. The optimization is done under the realistic assumption of limited front-end bandwidth, varying between 3 and 24.552 MHz double-sided bandwidth.

This paper is organized as follows: first, we present the MGD structure with adjustable parameters and a method to optimize these parameters. The performances of optimized MGD structure in multipath channels is shown in terms of Multipath Error Envelope (MEE). Finally, we verify the optimized MGD in a Simulink-based GNSS software receiver, developed at Tampere University of Technology (TUT) within the GRAMMAR Eu-FP7 project.

II. Multiple Gate Delay Tracking Loop

A generic block diagram of MGD structure considered in this paper has several early and late shifted correlator pairs in the delay tracking loop. A maximum of N=3 early-late correlator pairs (meaning a total of 7 complex correlators if in-prompt correlator is considered) is currently employed in the optimization, but the general structure is valid for any $N >= 1$. The discriminator, which is the sum of weighted correlator pairs is then as the input of delay estimator. The delay is calculated, simply by searching for the zero crossing along the discriminator function. The discriminator of MGD structure is given by:

$$D(\tau) = \begin{cases} \sum_{i=1}^{N} a_i \left(\left| R_I\left(\tau + \frac{\Delta_i}{2}\right) + jR_Q\left(\tau + \frac{\Delta_i}{2}\right) \right|^P \right. \\ \left. - \left| R_I(\tau - \frac{\Delta_i}{2}) + jR_Q(\tau - \frac{\Delta_i}{2}) \right|^P \right), P = 1, 2 \\ \sum_{i=1}^{N} a_i \left(\left| R_I\left(\tau + \frac{\Delta_i}{2}\right) \right| + \left| R_Q\left(\tau + \frac{\Delta_i}{2}\right) \right| \right. \\ \left. - \left| R_I(\tau - \frac{\Delta_i}{2}) \right| - \left| R_Q(\tau - \frac{\Delta_i}{2}) \right| \right), P = -1 \end{cases} \quad (1)$$

where N is the number of correlation pairs; $R_I(\cdot)$ and $R_Q(\cdot)$ are the in-phase and quadrature phase of correlation function between received signal and reference code, respectively; the spacing between the i-th early and i-th late correlator equal to Δ_i; uniform spacing is used, which means $\Delta_i = i\Delta_1$. The factor P determines the type of nonlinearity: P=2 (square of envelope) and P=1 (envelope). For sake of a uniform model, we also introduced the notation P=-1, which stands for the sum of absolute value of real part and imaginary part of correlation function.

In this paper, we use the delay tracking loop structure shown in Figure 1. The in-phase (R_I) and quadrature (R_Q) correlations with Early(E) and Late(L) values are generated and shifted according to the estimated delay from the discriminator. A Numerically Controlled Oscillator (NCO) adjusts the code phase according to the smoothed error coming from the discriminator function. The smoothing is done via the loop filter, here using a code loop bandwidth of 3 Hz.

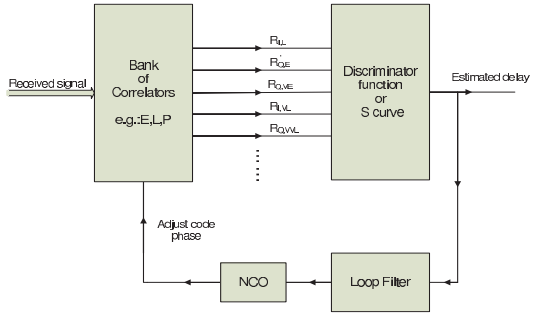

Fig. 1. The block diagram of tracking loop used

III. Optimization scheme

In order to decide the optimum coefficient, we use an optimization criterion for multipath performance assessment called Multipath Error Envelopes (MEE), which was also used in [5] and [7]. MEEs are widely used for illustrating the multipath performance of code tracking algorithms. The smaller the enclosed area between upper and lower multipath error envelope is, the better the performance in multipath is. The optimum coefficients would be those which offer the minimum MEE enclosed area for a variety of multipath profiles. The illustration of this enclosed MEE area principle is shown in Figure 2 for a Narrow Correlator structure and 3 MHz double-sided bandwidth.

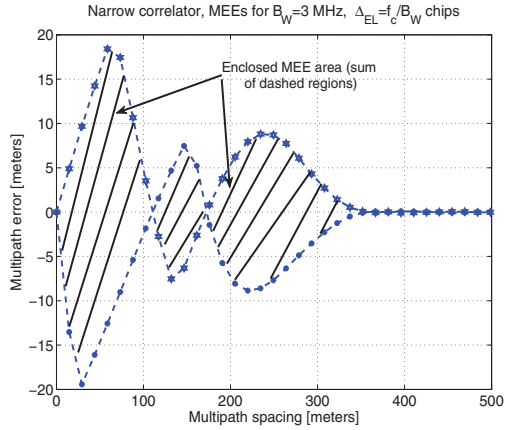

Fig. 2. Illustration of enclosed MEE area for Narrow Correlator case. $\Delta_1 = \Delta_{EL} = 0.34$ chips

The optimum coefficients are calculated as follows: first, we define a vector v_i, with a resolution of 0.1 and range of values between -1 and 1, which contains the search range for the optimum coefficients. The weighting coefficient a_1 is set at 1, without loss of generality. The channel is considered as a two-path static channel with the first path has unit amplitude

and the second path amplitude varies from 0.5 to 0.95, and the multipath spacing varies between 0 and 1.1 chips with a step of 0.05 chips. These assumptions on the channel multipath profiles are used in order to evaluate the best MGD structure for medium-to-strong multipath components, which are most likely to affect significantly the delay tracking accuracy. The final MEE will be obtained as an average of all MEE for each channel profile. In addition, under front-end limited bandwidth assumption, the spacing of first correlator pair is determined by the Equation (2), according to [9]:

$$\Delta_1 = \frac{f_c}{B_W} \tag{2}$$

where f_c is chip rate, $f_c = 1.023$MHz for E1 signal; B_W is the receiver double-sided front-end bandwidth in MHz. The successive spacings are given by $i\Delta_1$, $i = 2, 3$. Moreover, the correlation functions between received signal and reference code are built in such a way that CBOC(+) signal are correlated with CBOC(+) or SinBOC(1,1) reference code, and CBOC(-) signal is correlated with CBOC(-) or SinBOC(1,1) reference code, according to the used receiver type. Based on the above configurations, the optimum coefficient values a_2 and a_3 were found via s two dimensional searches for the second and third correlator pairs correspondingly.

IV. Tables with optimization parameters

Based on simulations, we noticed that the enclosed areas and optimum coefficients of MGD with $P = -1$ are exactly the same as those for $P = 1$. Therefore, we will not list those parameters for P=-1 separately.

If we compare the enclosed areas of optimum MGD for $P = 1$, $P = -1$, and $P = 2$ in Table I and Table II, the using of envelopes (i.e., $P = 1$ or $P = -1$) gives smaller or equal enclosure area compared to using of squaring envelopes ($P = 2$) for all signal types. Therefore using the envelopes or sum of absolute values in the implementation of code delay tracking is better than using the squared envelopes. This fact was also remarked in [7] for SinBOC(1,1).

Two well known reference structures are also shown in Table III and IV for comparison: the Narrow Correlator (NCORR) and the High Resolution Correlator (HRC) with $P = 1$. In fact, these two structures are particular cases of the MGD structure used in this paper: NCORR has the weighting coefficients vector a equal to $a = [1\ 0\ 0]$ and HRC has $a = [1\ -0.5\ 0]$ and $\Delta_2 = 2\Delta_1$. We found that the optimum MGD has a smaller enclosed average area than both Narrow Correlator and HRC. We also remark that, when the B_W is small, or the early-late spacing is high, the HRC has bigger enclosed area than NCORR. This points out towards the fact that HRC is not robust enough for narrow receiver front-end bandwidths.

The optimum MGD weighting parameters a are shown in Table V and Table VI for CBOC(-) and CBOC(+) modulation, respectively. We recall that CBOC(-) is used for the pilot E1-C channel and CBOC(+) is used for the data E1-B channel. In the both tables, various front-end filters are shown, as well as the two receiver options: one with reference CBOC-modulated code, and another one with reference SinBOC(1,1)-modulated code.

Figures 3 and 4 show the averaged MEE (over varying second path amplitude) for the Narrow Correlator (NCORR), High Resolution Correlator (HRC) and optimum MGD with B_W=3 MHz and CBOC(-) signal with SinBOC(1,1) reference code and CBOC reference code, respectively. The slight variations in the MEE curves are explained by the fact that, some spurious peaks might be obtained under certain second path amplitudes (e.g., second path very close in amplitude to the first path), and these spurious peaks make the averaged MEE less smooth than what is usually reported in literature under fixed second path amplitude.

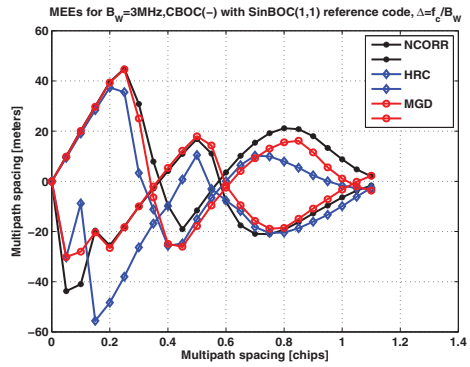

Fig. 3. The averaged MEE for NCORR, HRC and MGD with optimum parameters a=[1 -0.1 -0.2]. $P = 1$, $B_W = 3$ MHz, CBOC(-) signal with SinBOC(1,1) reference code.

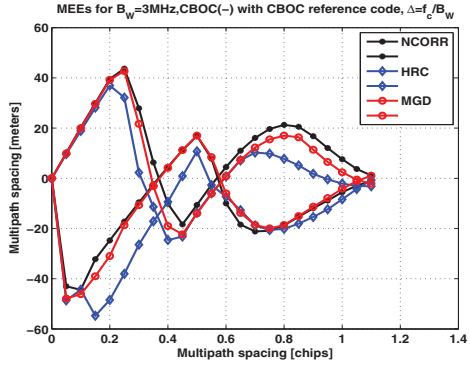

Fig. 4. The averaged MEE for NCORR, HRC and MGD with optimum parameters a=[1 -0.1 -0.1]. $P = 1$, $B_W = 3$ MHz, CBOC(-) signal with CBOC(-) reference code.

Figure 5 and Figure 6 show the average MEE for the Narrow Correlator, High Resolution Correlator and optimum MGD with B_W=24.552 MHz and CBOC(-) signal with SinBOC(1,1)

TABLE I
AVERAGED ENCLOSED MEE AREAS [CHIPS] FOR MGD STRUCTURES WITH OPTIMUM WEIGHTING COEFFICIENTS.

P=1 and P=-1				
Tx	CBOC(-)		CBOC(+)	
Rx	CBOC(-)	SinBOC(1,1)	CBOC(+)	SinBOC(1,1)
$B_W = 3MHz$	0.0296	0.0298	0.0312	0.0302
$B_W = 4MHz$	0.0261	0.0266	0.0301	0.0288
$B_W = 20.46MHz$	0.0024	0.0033	0.0035	0.0035
$B_W = 24.552MHz$	0.0021	0.0023	0.0029	0.0024

TABLE II
AVERAGED ENCLOSED MEE AREAS [CHIPS] FOR MGD STRUCTURES WITH OPTIMUM WEIGHTING COEFFICIENTS.

P=2				
Tx	CBOC(-)		CBOC(+)	
Rx	CBOC(-)	SinBOC(1,1)	CBOC(+)	SinBOC(1,1)
$B_W = 3MHz$	0.0297	0.03	0.0317	0.03
$B_W = 4MHz$	0.0287	0.0294	0.0327	0.032
$B_W = 20.46MHz$	0.0025	0.0035	0.0037	0.0038
$B_W = 24.552MHz$	0.0024	0.0027	0.0031	0.0024

TABLE III
AVERAGED ENCLOSED MEE AREA [CHIPS] OF OPTIMUM MGD, HRC AND NCORR FOR CBOC(-) TRANSMITTED SIGNAL

P=1 and P=-1						
Tx	CBOC(-)					
Rx	CBOC(-)			SinBOC(1,1)		
	MGD	HRC	NCORR	MGD	HRC	NCORR
$B_W = 3MHz$	0.0296	0.0307	0.0306	0.0298	0.0308	0.0313
$B_W = 4MHz$	0.0261	0.0357	0.0326	0.0266	0.039	0.0335
$B_W = 20.46MHz$	0.0024	0.0031	0.0047	0.0033	0.0033	0.0096
$B_W = 24.552MHz$	0.0021	0.0024	0.0043	0.0023	0.0025	0.0084

TABLE IV
AVERAGED ENCLOSED MEE AREA [CHIPS] OF OPTIMUM MGD, HRC AND NCORR FOR CBOC(+) TRANSMITTED SIGNAL

P=1 and P=-1						
Tx	CBOC(+)					
Rx	CBOC(+)			SinBOC(1,1)		
	MGD	HRC	NCORR	MGD	HRC	NCORR
$B_W = 3MHz$	0.0312	0.0338	0.0335	0.0302	0.0324	0.0328
$B_W = 4MHz$	0.0301	0.0428	0.0359	0.0288	0.0415	0.0349
$B_W = 20.46MHz$	0.0035	0.004	0.0067	0.0035	0.0038	0.0112
$B_W = 24.552MHz$	0.0029	0.0029	0.0059	0.0024	0.0024	0.0097

TABLE V
OPTIMUM WEIGHTING COEFFICIENT VECTOR a=[1 a_2 a_3] FOR MGD WHEN P=1 (OR P=-1) NON-LINEARITY

P=1 and P=-1								
Tx	CBOC(-)				CBOC(+)			
Rx	CBOC(-)		SinBOC(1,1)		CBOC(+)		SinBOC(1,1)	
	a2	a3	a2	a3	a2	a3	a2	a3
$B_W = 3MHz$	-0.1	-0.1	-0.1	-0.2	-0.2	-0.2	0.1	-0.3
$B_W = 4MHz$	0.3	-0.6	1	-1	0.4	-0.6	1	-1
$B_W = 20.46MHz$	0.1	-0.4	-0.2	-0.2	0.1	-0.4	-0.2	-0.2
$B_W = 24.552MHz$	0.3	-0.5	-0.8	0.2	-0.5	0	-0.8	0.2

TABLE VI
OPTIMUM WEIGHTING COEFFICIENT VECTOR a=[1 a_2 a_3] FOR MGD WHEN P=2 NON-LINEARITY

P=2								
Tx	CBOC(-)				CBOC(+)			
Rx	CBOC(-)		SinBOC(1,1)		CBOC(+)		SinBOC(1,1)	
	a2	a3	a2	a3	a2	a3	a2	a3
$B_W = 3MHz$	0.1	-0.2	0.1	-0.2	0.1	-0.4	0.1	-0.3
$B_W = 4MHz$	0.9	-1	0.9	-1	1	-1	1	-1
$B_W = 20.46MHz$	0.2	-0.6	-0.3	-0.2	0.1	-0.5	-0.3	-0.2
$B_W = 24.552MHz$	0.3	-0.6	-0.8	0.2	-0.8	0.2	-0.8	0.2

reference code and CBOC reference code, respectively. We remark that, for low receiver bandwidth (i.e, 3 or 4 MHz), typical in mass-market receivers, it makes sense to use a reference SinBOC(1,1) receiver in order to preserve a low complexity, while for higher front-end bandwidth (e.g., 24.552 MHz as specified in Galileo OS SIS ICD), a reference CBOC receiver will achieve the best performance.

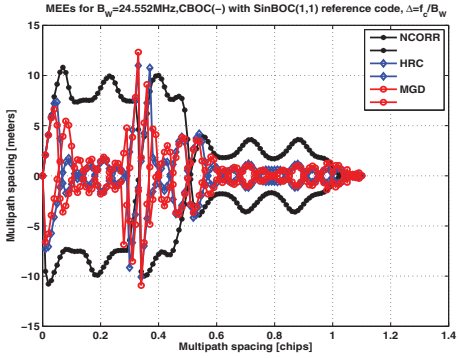

Fig. 5. The average MEE for NCORR, HRC and MGD with optimum parameters a=[1 -0.8 0.2]. P=1, B_W=24.552MHz, CBOC(-) signal with SinBOC(1,1) reference code

The results shown in Figures 3 to 6 showed that HRC is clearly not a good option in terms of MEE performance at low receiver bandwidths. For low bandwidths, MGD is slightly better than NCORR, but the gap is not significant. For high bandwidths, HRC and MGD outperforms the NCORR, while having a very similar performance. It seems that, in terms of MEE, the only advantage of using MGD versus NCORR at low bandwidths and HRC at high bandwidths is its higher flexibility and ability to offer a patent-free solution, adjusted to the designer needs (e.g., according to desired correlator spacing and sampling frequency).

V. SIMULINK-BASED IMPLEMENTATION

The results so far were obtained under zero noise (only the multipath presence was considered, as it is typically done when computing MEE curves). However, the noise presence may affect significantly the performance of the analyzed algorithms. The task of this section is to validate the MGD

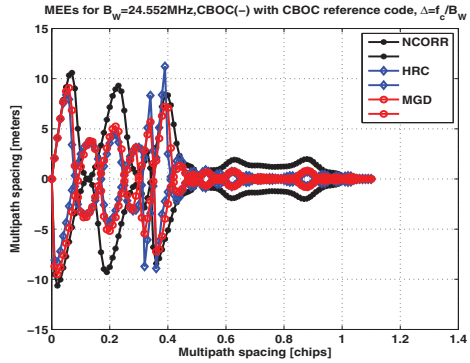

Fig. 6. The average MEE for NCORR, HRC and MGD with optimum parameters a=[1 0.3 -0.5]. P=1, B_W=24.552MHz, CBOC(-) signal with CBOC(-) reference code

algorithms via simulations in the presence of both noise and multipath, carrier out via a Simulink model for Galileo E1 signals.

A. Model description

Simulation is a powerful method in the analysis and design communication device. The performance of algorithm can be assessed before it is implemented on a real model. The simulator used in this paper for testing the MGD structure is a Galileo E1 Open Service (OS) simulator, which was created at Tampere University of Technology (TUT). The simulator model simulates the whole E1 channel, which consists of four parts: transmitter, propagation channel, acquisition and tracking block, as shown in Figure 7. Since the model is created based on Simulink tool in Matlab, it is easy to modify the key parameters and functions, such as code tracking discriminator function and modulation type of reference code.

The transmitter block is implemented with CBOC modulation, which exactly matches the latest Galileo OS SIS ICD. The propagation channel model takes the multipath and Additive White Gaussian Noise (AWGN) into account. The signal reception consists of acquisition and tracking unit block. Both SinBOC(1,1) and CBOC modulated code replica can be generated in tracking unit. The discriminators for E1B and E1C are implemented separately. Then the reference codes can

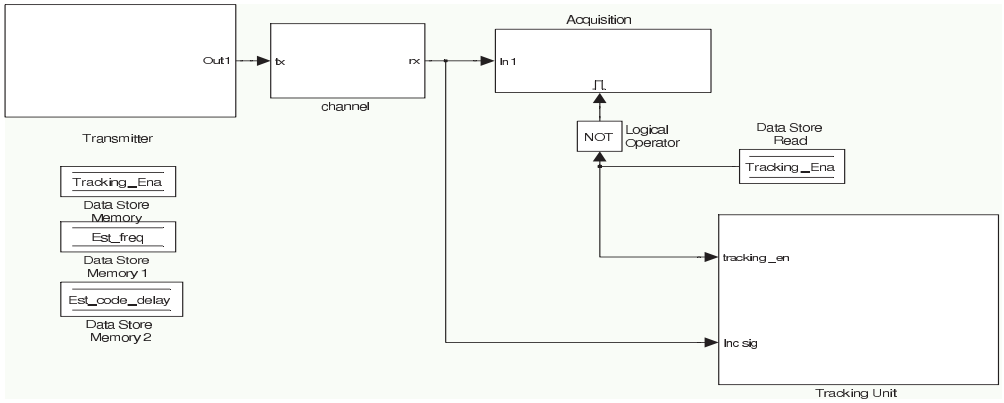

Fig. 7. The Simulink-based software receiver at TUT

be generated for E1B and E1C, separately. The MGD parameters used in discriminator can be also set differently, according to the modulation. In the reported simulation, SinBOC(1,1) modulated reference codes are used (similar results were obtained with a reference CBOC receiver). Therefore, the MGD parameters used in E1B channel are chosen for CBOC(+) transmitted signal with SinBOC(1,1) reference code and in E1C channel are the one for CBOC(-) with SinBOC(1,1) reference code. The receiver RF front-end filter is Chebyshev type I of filter and implemented in the channel block.

For optimized MGD structure, three pairs of correlator are needed: E-L, Very Early(VE)-Very Late(VL), Very Very Early(VVE)-Very Very Late(VVL). The correlator spacing between the E-L, VE-VL and VVE-VVL are uniformly increasing, Δ_1,$2\Delta_1$ and $3\Delta_1$, as presented in the previous section. The Δ_1 was dependent on the front-end bandwidth, via eq. (2).

In order to deal with the gain variations in the Simulink model, the discriminator function of 1 has to be normalized via a sum of early and late correlator. The envelope combining ($P = 1$) is used here, since it gives smaller code tracking error, as shown in Table I. The weighting coefficient vector a is a=[1 0 0] for Narrow Correlator; a=[1 -0.5 0] for High Resolution Correlator; a for MGD chosen from the Table IV has been used.

B. Simulation results

In order to test the performance of new structure, Root Mean Square Error (RMSE) between the estimated delay and the true Line-Of-sight (LOS) delay is calculated. The channel profile is set as two-path static channel with [0.08 0.24] chips delay and [0 -3] dB path gain. The front-end bandwidth are set as 3 MHz and 24.552 MHz, respectively. The early-late spacing is chosen as 0.34 chips for 3 MHz front-end bandwidth, according to min f_c/B_W rule. Here, $f_s = 13$ is sampling frequency in MHz. The MGD parameters for 3 MHz bandwidth are given in Table V, which are a=[1 -0.1 -0.2] for E1B and a=[1 0.1 -0.3] for E1C.

The early-late spacing for 24.552 MHz front-end bandwidth was set at 0.1 chips, slightly higher than the f_c/B_W rule. The reason why we chose 0.1 chips early-late spacing instead of $f_c/B_W = 0.04$ correlator spacing is due to the fact that a too small early-late spacing brings the problem of locking to false points with HRC and MGD, as illustrated in Figure 8. From this figure, it can be seen that the code tracking error with 0.04 chips early-late spacing converges to a higher value than for 0.1 chips early-late spacing , since it locks to a false point caused by the shape of the CBOC correlation function with SinBOC(1,1) receiver. The MGD parameters for 24.552 MHz bandwidth and 0.1 chips early-late are a=[1, -0.8, 0.2] for both CBOC(+) and CBOC(-) signal with SinBOC(1,1) reference code.

Figure 9 shows the RMSE versus Carrier-to-Noise Ratio(C/N0) for 3 MHz front-end bandwidth. Both HRC and optimum MGD have higher RMSE than Narrow Correlator, and MGD and HRC have almost the same performance. The fact that NCORR gives better results than MGD in terms of RMSE (which contradicts the table results where MGD had

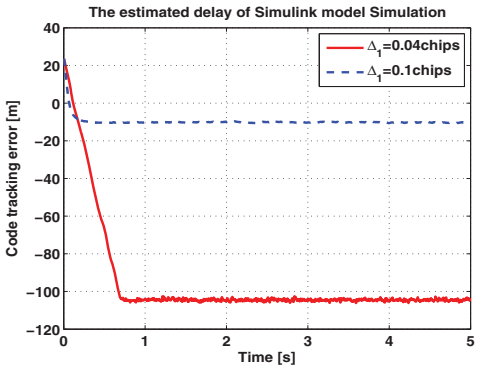

Fig. 8. An example of code tracking error versus simulation time for HRC with Δ_1=0.04 chips and Δ_1=0.1chips (false lock problem for low early-late spacings).

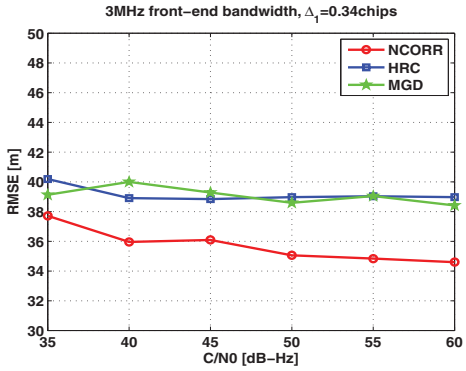

Fig. 9. The RMSE simulation results in two-path static channel, SinBOC(1,1) reference code, $\Delta_1 = 0.34$chips, MGD parameters [1, -0.1, -0.2] for E1B and [1, 0.1, -0.3] for E1C

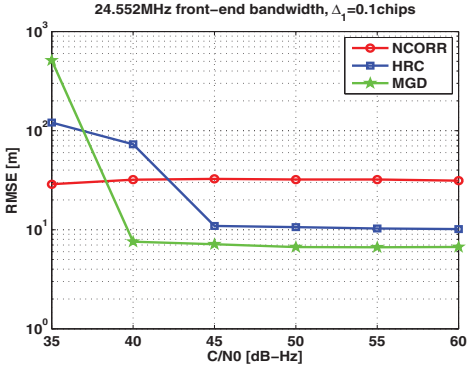

Fig. 10. The RMSE simulation results in two-path static channel, SinBOC(1,1) reference code, $\Delta_1 = 0.1$chips, MGD parameters [1, -0.8, 0.2] for both E1B and E1C

better envelope) is due to the fact that noise is not taken into account in the MEE curves and MGD optimization and noise robustness of NCORR is better than noise robustness of HRC and MGD. Figure 10 shows the RMSE versus C/N0 for 24.552 MHz front-end bandwidth. The MGD with optimum coefficient (a=[1 -0.8 0.2] for both CBOC(+) and CBOC(-) with SinBOC(1,1) reference code), outperforms the HRC and Narrow Correlator at higher C/N0. At lower C/N0, MGD and HRC have worse performance than NCORR, since the additional correlator pairs are more sensitive to the noise. A combined two-stage solution, using for example NCORR in the first stage, followed by MGD in a second stage could be further used to improve the performance at low C/N0 and it is currently under investigation. The RMSE curves from Figures 9 and 10 are almost flat with C/N0 variations because the mean bias (due to multipath propagation) is more severe than the code delay tracking error variance.

VI. Conclusions

In this paper, an analysis of Multiple Gate Delay tracking structure for Galileo E1 signal with limited front-end bandwidth in multipath environment has been done. We presented the steps of optimization of MGD parameters according to theoretical multipath Error Envelopes, and we showed their implementation in Simulink-based software receiver at Tampere University of Technology. We also compared the performance of the optimized MGD structures with that of NCORR and HRC structure. The results in both theory and simulations showed that the optimum MGD gives significantly better code delay tracking performance than the Narrow Correlator and High Resolution Correlator only with wide front-end bandwidth and under good C/N0 conditions. We also found that both MGD and High Resolution Correlator are not robust enough with narrow front-end bandwidths, and therefore NCORR structure is to be preferred in mass-market receivers with 3 or 4 MHz double-sided receiver bandwidth. Also, joint solutions of NCORR and MGD are possible and remain to be investigated.

Acknowledgment

The research leading to these results has received funding from the European Communitys Seventh Framework Programme (FP7/2007-2013) under grant agreement number 227890 and from Academy of Finland, which are gratefully acknowledged. The authors also want to thank Xuan Hu, a former member of the Department of Communications Engineering at Tampere University of Technology, who created the basic version of the Simulink model used within these studies. The Simulink model used in this paper is partly available as open-source model, distributed by Tampere University of Technology. For more details, contact the paper's authors.

References

[1] Galileo Open Service, Signal In Space Interface Control Document,OS SIS ICD (2008), Draft 1. http://www.gsa.europa.eu/go/galileo/os-sis-icd

[2] A. V. Dierendonck, P. Fenton, and T. Ford, Theory and performance of narrow correlator spacing in a GPS receiver, Journal of the Institute of navigation, vol. 39, pp. 265283, Fall 1992.

[3] G.A. McGraw, Rockwell Collins, M.S.Braasch, "GNSS Multipath Mitigation Using Gated and High Resolution Correlator Concepts," pp. 333-342, ION NTM 1999, Jan.1999.
[4] D. de Castro, J. Diez, and A. Fernandez, A New Unambiguous Low-Complexity BOC Tracking Technique, in Proc. of ION GNSS, 2006.
[5] D. Skournetou and E.S. Lohan, "Non-coherent multiple correlator delay structures and their tracking performance for Galileo signals," In Proc. of International Conference on ITS
[6] X. Hu and E. S. Lohan, GRANADA validation of optimized Multiple Gate Delay structures for Galileo SinBOC(1,1) signal tracking, in ITST Proceedings, (Sophia Antipolis, France), Jun 2007. Telecommunications (ITST), May/Jun 2007, Switzerland.
[7] H. Hurskainen, E. S. Lohan, X. Hu, J. Raasakka, and J. Nurmi, "Multiple gate delay tracking structures for GNSS signals and their evaluation with simulink, systemC, and VHDL," in International Journal of Navigation and Observation, vol. 2008, Article ID 785695, 17 pages, 2008.
[8] Irsigler, M. and Eissfeller, B., Comparison of Multipath Mitigation Techniques with Consideration of Future Signal Structures," Proceedings of International Technical Meeting of the Satellite Division of the Institude of Navigation, ION-GPS/GNSS 2003, Sept. 9-12, 2003, Portland, 2584-2592.
[9] J. W. Betz and K. R. Kolodziejski, Extended Theory of Early-Late Code Tracking for a Bandlimited GPS Receiver, to be Published in Navigation: Journal of The Institute of Navigation, Fall 2000.

Publication V

J. Zhang, D. Skournetou, W. Wang, S. Sand, E. S. Lohan, "Performance analysis of dual-frequency range estimation methods in the presence of ionospheric and multipath propagation effects," *Proc. of the International Conference on Localization and GNSS ICL-GNSS*, June 2012, Starnberg, Germany.

Performance Analysis of Dual-Frequency Range Estimation Methods in the Presence of Ionospheric and Multipath Propagation Effects

Jie Zhang, Danai Skournetou and Elena-Simona Lohan
Department of Communications Engineering
Tampere University of Technology
Tampere, Finland
Email: jie.zhang, danai.skournetou, elena-simona.lohan@tut.fi

Wei Wang and Stephan Sand
Institute of Communications and Navigation
German Aerospace Center (DLR)
Wessling, Germany
Email: Wei.Wang, Stephan.Sand@dlr.de

***Abstract*— In the global navigation satellite systems (GNSS), the performance of GNSS is subject to various errors, such as ionosphere delay, receiver noise and multipath. Among all these errors, the ionosphere delay error and multipath error are commonly regarded as the most limiting factors. In theory, a dual-frequency receiver can eliminate the ionospheric effect. However, in reality, the tracking error has effects on the ionospheric delay correction. This effect has not been studied, especially in realistic channel scenarios. In this paper, the authors investigate the effect of tracking error, obtained from Galileo signal Simulink-based simulators with realistic channel models on the range estimation in dual frequency receivers and compare the performance of three dual frequency ionosphere delay correction methods, namely the least square (LS), constrained LS (CLS) and Bruce Force Constraint (BFC). The results showed that the BFC performed the best below a fairly high ionosphere delay error. The LS method was only affected by multipath error, but the effect was small. CLS performance was better than or equal to LS at the expense of increased complexity.**

I. Introduction

Among the various error sources present in Global Navigation Satellite Systems (GNSSs), ionosphere accounts for the biggest part of signal's total delay [1] which has to be estimated and removed. Typically, the ionosphere layer is considered to start at 50 km from the earth surface and to end at 1000 km. Unlike the lower layers of atmosphere (e.g. troposphere, stratosphere, etc.), ionosphere contains charged particles (electrons and ions), the content of which depends on various spatial and temporal parameters (e.g. altitude, season, time of the day, etc.), as well as on the occurrence of natural phenomena (e.g. electromagnetic storms and traveling ionospheric disturbances). The presence of the charged particles makes ionosphere a dispersive medium, thus, signals transmitted at different carrier frequencies have different phase advances and time delays.

When the signal propagates through ionosphere, its velocity changes due to the interaction with particles present in it. As a result, the signal's code is delayed and its phase is advanced. In particular, the signal is delayed almost by as much as the carrier phase is advanced, thus, it is sufficient to estimate one of the two parameters (if higher order and bending effects are ignored, then the values of code delay and carrier phase advance are exactly the same [2]).

In order to mitigate the refraction effects, the knowledge of the involved refractive indices and signal's frequency is required. However, because ionosphere is an heterogeneous medium, meaning that the density of the ionised particles within it is not uniform (from now on we will consider only electrons since ions are much heavier [3]), its refractive index is defined by the electron density. Appleton and Lassen have derived a formula for computing the ionospheric refractive index [4], with which the ionospheric delay can be defined as the sum of first, second, third order and bending effects [2]. These effects are a function of the Total Electron Content (TEC), which is a space-time varying parameter to be estimated. It can be shown that for E1 signal, the second and third order effects contribute to the total ionospheric delay by a sub-meter and centimeter level, respectively (we remark, that the contribution of these two effects is similar for the rest of GNSS signals). Therefore, when mass-market receivers are considered, it suffices to consider only the first-order effect which accounts for almost 99% of the total delay [2]. For this reason, we ignore higher-order terms in our model and whenever ionospheric effects are mentioned, they shall be associated only with first-order terms.

Most of the methods for ionospheric delay estimation have been proposed for single-frequency receivers since this is the dominant design when mass-market production is regarded. However, the performance of a single-frequency method can be useful also for receivers which operate at more than one frequency. For example, if signals from other frequencies are lost and the time needed to re-acquire/re-track a lost signal is more than what can be afforded, the single-frequency method could be employed as backup option [5]–[8].

As mentioned earlier, the ionospheric delay depends mainly on two parameters: the total electron density and the carrier frequency. While the latter is a known constant, the former needs to be estimated in order to further estimate the ionospheric delay. In single-frequency receivers, TEC is found with the help of an appropriately chosen model which shows

the ionosphere status (i.e. TEC levels) for different locations and at different time periods. Moreover, such models are also responsible for making the necessary corrections for the ionospheric delay to a good degree of accuracy [9].

Unlike single-frequency receivers, no modeling of the ionosphere is needed when more than one carrier frequencies are available. For example, a dual-frequency receiver measures the pseudorange for each of the two received signals, both of which are contaminated by the same ionospheric effect. In theory (i.e., error-free scenario), proper combination of the available measurements allows the receiver to completely remove the ionospheric delay caused by first order effects [10] and this is one of the main advantages of dual-frequency receivers over single-frequency ones.

Navstar Global Positioning System (GPS) -based dual frequency receivers utilize the L1 and L2 frequencies since these are the two signals currently transmitted from GPS satellites; however, with the advent of the new modernized signals the designers will have the flexibility to choose a better combination. Considering the future Galileo system, the research on dual-frequency receivers is in its infancy. In author's earlier work, it was shown that the ability of dual-frequency methods to remove the first-order ionospheric delay is significantly affected by the presence of multipath propagation errors [12]. In this paper, we extend our earlier work by studying the performance of dual-frequency methods in more realistic channel environment. The multipath errors existing in the measured pseudorange are obtained from Galileo signal Simulink simulators in where the Channel Impulse Response (CIR) is generated within a parameterized artificial unban canyon scenario. We compare the performance of range estimation of three dual-frequency ionosphere correction methods. The novelty of this paper comes from analyzing the performance of dual-frequency ionospheric delay correction methods in the presence of realistic urban-canyon channels.

The remainder of this paper is organized as follows: Section II describes the three ionosphere delay algorithms for estimation of the pseudorange. Section III presents the setup used in the simulations. Section IV includes the results and discussion. Finally, Section V concludes the most important findings of this work.

II. Background

In code-based GNSS receivers, we can model the measured pseudorange in units of length as [7], [11]

$$\rho_i = \rho + E + I_i + \varepsilon_i \tag{1}$$

where ρ is the true satellite-receiver range, E encompasses all the error sources which are common to all received signals (e.g. clock bias, tropospheric delay) and I_i is the ionospheric delay corresponding to the signal transmitted in f_i carrier frequency and ε_i is the measurement error. More precisely, the ionospheric delay via a first-order approximation is as [2]

$$I_i = \frac{40.3}{f_i^2} TEC \tag{2}$$

where TEC is the total electron content measured in TEC Units (TECUs) with 1 TECU=10^{16} electrons/m^2. The measurement error, ε_i, is a residue of the processing done in the code tracking stage and is equal to $c(\hat{\tau}_i - \tau)$, where c is the speed of light, $\hat{\tau}_i$ and τ are the estimated and the true code delay, respectively, both given in units of time. We notice that the code tracking error is different for different signals because it depends on signal-specific characteristics such as type (i.e. data or pilot), modulation, frequency, etc. and it represents mostly the effects of noise and multipath propagation.

Starting from Eq. (1), we can form the following system of linear equations for a dual-frequency receiver if we assume E is zero (i.e. $i = 1, 2$)

$$\begin{cases} \rho_1 = \rho + \dfrac{40.3}{f_1^2} TEC + \varepsilon_1 \\ \rho_2 = \rho + \dfrac{40.3}{f_2^2} TEC + \varepsilon_2 \end{cases} \tag{3}$$

With the help of vector notations, we can write the system given in (3) in a compact form as

$$\begin{aligned} \begin{bmatrix} \rho_1 \\ \rho_2 \end{bmatrix} &= \begin{bmatrix} 1 & \frac{40.3}{f_1^2} \\ 1 & \frac{40.3}{f_2^2} \end{bmatrix} \begin{bmatrix} \rho \\ TEC \end{bmatrix} + \begin{bmatrix} \varepsilon_1 \\ \varepsilon_2 \end{bmatrix} \\ \mathbf{r} &= \mathbf{A}\mathbf{x} + \mathbf{e} \end{aligned} \tag{4}$$

where $\mathbf{r}$ is the observation vector that contains the pseudorange measurements, $\mathbf{A}$ is a 2×2 matrix, $\mathbf{x}$ is the unknown parameter vector to be estimated and $\mathbf{e}$ is the measurement error vector. Such a model can be extended straightforwardly to more than 2 frequencies if more are available (e.g., GPS L1, L2, L5 or Galileo E1, E5a/b, E6).

One of the most popular methods of solving a system of linear equations is the one that tries to minimize the squared difference between the observed data and $\mathbf{A}\mathbf{x}$, known as ordinary linear Least Square (LS) method. In particular, the LS solution is

$$\hat{\mathbf{x}}_{LS} = (\mathbf{A}^T\mathbf{A})^{-1}\mathbf{A}^T\mathbf{r} \tag{5}$$

where T denotes the operation of transposition.

The main disadvantage of LS methods is that its solution is unrestricted and thus highly sensitive to noise. Consequently, the estimate of the unknown vector $\mathbf{x}$ may violate certain physical limitations, associated with the unknown parameters. One way to avoid the aforementioned problem is to impose certain constraints in the solution of the ordinary LS, leading to what is commonly known as Constrained Least Square method (CLS). More precisely, the idea is to minimize the squared difference between the observed data and $\mathbf{A}\mathbf{x}$, subject to the linear inequality constraint $\mathbf{A}\hat{\mathbf{x}}_{CLS} \geq \mathbf{b}$, where $\mathbf{b}$ =[0 0] which means that both range and TEC estimates are forced to be non-negative. CLS is expected to provide a more accurate solution than LS at the expense of increased computational burden.

In order to reduce the computational complexity of CLS method and retain the advantage of increased accuracy via constrained solution, the authors have previously designed

TABLE I

SIMULATOR PARAMETERS

Parameters	Value
C/N_0 [dB-Hz]	[22:4:38]
fs [MHz]	26
IF [MHz]	E1: 7.9, E5a: 21.795
Tracking algorithm	Narrow Correlator

a simple method for estimating the range and the TEC parameters, called Brute Force Constraint (BFC), a detailed description of which can be found in [12].

III. SIMULATION SETUP

In our research here, we consider the carrier frequencies E1 (1575.42 MHz) and E5a(1176.45 MHz), assigned to Galileo Open Service (OS). The simulation setup is as follows: we generate 4 second of E1 signal measured range data and 1 second of E5a signal measured range data, which means for both signal, we have 1000 points of the measured range data (4 ms integration in E1 signal simulator and 1 ms in E5a signal simulator). This data includes true satellite-receiver rang, multipath error and ionospheric delay corresponding to the signal transmitted in E1 and E5a frequencies. More precisely, the true range is uniformly distributed between 18000 and 25000 km. Ionosphere delay is modeled as in Eq.2 for E1 and E5a frequencies, respectively. TEC parameter has been chosen in such a way that typical values encountered in various latitude are included [13]–[16] and is assumed to be constant within the data duration. The multipath errors for E1 and E5a signals are obtained with the help of two Simulink simulators, which are built at Tampere University of Technology for Galileo E1 and E5a signals, respectively. The detail about the structure and functionality of these simulators can be found in [17]. The simulators are freely available under open access license term at [18]. A general diagram of the simulator is shown in Fig. 1. The multipath error are obtained under two different channel profiles. One of them is single path static channel, in which the Channel Impulse Response (CIR) is static during the simulation. The other channel profile is a dynamic channel, where the CIR is generated within a parameterized artificial unban canyon scenario with house fronts, lamppost and so on. The channel profile takes also the position of satellite and receiver movement into account. Moreover, we use exact the same channel profiles for Galileo E1 and E5a signals in order to simulate that E1 and E5a signals are transmitted from the same satellite, so that both signals passes through the same satellite-receiver route. We also assume that the multipath error for E1 and E5a are uncorrelated. More detailed information about the dynamic channel generation can be found in [19]. The parameters of this dynamic channel and other simulator parameters, Carrier to Noise Density ratio C/N_0, sampling frequency f_s and Intermediate Frequency (IF) used in the simulation are summarized in Table II and Table I.

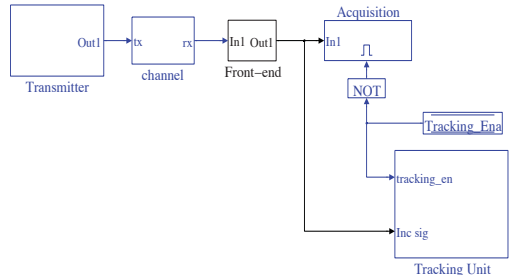

Fig. 1. Generic Simulink block of Galileo simulator at TUT (Open-source).

TABLE II

REALISTIC CHANNEL PROFILES

Scenario	I	II	III
Track type	Pedestrian		
Max receiver speed [m/s]	1		
Road width [m]	9		
Max No. of path	5	5	5
Path power [dB]	Dynamic		
Elevation of satellite [degree]	20	45	80

IV. SIMULATION RESULTS

In this section, we compare the range estimation performance of dual frequency receiver methods under different ionosphere and multipath errors in terms of Root Mean Square Error (RMSE). Fig. 2 and 3 show the RMS of multipath error obtained from the simulators under different channel profiles. These tracking errors are used in the measured range. The fluctuation in the curves is due to the fairly low C/N_0. In Fig. 4 and 5, we see the RMSE values for the case of single static channel. We observe that BFC performs the best at low TECU value. With the higher TECU, the performance of BFC is not always the best among three methods. On the other hand, if we compare Fig. 4 and Fig. 5, the LS performs more stable, it does not vary with the change of TECU value. The performance of CLS is getting closer to LS with higher TECU.

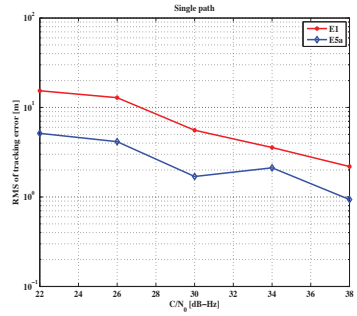

Fig. 2. Tracking error of E1 and E5a signals in static single path channel profile

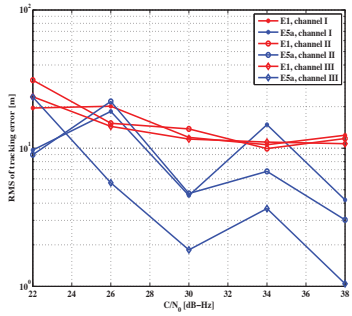

Fig. 3. Tracking error of E1 and E5a signals in dynamic channel profile

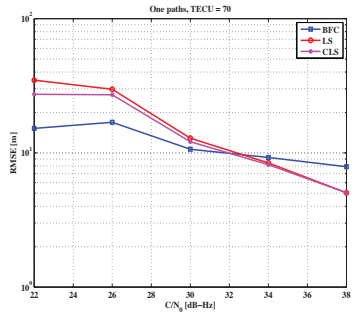

Fig. 5. RMS of range estimation error with TECU = 70 in static channel

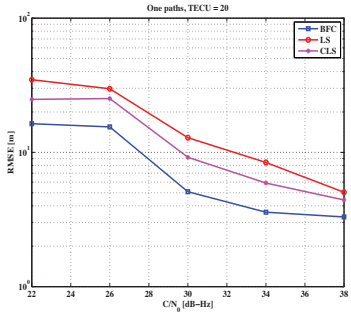

Fig. 4. RMS of range estimation error with TECU = 20 in static channel

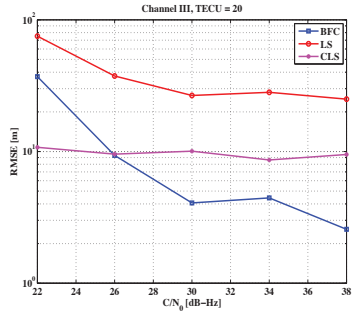

Fig. 6. RMS of range estimation error with TECU = 20 in channel III

Fig. 6 and Fig. 7 show the comparison between LS, CLS and BFC under dynamic channel profile with high satellite elevation. We observe that the LS method has the worst performance among three methods, but the performance of LS does not change with the TECU value. CLS method gives higher error with 70 TECU than that with 20 TECU. The performance of BFC changes dramatically with the increase of TECU.

Fig. 8 shows the performance of three methods versus different TECU values with C/N_0 at 38 dB-Hz. We observe that the RMSE of LS is constant with the same multipath error. The CLS method has better results than LS at low TECU and is merging to LS with the increasing of TECU. In all these three channel conditions, BFC has the best performance when TECU is under 100. The BFC has minimum RMSE at 40 TECU. This is because at this point, the ionosphere delay error and multipath error canceled with each other the most in the BFC method. Therefore, the totally error in the estimated range is smaller.

V. Conclusion

This paper focuses on the performance evaluation of dual frequency ionosphere delay correction methods in the presence of multipath error. First, we described three dual frequency ionosphere delay correction methods, LS, CLS and BFC. Next we examined the effect of code tracking error with realistic channel models in the performance of the above mentioned methods and provided comparative discussion of them.

The simulation results showed that the LS method was only affected by the tracking error, but not by the TECU. The performance of LS was constant with different ionosphere delay error if tracking error is the same. Moreover, the results showed that CLS method performed better than or equally to LS at the expense of increased computational complexity. The BFC methods was shown the best performance with TECU below 100. However, the performance of BFC deteriorated significantly with the increase of ionosphere delay error when the tracking error was low. Based on the observations and the fact that the measurement error was highly likely in multipath propagation channels, we would suggest that the BFC method would be used in dual frequency ionosphere correction. BFC method offered average the best performance than LS and CLS.

Acknowledgment

The author would like to thank Tampere Doctoral Programme in Information Science and Engineering (TISE) and Tekniikan edistämissäätiön (TES) for their support. This work has also been supported by th Academy of Finland, which is gratefully acknowledged.

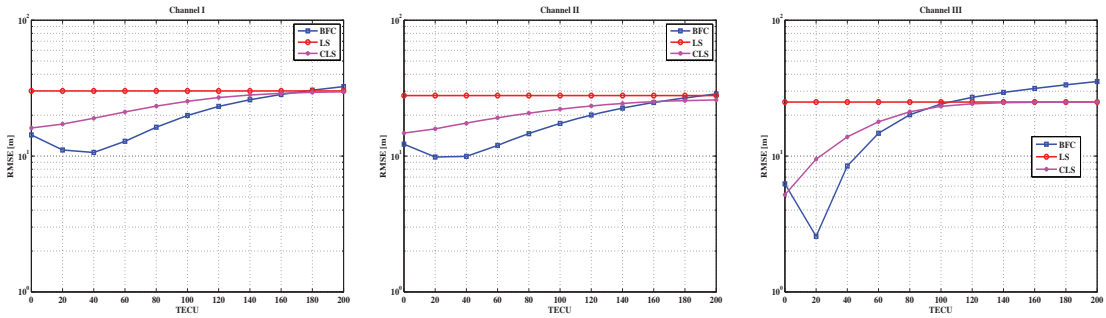

Fig. 8. RMSE vs. TECU in dynamic channel profiles

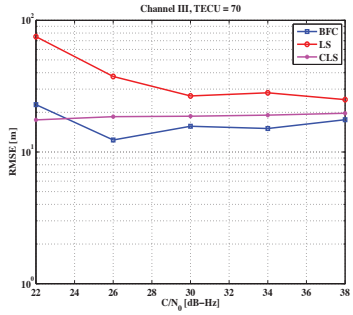

Fig. 7. RMS of range estimation error with TECU = 70 in channel III

REFERENCES

[1] E. Kaplan, Understanding GPS: Principles and Applications. Artech House, 1996.

[2] D. Odijk, Fast precise GPS positioning in the presence of ionospheric delays, Ph.D. dissertation, Publications on Geodesy 52, Netherlands Geodetic Commission, Delft, Netherlands, November 2002.

[3] P. Misra and P. Enge, Global Positioning System: Signals, Measurements, and Performance. Lincoln, Massachusetts: Ganga-Jumuna Press, 2001.

[4] E. V. Appleton, U. R. S. I. papers, 1927, washington.

[5] B. Bidaine, R. Prieto-Cerdeira, and R. Orus, Nequick: In-depth analysis and new developments, in In proc. of the 3rd ESA Workshop on Satellite Navigation User Equipment Technologies NAVITEC 2006 [CD-Rom], Noordwijk, The Netherlands, 2006.

[6] J. Seo, T. Walter, and P. Enge, Availability benefit of future dual frequency gps avionics under strong ionospheric scintillation, in ION GPS/GNSS, Savannah, GA, September 2009.

[7] Y. Yang, R. Sharpe, and R. Hatch, L1 backup navigation for dual frequency gps receiver, in ION GPS/GNSS, Portland, Oregon, September 2003, pp. 12581263.

[8] A. Batchelor, P. Fleming, and G. Morgan-Owen, Ionospheric delay estimation in the european global navigation overlay service, in Remote Sensing of the Propagation Environment (Digest No: 1996/221), IEE Colloquium on, nov 1996, pp. 3/1 3/6.

[9] G. S. B. Rao and R. Goswami, Ionospheric delay estimation for improving the global positioning system position accuracy, IETE Journal of Research, vol. 54, no. 1, pp. 2329, 2008.

[10] U. Engel, A theoretical performance analysis of the modernized GPS signals, in Position, Location and Navigation Symposium, 2008 IEEE/ION, May 2008, pp. 10671078.

[11] J. A. Farrell and M. Barth, The Global Positioning System and Inertial Navigation. McGraw-Hill, 1999, (ISBN-0-07-022045-X).

[12] D. Skournetou and E.-S. Lohan, Ionosphere-corrected range estimation in dual frequency global navigation satellite systems receivers, Radar, Sonar Navigation, IET, vol. 5, no. 3, pp. 215 224, March 2011.

[13] G.X.Gao, S. Datta-Barua, T.Walter, P.Enge, "Ionosphere effects for wideband GNSS signals", ION Annual Meeting, Cambridge, MA, 2007

[14] G.W.Hein, , J.A. Avila-Rodriguez,; "Combining Galileo PRS and GPS M-Code", Inside GNSS, 2006, 1, (1), pp. 4856

[15] A.J.Mannucci,"Ionosphere and ionospheric delay", www.cosmic.ucar.edu/summercamp2005/presentations/MannucciAnthony20050602. pdf (2005), presentation available online; accessed 5 January 2010

[16] Australian Government IPS Radio and Space Services TEC Global Map, http://www.ips.gov.au/Satellite/2/1/5

[17] J. Zhang, E. S. Lohan, *Galileo E1 and E5a link-level performances in single and multipath channels*, International ICST Conference on Personal Satellite Services (PSATS), Malaga, Spain, 2011.

[18] Simulink open-source software for Galileo E1 signals, *http://www.cs.tut.fi/tlt/pos/Software.htm*, Tampere University of Technology, accessed Mar 2011.

[19] W. Wang, T. Jost, A. Lehner, F. Perez-Diaz and U.-C. Fiebig, "Towards a Channel Model for Joint GNSS and Mobile Radio based Positioning," in Proc.of COST Action IC1004, Cooperative Radio Communications for Green Smart Environments, Lisbon, Portugal, 2011.

Publication VI

J. Zhang, J. Salmi, E. S. Lohan, “Analysis of kurtosis-based LOS/NLOS identification using indoor MIMO channel measurements,” *IEEE Transactions on Vehicular Technology*, vol. 62, issue 6, pp. 2871-2874, July 2013.

Analysis of Kurtosis-based LOS/NLOS Identification using Indoor MIMO Channel Measurement

Jie Zhang, Jussi Salmi, *Member*, *IEEE*, and Elena-Simona Lohan

***Abstract*— The location of the mobile station (MS) can be estimated from the distance measures between MS and several base stations (BS). However, the distance measure accuracy is degraded due to the complicated indoor environment, particularly Non Line-of-Sight (NLOS) propagation. In order to improve the accuracy of wireless localization, the knowledge of whether the BS - MS path is Line-of-Sight (LOS) or NLOS may be of significant importance. Several papers have proposed to use kurtosis for the NLOS identification in ultra wide band systems. In this paper, we investigate the kurtosis of different channel impulse response (CIR) forms and explore the potential of kurtosis for LOS/NLOS identification with two sets of bandwidth and number of frequency tap configurations in terms of simulations. The statistical analysis of kurtosis is also conducted with an extensive set of Multiple-Input and Multiple-Output (MIMO) channel measurement data collected at Aalto University. Both simulation and measurement results indicate that using decibel of CIR amplitude in kurtosis calculation provides consistent information about the LOS/NLOS condition regardless of system parameters. The results also show that average kurtosis over the MIMO channels, when available, gives a better indication of the LOS/NLOS conditions.**

***Index Terms*—Identification, kurtosis, LOS, MIMO measurement, NLOS**

I. Introduction

OVER the last few years, localization and navigation services in wireless mobile networks have gradually entered into the daily life of the people all over the world, in most of the cases through applications such as route guidance. This trend will continue in the future and more people will become direct or indirect users of such services. Basically, the mobile station (MS) location may be determined based on the distance measures between MS and several base stations (BS). The distance measures can be estimated based on, for example, a logarithm-distance path-loss model [1]-[4] as shown in (1):

$$PL\ [\mathrm{dB}] = PL_0 + n10\log_{10}\frac{d}{d_0} + X_g \tag{1}$$

where PL is total path loss measured in decibel (dB); PL_0 is the path loss in dB at the reference distance d_0; d is the length of the path; n is the path loss exponent, X_g is a Gaussian random variable with zero mean. In this path-loss model, PL and PL_0 are usually obtained by the measurement. Therefore, the distance d between MS and BS can be estimated if n and X_g are known. However, the accuracy of n and X_g estimation depends on the wireless propagation channel. If the path between MS and BS is in the Line-of-Sight (LOS), accurate n and X_g estimation yields high quality distance d estimates, and thus enables MS localization. However, Non Line-of-Sight (NLOS) conditions in MS-BS path often occur indoors due to complex building structures, which block the direct radio link. The precision of path-loss parameters estimation is degraded, which results in poor estimation of MS location. It is therefore critical to identify NLOS conditions so that the accuracy of path-loss model could be improved.

Several papers have proposed different techniques based on kurtosis for NLOS identification [5] - [7]. However, these identification techniques are mainly used in Ultra Wide Band (UWB) system, which has >500MHz absolute bandwidth or a large relative bandwidth (larger than 20%) [8]. The distribution of Channel Impulse Response (CIR), hence the kurtosis in other systems might be very different from those in UWB systems. The kurtosis-based NLOS identification may not be valid with different system configurations. This research investigates the kurtosis of different CIR forms with two sets of bandwidth and number of frequency tap configurations in the simulations. With an extensive set of Multiple-Input and Multiple-Output (MIMO) channel measurement data, which were collected at Aalto University [9], the statistical analysis of kurtosis in MIMO channel and Single-Input and Single-Output (SISO) channel is conducted.

Manuscript received August 29, 2012; revised December 18, 2012, January 30, 2013. The author would like to thank Graduate School in Electronics, Telecommunications and Automation (GETA) and Tampere Doctoral Programme in Information Science and Engineering (TISE) for their support. This work has also been supported by the Academy of Finland, which is gratefully acknowledged.

Jie Zhang is with the Department of Electronics and Communications Engineering, Tampere University of Technology, Tampere, Finland (e-mail: jie.zhang@tut.fi).

Jussi Salmi is with the Aalto University School of Electrical Engineering, SMARAD CoE, Department of Signal Processing and Acoustics, Espoo, Finland (e-mail: jussi.salmi@aalto.fi).

Elena-Simona Lohan is with the Department of Electronics and Communications Engineering, Tampere University of Technology, Tampere, Finland (e-mail: elena-simona.lohan@tut.fi).

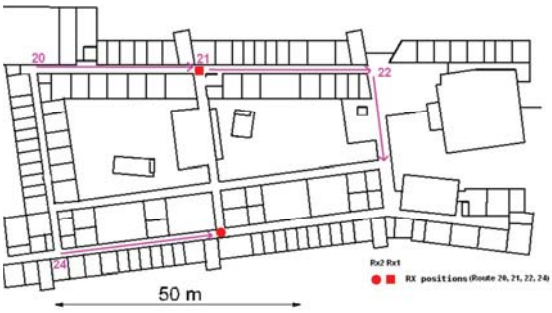

Fig. 1: The map of routes.

The contribution of this paper is two-fold. First, it utilizes a different form of CIR for kurtosis calculation, in which way the kurtosis values in both LOS and NLOS conditions are more consistent regardless of system configurations than the conventional method. Second, it provides statistical analysis of kurtosis in both MIMO channel and SISO channel.

The remainder of this paper is organized as follows: Section II describes the channel measurement environment; Section III presents the definition of kurtosis; Section IV and V show the statistical results and discussion in terms of simulations and measurements, respectively; finally, conclusions are drawn in Section VI.

II. Measurement Description

Radio channel measurements were carried out at Aalto University, Computer Science Building. The building has typical office or library structure: it is a three-storey building with a large hall in the middle. The hall occupies the whole height of the building and is surrounded by the classrooms and offices. The measurements use a MIMO channel sounder [9] with 5.3 GHz center frequency, 120 MHz signal bandwidth and two separate receiver units. Four measurement routes considered in this article are shown in Fig. 1. The location of RX1 and RX2 are fixed and the transmitter is moving along the route in the direction of the arrow. These routes cover both of LOS and NLOS conditions. Each route has a large number of snapshots (instantaneous MIMO channel realizations, spaced 39.32 ms apart). With two receivers, we have CIR of TX-RX1 and TX-RX2 links with MIMO matrix size of 30 × 32 and 30 × 30, respectively. More details about the antenna structure and measurement configurations can be found in [9].

III. Parameter Definition and Statistical Analysis

Kurtosis is defined here as the ratio of the fourth-order moment of the data to the square of the second-order moment. It characterizes the peakedness of the data samples. The kurtosis has also been defined as "a measure of whether the data is peaked or flat relative to a Gaussian distribution" [10]. For example, the data samples with high kurtosis tend to have a distinct peak near the mean, while data sets with low kurtosis tend to have a flat top near the mean rather than a sharp peak. Thus, the kurtosis metric can be used to identify LOS channel since the CIR are peakier with respect to flatter NLOS channels. Mathematically, the kurtosis can be expressed as in (2),

$$\kappa = \frac{E\left[\left(X-\mu_X\right)^4\right]}{E\left[\left(X-\mu_X\right)^2\right]^2} = \frac{E\left[\left(X-\mu_X\right)^4\right]}{\sigma_X^4} \tag{2}$$

where X is the random variable under evaluation, μ_X and σ_X are the mean and standard deviation of X, respectively. In [5]-[7], the authors have taken the CIR amplitude, X=|h(t)| as the data samples for kurtosis calculation in UWB system. However, the properties of the CIR and hence the kurtosis might be different depending on the system parameters. Moreover, the kurtosis calculation by using the |h(t)| may not be the best option for NLOS identification, since the linear scale amplitude is positive and thus always different from Gaussian. In this paper, we evaluate the kurtosis of the CIR amplitude in logarithmic scale. The kurtosis is the same with any logarithm with any scale factor in front, but in this article, we use X=20log$_{10}$(|h(t)|), which is supported by the often assumed log-normal of the CIR amplitude fading. We assume the kurtosis to have a high value for LOS and a low value for NLOS (ideally 3 for a pure Gaussian random variable). For this reason, the decision can be taken for NLOS when κ is smaller than a certain threshold [12]. Moreover, we use different MIMO channels to average over the kurtosis estimates computed from each individual CIR.

IV. Simulation Results

In order to evaluate the kurtosis of different CIR forms in LOS/NLOS conditions and the dependence of kurtosis value on the bandwidth and the number of frequency tap, the computer simulations have been carried out using the

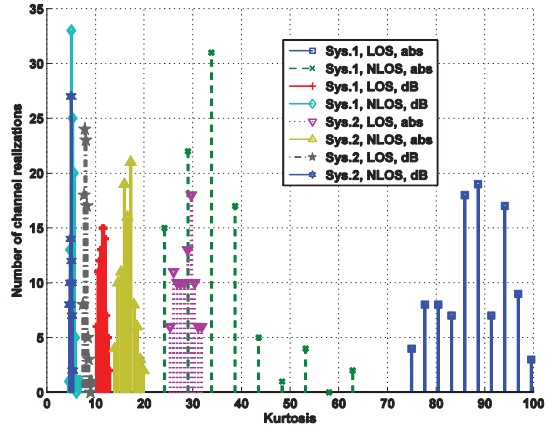

Fig. 2: Histograms of kurtosis with simulated channel impulse response. The dB based kurtosis yields reasonable threshold selection for both system parameter sets, whereas absolute value based is more sensitive on the system settings.

calibrated model of the same cylindrical dual-polarized antenna arrays that was used in the measurements. In the simulation, the transmitter location is fixed. The receiver is randomly placed within +/- 25m away from the transmitter and the scatters are randomly placed +/- 50 meters away from the transmitter. There are 30 scatters in NLOS condition and one direct path with five scatters in LOS condition. The simulation generates CIR vectors for two different system parameters: 1) 120 MHz bandwidth and 192 frequency taps (CIR length = 192/120 MHz = 1.6 micro seconds (μs)), which corresponds to the data from the sounder in the measurements, and 2) 20 MHz bandwidth and 64 frequency taps (CIR length = 64/20 MHz = 3.2 μs), which corresponds to 802.11 Wireless Local Area Network (WLAN) Orthogonal Frequency Division Multiplexing (OFDM) standards. For each set of parameters, we have 100 channel realizations. In each channel realization, 30×32 CIR vectors are generated and the kurtosis is calculated as the average of all the kurtosis values of each CIR vector. The variable X is by taken CIR h(t) samples with two different methods: 1) the amplitude of CIR, X=|h(t)|; 2) logarithm of CIR amplitude, X=20log10(|h(t)|).

The histograms of kurtosis values in LOS and NLOS conditions with two sets of system parameters ("Sys.1" and "Sys.2" in the plot) are shown in Fig. 2. The distribution of kurtosis by using CIR amplitude ("abs" in the plot) has significant dependence on the system parameters for both LOS and NLOS conditions. A general threshold for NLOS identification is hard to select due to the high variation in kurtosis between system parameters. On the other hand, by using dB of CIR amplitude ("dB" in the plot) as variable, the kurtosis is less sensitive to the system parameters. The kurtosis values in LOS and NLOS conditions for both systems have small variance between channel realizations. The kurtosis value in NLOS conditions is close to 3, which indicates that the probability density function of variable is close to Gaussian distribution. From the NLOS identification point of view, by using dB of CIR amplitude as variable, the kurtosis shows good consistence and separation between LOS and NLOS, regardless the system parameters. Therefore, a general threshold can be easily selected for NLOS identification even the system parameters would change.

V. Measurement Results

The kurtosis was also evaluated with measurement data. In the measurement, we obtain 30×32 CIR vectors for TX-RX link and 30×30 CIR vectors for TX-RX2 link at each snapshot. The kurtosis at each snapshot is calculated as the average of 30×32 kurtosis values for TX-RX1 link and 30×30 kurtosis values for TX-RX2 link. Figure 3 - Figure 6 show the average kurtosis of CIR amplitude in the logarithmic scale at different routes. As can be seen in Fig. 3, 4 and 6, the average kurtosis curves (solid lines) show a clear separation for LOS and NLOS conditions for all the routes under consideration. In Fig. 5, the average kurtosis curves are quite similar for TX-RX1 and TX-RX2 links, which are both in NLOS conditions. Figure 3 - Figure 6 also show the 90% quantiles and 10% quantiles of kurtosis values (960 kurtosis values for TX-RX1

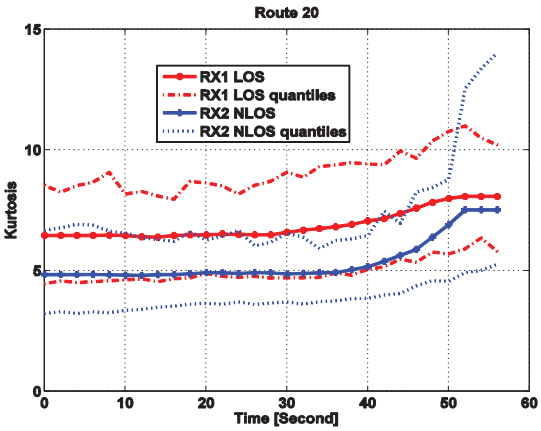

Fig. 3: Average kurtosis (solid lines) at each snapshot in Route 20. The dashed lines denote the 10% and 90% quantiles.

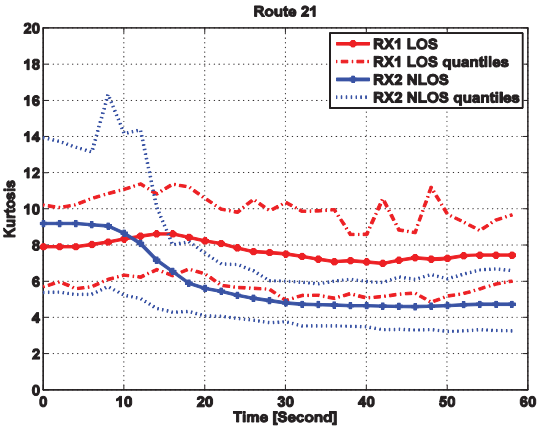

Fig. 4: Average kurtosis (solid lines) at each snapshot in Route 21. The dashed lines denote the 10% and 90% quantiles.

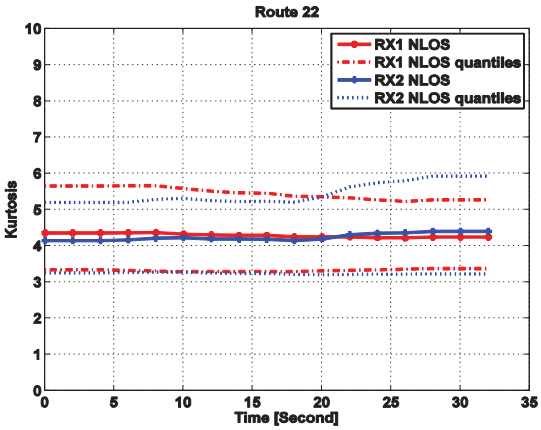

Fig. 5: Average kurtosis (solid lines) at each snapshot in Route 22. The dashed lines denote the 10% and 90% quantiles.

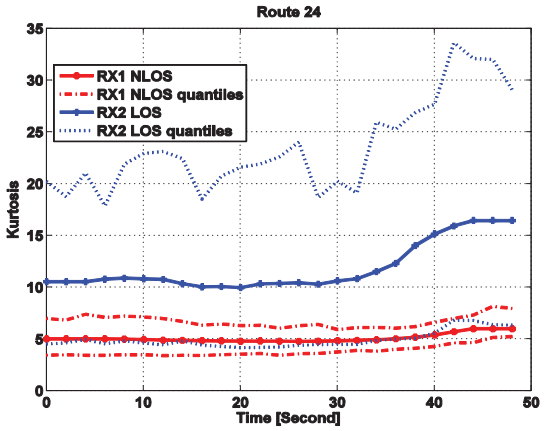

Fig. 6: Average kurtosis (solid lines) at each snapshot in Route 24. The dashed lines denote the 10% and 90% quantiles.

Link and 900 kurtosis values for TX-RX2 link) at each snapshot in the routes. The quantiles show the kurtosis in best/worst cases of all the Single Input Single Output (SISO) channels, depending on the antenna orientations. Comparing with the kurtosis in SISO channels, the average kurtosis over the MIMO channels, when available, gives a better indication of the LOS/NLOS conditions.

VI. Conclusions

This paper has presented the statistical analysis based on the MIMO channel measurements in an office building at Aalto University. The kurtosis of CIR in LOS and NLOS channels has been studied with two sets of system parameters in terms of both simulation and measurement. Both the simulation results revealed the kurtosis by using CIR amplitude had significant dependence on the system parameters.

By using only CIR amplitude as variable, the values of kurtosis varied over a wide range with the change of system parameters in both LOS and NLOS conditions. A general threshold was hard to select for NLOS identification in different system configurations. On the other hand, by using CIR amplitude in logarithmic scale as variable, the kurtosis was less sensitive to the system parameters and was more consistent and had clearer separation for NLOS and LOS conditions regardless of system parameters. Therefore, a general threshold could be selected and it would also work even if the system parameters would change based on the simulation results. The measurement results also showed that if multiple antennas were available, the average kurtosis, which was averaged over all the kurtosis values and a period of time, should give better indication of the LOS/NLOS conditions.

Reference

[1] S. Mazuelas et al., "Robust Indoor Positioning Provided by Real-Time RSSI Values in Unmodified WLAN Networks," IEEE J. Sel. Topics Signal Process, vol.3, no.5, pp.821-831, Oct. 2009

[2] E. Laitinen et al., "Comparison of Positioning accuracy of Grid and Path Loss-based Mobile Positioning Methods using Received Signal Strength", Proc. Signal Processing and Applied Mathematics for Electronics and Communications, Cluj-Napoca, Romania, 2011.

[3] S. Jung et al., "Wi-Fi fingerprint-based approaches following log-distance path loss model for indoor positioning," Intelligent Radio for Future Personal Terminals (IMWS-IRFPT), 2011 IEEE MTT-S International Microwave Workshop Series on , vol., no., pp.1-2, 24-25 Aug. 2011, doi: 10.1109/IMWS2.2011.6027190

[4] A. Hong et al., "Considerations on the relationship between path loss and spatial characteristics based on MIMO measurements," Proc. of International ITG/IEEE Workshop on Smart Antennas, Reisenburg , 13-14, Mar. 2006

[5] I. Guvenc et al., "NLOS identification and mitigation for UWB localization systems," Proc. of IEEE Wireless Communications and Networking Conf., vol., no., pp. 1571–1576, Hong Kong, 11-15 Mar. 2007.

[6] I. Guvenc et al., "NLOS identification and weighted least-squares localization for UWB systems using multipath channel statistics," EURASIP Journal on Advances in Signal Processing, Article ID 271984, 14 pages, 2008, doi:10.1155/2008/271984.

[7] L. Mucchi and P. Marcocci, "A new parameter for channel identification in UWB indoor environments," Proc. of International Conf. on Computer Communications and Networks, vol., no., pp.419-423, Turtle Bay Resort, Honolulu, Hawaii, USA, 13-16 Aug. 2007.

[8] A. Molisch, "Ultrawideband propagation channels theory, measurement and modeling," IEEE Trans. on Vehic. Tech., vol. 54, no. 5, pp. 1528-1545, Sept. 2005.

[9] V.-M. Kolmone et al., "A Dynamic Dual-Link Wideband MIMO Channel Sounder for 5.3 GHz," IEEE Trans. Instrum. Meas., vol.59, no.4, pp.873-883, April 2010

[10] O. Maimon and L. Rokach, Decomposition Methodology For Knoledge Discovery And Data Mining: Theory And Applications, World Scientific Pub Co Inc, July, 2005

[11] V.-M. Kolmonen et al., "5.3-GHz MIMO radio channel sounder," IEEE Trans. Instrum. Meas., vol. 55, no. 4, pp. 1263-1269, Aug. 2006.

[12] D. Dardari et al., Satellite and Terrestrial Radio Positioning Techniques, Academic Press, Oct. 2011.

Jie Zhang was born in Beijing, China, in 1985. She received the B.S. degree in Communications Engineering from Beijing University of Technology, China in 2007 and M.S. degrees in Radio Frequency Electronics from the Tampere University of Technology, Finland, in 2010. Currently, she is a Ph.D candidate and researcher in Department of Electronics and Communications Engineering at Tampere University of Technology, Finland. Her research interests include advanced signal processing for multi-mode multi-frequency operation in navigation devices.

Jussi Salmi (S'05-M'09) was born in Finland in 1981. He received the M.Sc. and D.Sc degree, both with honors, from Helsinki University of Technology (HUT) Finland, in 2005 and 2009, respectively.

In 2009-2010, he worked as a Postdoctoral Research Associate in the Department of Electrical Engineering, University of Southern California, Los Angeles, CA. currently, he works as Postdoctoral researcher in the Department of Signal Processing and Acoustics, Aalto University School of Electrical Engineering (former HUT),

Finland. His current research interests include RF-based vital sign detection, UWB MIMO radar, indoor positioning, measurement based MIMO channel modeling, and parameter estimation.

Elena-Simona Lohan received her M.Sc. degree in Electrical Engineering from the Politehnica University of Bucharest, Romania, in 1997, the D.E.A. degree in Econometrics, at Ecole Polytechnique, Paris, France, in 1998, and the Ph.D. degree in Telecommunications from Tampere University of Technology. Since December 2003, she has been working as an Adjunct Professor at TUT and she has been acting as a group leader for the mobile and satellite-based positioning activities at the Department of Electronics and Communications Engineering. Her research interests include wireless positioning techniques, GNSS receiver architectures, CDMA signal processing, and wireless channel modeling and estimation. She was also involved with the EU FP6 project GREAT and EU FP7 project GRAMMAR as technical team leader and working package leader, respectively.

Tampereen teknillinen yliopisto
PL 527
33101 Tampere

Tampere University of Technology
P.O.B. 527
FI-33101 Tampere, Finland

ISBN 978-952-15-3187-3
ISSN 1459-2045